UNIVERSITY OF CALIFORNIA SAN DIEGO

ARTICULATION OF HUMAN ARTICULAR CARTILAGE INDUCES ANISOTROPIC STRUCTURAL DETERIORATION AND AGE-DEPENDENT CELLULAR RESPONSES

A dissertation submitted in partial satisfaction of the
requirements for the degree Doctor of Philosophy

in

Materials Science and Engineering

by

Felix Hsu

Committee in charge:

Professor Robert L. Sah, Chair
Professor Shengqiang Cai
Professor Adam J. Engler
Professor Koichi Masuda
Professor Yingxiao Wang

2017

The Dissertation of Felix Hsu is approved, and it is acceptable in quality and form for publication on microfilm and electronically:

_____

_____

_____

_____

_____
Chair

University of California, San Diego

2017

DEDICATION

This dissertation is dedicated to my father, Charles, my mother, Teresa, my siblings, Alex and Rosalind, and my wife, Judy. Thank you for your sacrifice, your encouragement, your company, and your enduring love.

TABLE OF CONTENTS

LIST OF FIGURES

LIST OF TABLES

ACKNOWLEDGEMENTS

This work would not be possible without the invaluable mentorship, companionship, advice, guidance, and help from many people.

My most sincere thanks to my advisor, Dr. Robert Sah, for his continuous guidance and support throughout the years. During the past 6-7 years, only under the mentoring and motivation of Dr. Sah, have I been able to learn the art of scientific research, to overcome intellectual challenges presented by difficult studies, and to be rewarded by observing the truth. I am especially grateful to Dr. Sah for welcoming me into the lab at a time I reached a fork in my life and felt lost, for providing me with an opportunity to continue to pursue my interest in orthopaedic research. I am also thankful for Dr. Sah's generosity with his time, spending several late nights and some weekends to advise and prepare me for critical presentations, and for patiently holding me responsible for knowledge I have gained in the past.

I would also like to thank my thesis committee members, Dr. Shengqiang Cai, Dr. Adam Engler, Dr. Koichi Masuda, and Dr. Yingxiao Wang for sharing their expertise and provide valuable knowledge during the thesis work.

The collaborators also provided significant contributions to the thesis. Dr. Martin lotz contributed by providing valuable donor samples and performed sample processing, and insight into the area of aging in human cartilage. Dr. Koichi Masuda provided invaluable consultation and generously shared lab equipment and materials without hesitation.

I will always feel at home with the Cartilage Tissue Engineering lab. The lab culture is always friendly and warm, and everyone is willing to help each other out

even when busy. The elders or alumni never hesitate to answer questions and share past experience, while undergrads and younger graduate students are frequently talented and diligent. I thank Quynhhoa (Hoa) Nguyen for welcoming into the laboratory and training me and familiarizing me with a good number of lab practices. I also thank past members, in particular Dr. Alexander Hui, Dr. Jérôme Hollenstein, Johnny Du, Dr. Murray Grissom, Dr. Neil Chang, Barb Schumacher, Dr. Yang Sun, Dr. EunHee Han, Dr. Elaine Chan, Dr. Andrea Pallante, Dr. William McCarty, Dr. Alvin Su, for serving as great examples on how to become a successful researcher and making the laboratory an enjoyable place to work. I also thank the current graduate students for their friendship, advice, and support: Aimee Raleigh, Jason Caffrey, Haoran Qiu, Rebecca Drake, Erica Gacasan, Melissa Ledgerwood-Lee, Ismael Munoz, Alex Szewczyk, Sydnee Hyman, and Somaya Jafari – and wish them all the best in continuing and completing their graduate work.

I am thankful for the strong and willing staff members of the lab: Dr. Albert Chen, Van Wong, Dr. Michele Temple-Wong, and Esther Cory. I could always rely on you for help and suggestions. Van Wong was always patient in resolving any random issues in bioreactor design and on mechanical instruments I had presented to him, even the most tedious or obvious ones. I have always enjoyed our apart-from-lab conversations on hobby collecting, Walking Dead, and Marvel. Albert Chen taught me much of what I know about mechanical testing and tissue mechanics, and I am honored to be trusted to perform some of these tests independently. I am happy to share similar interests in food as you. Esther Cory was always very helpful in anything imaging related and with performing micro CT on cartilage samples. I am delighted for her, for having a newborn son this year. Although Michele has left the lab, she has

never hesitated to provide me with invaluable research and life advice. We do miss her during the last year of my thesis work.

I have also been fortunate to work with a very talented and hardworking group of undergraduates and Master's students. I would like to thank: Sherine Cheung in her design of the fluid-flow chamber, and discovery of fluid-flow induced PRG4 expression in bovine chondrocytes; Laurence Chen for working diligently and not giving up on optimization of chondrocyte isolation, and for increasing the sample size for the study on age-dependent PRG4 secretion in human monolayer chondrocytes; Matt Gong for always being positive and energized to test out new ideas, helping with harvesting of cartilage tissue and subjecting them to various types of shear loading. I am delighted to see both Sherine Cheung and Laurence Chen to proceed onto pursuing a PhD degree in Bioengineering at UC Los Angeles, and Matt Gong to continue at UC San Diego to pursue his MD degree. I would also like to sincerely thank my fellow histopathology graders: Haoran (David) Qiu and Leening Liu, whom graded and annotated up to 72 sections without any complaints, and moreover, helped with technical advice and proofreading the manuscripts.

Finally, I am grateful for my family for their unconditional love and continuously support; furthermore, for my parent's sacrifices in helping me achieve my dream while never giving me pressure to be someone else I am not. I would not be able to be the person I am today without them.

For their contributions to Chapter 2, the dissertation author thanks co-authors Haoran Qiu, Leening P. Liu, Neil Chang, and Robert L. Sah. This work was supported by grants from the National Institutes of Health.

For their contributions to Chapter 3, the dissertation author thanks co-authors Haoran Qiu, Leening P. Liu, Neil Chang, and Robert L. Sah. This work was supported by grants from the National Institutes of Health.

For their contributions to Chapter 4, the dissertation author thanks co-authors Alexander Y. Hui, Eloy Alonso, Albert C. Chen, and Robert L. Sah. This work was supported by grants from the National Institutes of Health.

VITA

2006	Bachelor of Science, Major: Biology, Minor: Chemistry Duke University, Durham, North Carolina
2007-2009	Master of Arts, Department of Anatomy and Neurobiology Boston University, Boston, Massachusetts
2010-2017	Doctor of Philosophy, Materials Science and Engineering Cartilage Tissue Engineering Laboratory University of California, San Diego, La Jolla, California

Journal Articles

Hsu FH, Haoran Q, Chang N, Saleh AA, Moran KL, Lotz MK, Sah RL. Histopathology of Human Knee Medial Femoral Condyle Articular Cartilage: Grading of Features and Understanding of Progression in Age-associated Degeneration. To be submitted June 2017.

Hsu FH, Alonso E, Raleigh AR, Saleh AA, Masuda K, Lotz MK, Chen AC, Sah RL: Biomechanics and mechanoBiology of human cartilage articulation. Trans Orthop Res Soc 41:1428, 2016. Manuscript in progress, targeting submission in 2017.

Sun Y, Jiang W, Cory E, Caffrey JP, Hsu FH, Chen AC, Wang J, Sah RL, Bugbee WD: Pulsed lavage cleaning of osteochondral grafts depends on lavage duration, flow intensity, and graft storage condition. PLoS One 12:e0176934, 2017.

Selected Abstracts

Hsu FH, Qiu H, Chang N, Liu LP, Sah RL. Human femoral condyle articular cartilage exhibits flow into aging-associated pre-osteoarthritic lesions. Trans Orthop Res Soc 42: 2017.

Chen L, Hsu FH, Hui A, Schumacher BL, Sah RL: Primary human articular chondrocytes exhibit age-dependent PRG4 secretion and TGF-beta1 responsiveness. Trans Orthop Res Soc 41:1457, 2016.

Hsu FH, Alonso E, Raleigh AR, Saleh AA, Masuda K, Lotz MK, Chen AC, Sah RL: Biomechanics and mechanoBiology of human cartilage articulation. Trans Orthop Res Soc 41:1428, 2016.

Hsu FH, Hui AY, Chen AC, Lotz MK, Sah R: Articulation-induced responses of superficial zone chondrocytes in human knee articular cartilage: Effects of shear and sliding. Trans Orthop Res Soc 40:256, 2015.

Hui AY, Chang MJ, Brown CC, Hsu FH, Temple-Wong MM, Bugbee WD, Masuda K, Sah RL: Normal and osteoarthritic human synovial fluid regulation of articular cartilage proteoglycan-4 secretion: role of O2, TGF-beta, and IL-1. Trans Orthop Res Soc 39:380, 2014.

Hsu FH, Nguyen QT, Hui AY, Noori NB, Schumacher BL, Chen AC, D'Lima DD, Lotz MK, Sah RL: Mechanobiology of human articular cartilage: age-dependent PRG4 biosynthetic response to dynamic shear. Trans Orthop Res Soc 36:138, 2011.

ABSTRACT OF THE DISSERTATION

ARTICULATION OF HUMAN ARTICULAR CARTILAGE INDUCES ANISOTROPIC STRUCTURAL DETERIORATION AND AGE-DEPENDENT CELLULAR RESPONSES

by

Felix Hsu

Doctor of Philosophy in Materials Science and Engineering

University of California, San Diego, 2017

Professor Robert L. Sah, Chair

Articulation (shear and sliding) has been increasingly studied during the last two decades with the realization of its substantial involvement in daily locomotion of the human knee joint. Conventional biological responses of mechanical stimulation on chondrocyte viability has been studied for shear and sliding; but in addition, the close relationship between articulation and lubrication has emphasized the importance of

cell-mediated expression of the key boundary lubricating protein proteoglycan 4 (PRG4). While, in the absent of lubrication, shear and sliding between abnormal congruency between joint surfaces can initiate spatially-varied early degeneration, both instantly by direct mechanical damage of the cartilage and through time by mechanobiology. Thus, the overall motivation of this dissertation was to understand the effect of articulation (shear and sliding) on maintaining joint health as well as causing early or progressed degeneration in human articular cartilage.

Spatially-oriented histopathological features were identified in cartilage lesions of human knee medial femoral condyles (MFCs) using a standardized, reliable grading system developed from primary literature, supporting the concept of mechanical articulation-driven cartilage deterioration. To recapitulate *in vivo* effects of articulation on human articular cartilage, human cartilage explants were subjected to mid to high amplitudes of articulation that can potentially stimulate chondrocyte response and cause matrix damage. Although articulation on cartilage explants induced superficial zone cell death and apoptosis (regardless of aging), only young and not old cartilage responded by secreting higher levels of PRG4 lubricant and continuously expressed enhanced levels of autophagy. However, the articulation regime applied in the absence of lubrication was insufficient to generate noticeable wear at the cartilage surface.

Elucidating the mechanobiology of early degeneration in human articular cartilage by assessing the effects of articulation (shear and sliding) on SZ chondrocyte response and the initiation of matrix damage is one step towards a systems-based understanding of synovial joint homeostasis and derangement in health, aging, and disease. Furthermore, understanding the mechanobiological environments that can

initiate cartilage degeneration can be critical to the development of preventive therapies for osteoarthritis.

CHAPTER 1:

INTRODUCTION

1.1 General Introduction to the Dissertation

During daily locomotion, knee articular cartilage that covers long bones of femur and tibia not only provides weight bearing function but with the help of lubricating proteins at the cartilage-cartilage interface, articulates with low friction and wear for smooth relative movements between apposing joint surfaces. However, with aging and disease, deterioration can be initiated at site-dependent articular cartilage surfaces as a response to altered mechanical loading or altered perception of superficial zone chondrocytes to similar loading due to changes in its surrounding matrix. The livelihood and phenotype of these chondrocytes can change and affect the normal lubricating properties of articular cartilage. ***The overall motivation of this dissertation was to contribute to an understanding of early degeneration of human knee cartilage, starting by analyzing the spatial pattern of degeneration in human MFC by histology, followed by subjecting human knee cartilage tissue to mid to high levels of articulation (shear and sliding) in vitro, to attempt to recapitulate similar biological and/or structural responses indicative of degeneration in human cartilage.***

Specifically, the objectives of this work were to: (1) derive quantitative feature definitions and create an image atlas for histopathology in human knee medial femoral condyle (MFC) cartilage and determine the reliability and reproducibility of the grading system (**Chapter 2**). Then, (2) to apply this grading system to examine spatial patterns in the histopathology of cartilage lesions in human knee MFCs, compared to corresponding, non-lesion regions of normal MFC controls (**Chapter 3**). Finally, (3) to assess the age-dependent effects of mid to high levels of articulation on the mechanical response of human knee cartilage and biological response of the superficial zone chondrocytes within (such as PRG4 secretion, cell death, cell apoptosis and autophagy expressions) (**Chapter 4**).

Chapter 1 begins with a review of the synovial joint system, its components and interactions during normal daily locomotion. Then, additional background on the composition, structure, and function of articular cartilage is provided. The mechanical properties of cartilage tissue are described, followed by the mechanobiology of cartilage and chondrocytes with articulation (shear and sliding). Finally, aging and degeneration of articular cartilage and the underlying mechanobiologically-driven mechanisms are reviewed.

Chapter 2, which will be submitted to *Journal of Orthopaedic Research*, aimed to develop a standardized and reliable grading system for human knee MFC with quantitative feature definitions supplemented by an image atlas. Several classical grading systems for osteoarthritic and degenerated cartilage such as Collins, Mankin that is also equivalent to Histologic Histochemical Grading System (HHGS), and Osteoarthritis Cartilage Research Society International (OARSI) were referenced and

analyzed to identify a total of 16 representative cartilage matrix and chondrocyte features for the grading system. Quantitative definitions for each feature was created by systematically summarizing measurements on these features in other primary literature. Then, by applying standardized resolutions and field-of-views, and assessing the histology images quantitatively based on the definitions, several representative images per score per feature were selected to formulate the image atlas. Following 3 separate trials of applying the grading system on examining MFCs of all four macroscopic grades, and further refining the quantitative definitions while compiling the image atlas, the proposed grading method achieved high overall intra- and inter-observer reliability and reproducibility.

In Chapter 3, this grading system was applied to study cartilage lesions in human knee MFCs and found spatially-oriented histopathological features in the anterior-posterior direction of lesion MFCs, relative to matched normal MFC controls. Specifically, “cartilage flow”, which is described as bending of collagen fibril networks, was only located at the anterior (and not the posterior) transitional region of the cartilage lesion, implicating cartilage degeneration that is driven by mechanical articulation.

Chapter 4, thus, assessed the relationship of mechanical articulation (shear and sliding) and human knee cartilage, and the mechano-biological response of superficial zone chondrocytes, under the context of aging. Aging was associated with diminished PRG4 secretion, a boundary lubricant of cartilage, in normal human femoral condyles, and the stimulatory effect of mechanical articulation was only observed in young but not old donor cartilage. SZ cell apoptosis and necrosis were induced similarly by high

articulation, irrespective of age. Conversely, autophagy was higher in young than old in the absence of articulation, but was substantially higher with articulation in old cartilage. Certain biological responses by chondrocytes were correlated to the behavior of the bulk tissue (ie. cell death and PRG4 secretion with shear stress), while some biological responses were correlated to each other (ie. cell autophagy expression and PRG4 secretion). The age-associated attenuation in responses that can be categorized as reparative (autophagy) or preventive of further damage (lubrication) may be related to the age-associated predisposition to cartilage degeneration in OA.

Chapter 5 discusses the major findings and future directions for this work.

1.2 Synovial Joint Overview

Synovial joints are the most common joints of the human body and allow load-bearing, low-friction, wear-resistant movement between apposing bone surfaces [1]. Synovial joints normally consist of several bone compartments lined with articular cartilage, such as the femur, tibia, and patella in the knee joint, which are surrounded by synovial fluid that is further encapsulated by a fibrous capsule that includes the synovium. Each individual joint component possesses specialized biological and chemical properties for self-renewal and remodeling for adaptation to the environment; as well as unique structural and mechanical properties, to provide synchronized movements for daily locomotion [2] [3].

Of the synovial joint, articular cartilage serves as a critical tissue that withstands load experienced between the joint interfaces. Articular cartilage is quite durable, exhibiting substantial stiffness in compression while effectively distributing load [4]. During daily locomotion, as certain joint components move relative to each other, the articular cartilage is subjected to varying types (compression, shear, tension) and regimes (load, displacement, amplitude) of mechanical loading. Several factors determine the loading experienced by articular cartilage, such as the physical alignment and lubrication between the different joint components. Unfortunately, as a complex, mechanically-driven structure consisted of multiple components that are required to work in synchrony, the human knee can experience undesirable changes with one or more of the joint components being affected by aging, injury, and/or disease.

Joint disease and injury can result in pain and dysfunction of synovial joints. OA is a degenerative disease that results in destructive changes to joint structures including cartilage, synovium, and bone. OA has been classified as idiopathic or secondary to other factors, such as joint trauma and congenital diseases. Knee OA has been classified according to clinical, laboratory, and radiographic criteria [5]. Rheumatoid arthritis (RA) is a systemic inflammatory disease characterized by joint swelling, joint tenderness, and destruction of synovial joints [6]. Traumatic joint injury can result in cartilage damage, articular and bone fractures, damage to soft tissues such as ligaments and menisci, and lesions in the joint capsule and synovium. Such damage is associated with a number of mechanical and biological changes in the synovial joint that contribute to the development of post-traumatic OA [7-9].

Since articular cartilage is the key structure that bears load and enables smooth articulation in the human synovial joint, it is important to understand how articular cartilage normally functions to resist being damaged and if damaged, what are the mechanical factors that could initiate and accelerate the progression of such cartilage deterioration. The mechanical and biological responses of articular cartilage to loading are dependent on the composition and structure of the cartilage matrix as well as the activity of the chondrocytes embedded within.

1.3 Articular Cartilage Composition and Structure

Articular cartilage is mainly comprised of its cells, also termed chondrocytes, which are distributed sparsely within its matrix macromolecular network that is also filled with matrix fluid [3]. In normal mature cartilage, highly specialized

chondrocytes are the main if not the sole type of cells that regulate their surrounding matrix by being metabolically active. Chondrocytes are fairly active individually, but presented at low cell density in articular cartilage, constituting a tissue with low metabolic activity overall. Not only is the synthesis of matrix molecules dependent on chondrocytes and their metabolic activity, the organization of these macromolecules are also based on the distribution of the chondrocytes. Normal chondrocytes can perform remodeling activities constantly via synthesis and degradation of matrix molecules, as a response to the current chemical and mechanical environment.

The cell-mediated composition and organization of macromolecules can dictate the overall mechanical properties and behavior of articular cartilage. The extracellular matrix of articular cartilage is consisted of mainly tissue fluid (80% wet weight) and macromolecules (20-40% wet weight). The macromolecules are predominantly of two types: collagens and proteoglycans, each contributing 25-30 and 15-20% of the dry weight of cartilage, respectively. Collagen and proteoglycans provide articular cartilage with its mechanical stiffness and strength based on different underlying mechanisms.

Tight networks formed of collagen fibrils contribute to the tensile stiffness and strength of the cartilage. Proteoglycans (PG), negatively charged macromolecules with a protein core and several glycosaminoglycan (GAG) chains attached, can provide cartilage with compressive stiffness and resilience. The collagen network affects the mechanical properties provided by PG also, by constraining the negatively charged GAG chains that repel each other in a fixed volume as well as allowing for the

concentration of positively charged ions within the tissue fluid and increasing osmolarity.

Both chondrocyte and matrix exhibit depth-dependent properties in articular cartilage (**Figure 1.1**). Individual chondrocyte shapes are discoidal in the superficial zone, but round in the transitional and deep zones. Chondrocyte density is higher in the superficial zone relative to deeper zones (**Figure 1.1A**) [10]. For cell orientation, superficial, transitional, and deep zone cells are generally oriented parallel, diagonal, and vertical to the articular surface, respectively [11]. Also, certain cell phenotypes are only expressed in superficial zone chondrocytes (or a population of it), such as the secretion of an important joint lubricant protein superficial zone protein/proteoglycan 4 (SZP/PRG4) and progenitor-like gene expressions of cell fate selector gene Notch 1 [12].

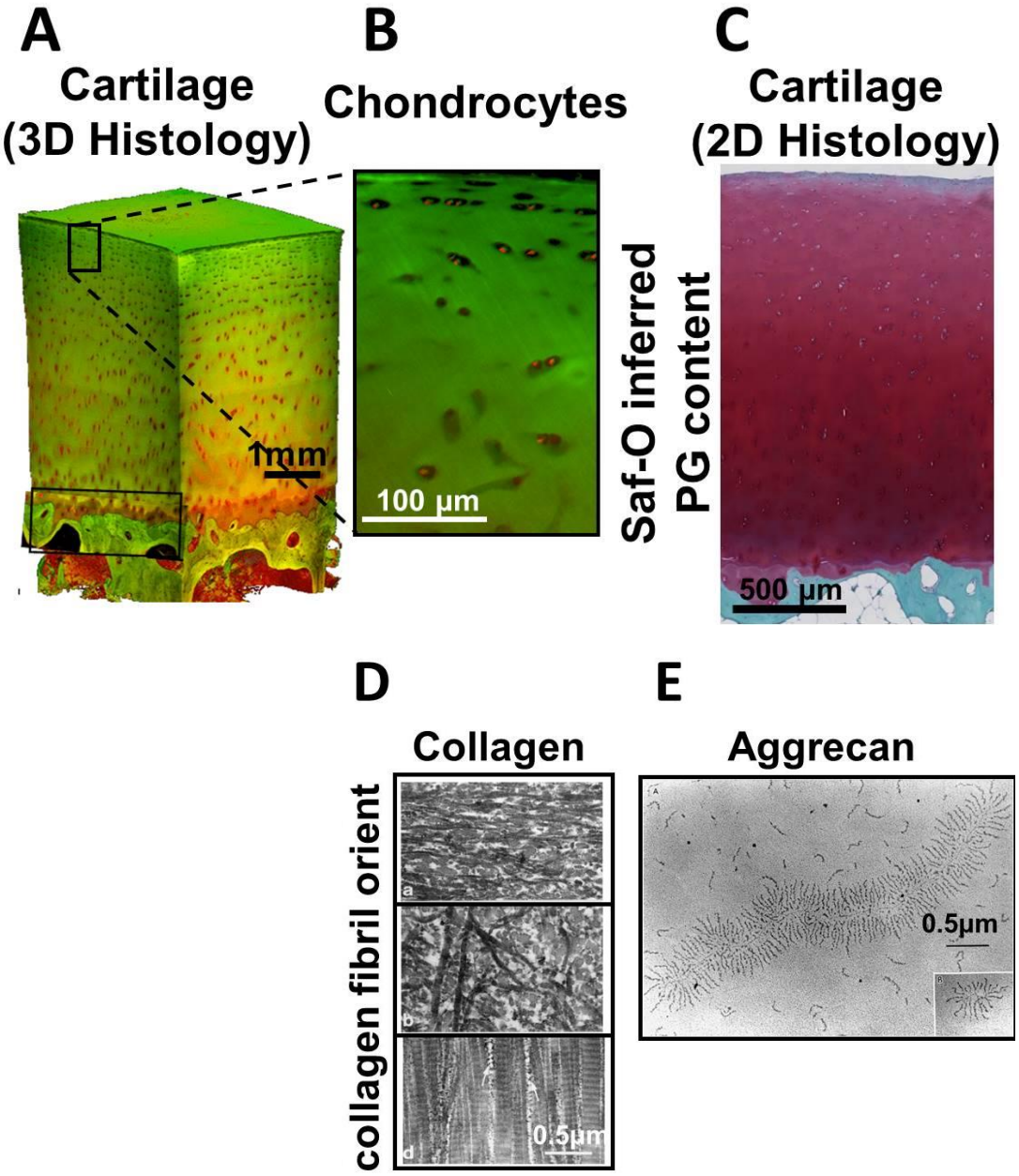

Figure 1.1: Depth-dependent properties of cartilage matrix and chondrocytes shown in (A) three- and (C) two-dimensional histology. (B) Chondrocyte and (D) collagen fiber orientations are also depicted by digital volumetric imaging and electron micrograph. (E) is an electron micrograph of a proteoglycan aggregate. Depth-dependent differences are shown, in (B) chondrocyte and (D) collagen orientation as well as (C) Saf-O inferred proteoglycan content.

The concentration and distribution of matrix molecules of collagen and proteoglycan are strongly dependent on chondrocytes, which regulate their synthesis and degradation. In normal human knee articular cartilage, although the collagen content does not appear to differ across the different zones, the orientation of the collagen fibrils are aligned according to the Benninghoff arcade, where the fibrils are parallel, diagonal, and perpendicular, in the superficial, middle, and deep zones of cartilage, respectively (**Figure 1.1D**) [13]. The content of proteoglycan, on the other hand, is depth-dependent and increases with increasing depth from the articular surface (**Figure 1.1B**, can be inferred by the stronger Safranin-O staining intensity in the deeper regions).

Chondrocytes, specifically ones in the superficial zone, also function to synthesize and secrete lubricant molecules such as proteoglycan 4 (PRG4) and Hyaluronan (HA) that helps reduce friction and wear at the articular surface. PRG4 (also known as lubricin and superficial zone protein) [14, 15] and HA [16] are the key proteins found at the surface of cartilage and in synovial fluid, which provide boundary and fluid film modes of lubrication to the joint, respectively [17-20]. PRG4 is encoded by the *PRG4* gene, which also encodes for superficial zone protein and lubricin, and are mucinous glycoproteins with multiple O-linked β(1-3)Gal-GalNAc oligosaccharides that mediate boundary lubrication of articular cartilage [21]. SZP is a ~345 kDa glycoprotein synthesized and secreted by chondrocytes in the superficial zone of cartilage, and not from other depths of cartilage [18].

1.4 Functions of Articular Cartilage

During daily locomotion, human knee joints undergo thousands of cycles of loading (and unloading), each lower limb alternating between the stance and swing phases. The stance phase when joints are loaded, is dissected into at least 7 positions of heel strike, flatfoot, mid stance, push off, acceleration, midswing, and deceleration. As we transition through these positions, our femoral condyle is subjected to compression as well as shear and sliding, against its counter-surface of the meniscus and tibial plateau cartilage. To understand the precise movements of these joint compartments in space and time, joint kinematic monitored the femur and tibia using dual fluoroscopic imaging. Based on the relative location measurements in **Figure 1.3A** of the femoral condyle relative to the tibial plateau, **Figure 1.3B** serves as a schematic that depicts visually the motions of the relative movements between the 2 joint components (with the femoral condyle fixed). A close analysis of relative joint movement suggests that the largest transitions in degrees or distances seem to occur between flat foot and mid stance, which is followed by similarly large transitions in the apposite direction between pushoff and acceleration.

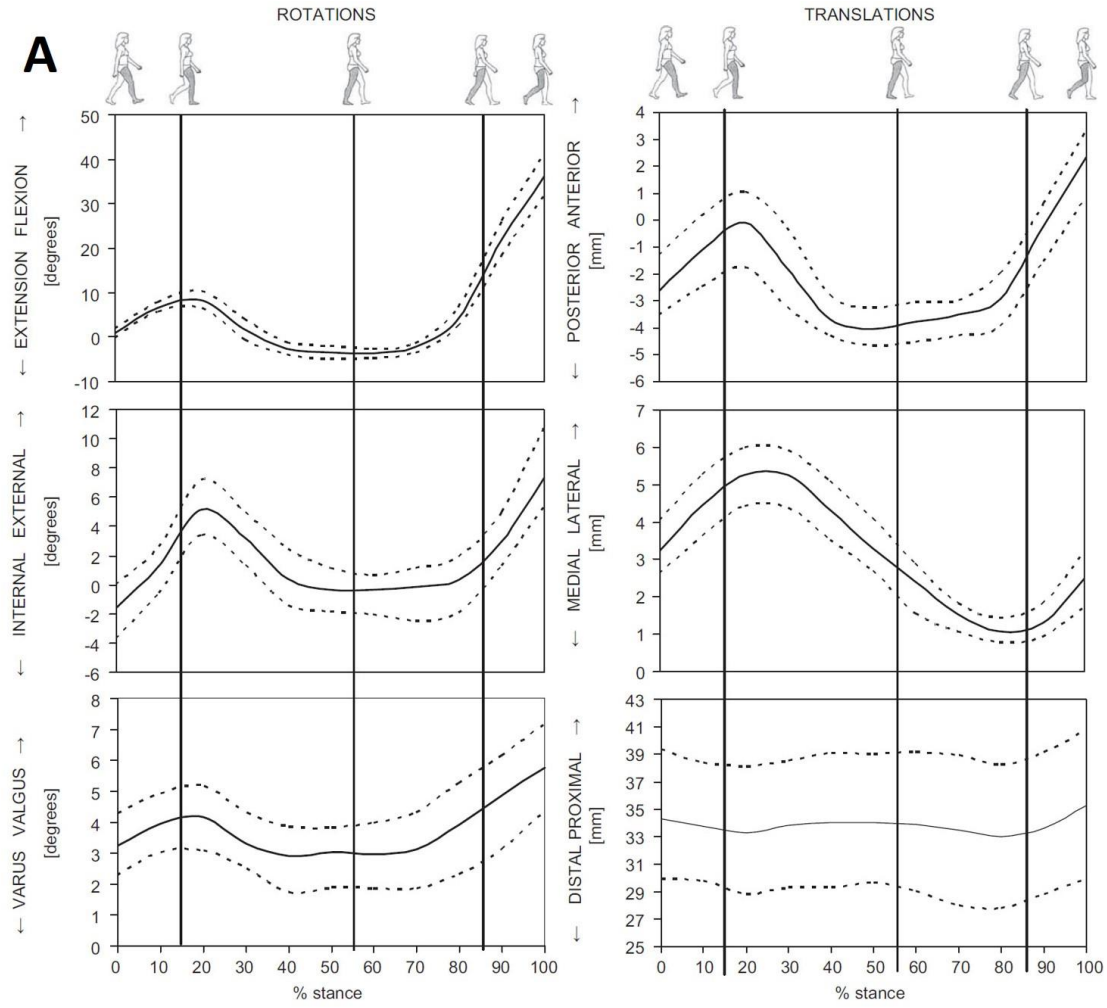

Figure 1.2: (A) Relative rotational and transitional positions of the femoral condyle to the tibial plateau during human gait and (B) corresponding schematic. (**A**) Relative positions of the femoral condyle versus the tibial plateau during locomotion, dissected into 6 degrees of freedom, 3 rotational and 3 transitional (adapted from [22]), and (**B**) schematic representation to depict visually the relative motions between these 2 joint components.

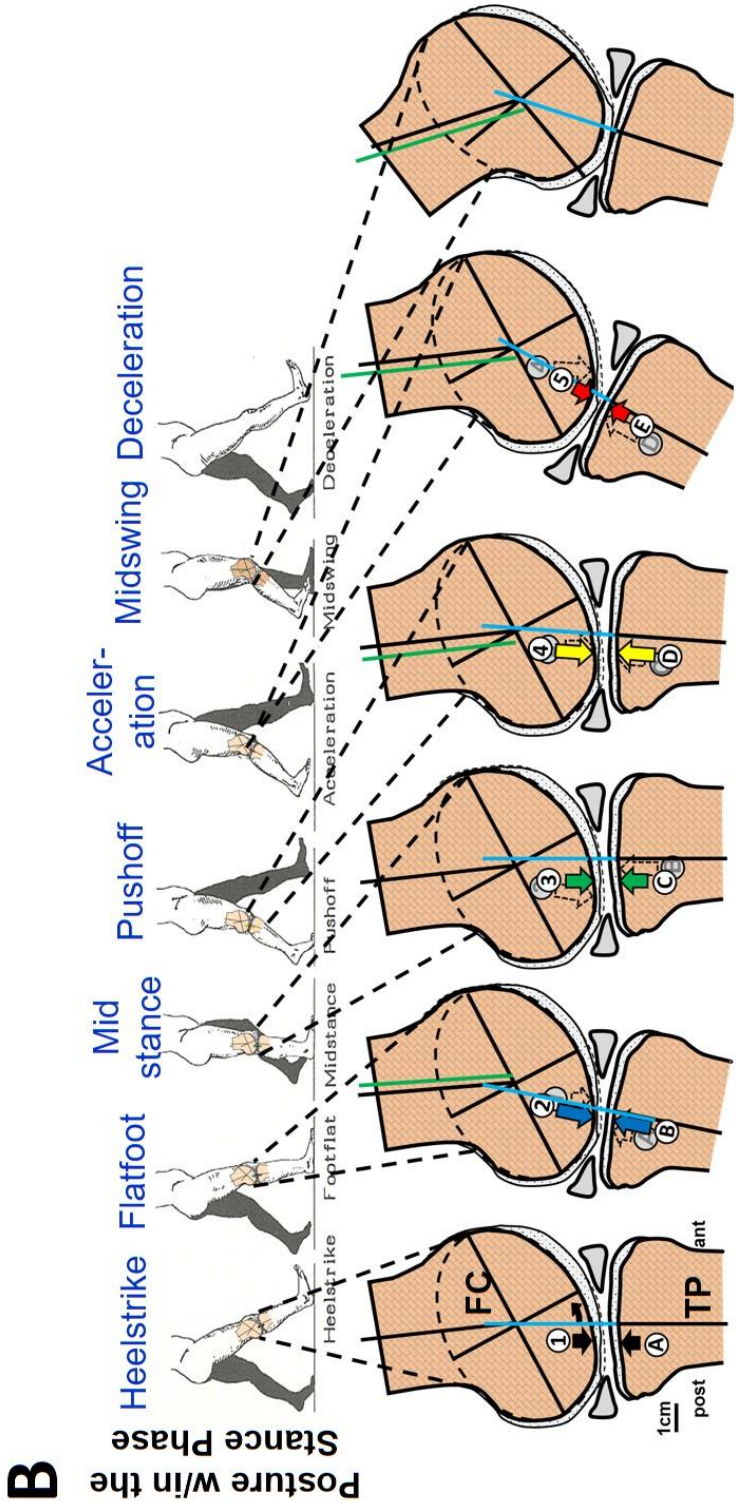

Figure 1.2: (A) Relative rotational and transitional positions of the femoral condyle to the tibial plateau during human gait. and (B) corresponding schematic. (cont'd)…(**B**) schematic to depict visually the relative motions between these 2 joint components.

1.4.1 Compression

The articular cartilage is a viscoelastic material which exhibits a biphasic response to compressive loading. The compressive properties of cartilage represent the product of proteoglycan molecules that are negatively charged and attracts water to swell, while being restrained in space by the collagen framework. When experiencing compression, not only does hydrostatic pressure build up to trigger the flow of interstitial fluid, the aggrecan molecules that electrostatically repulse each other are forced into smaller spaces. Consequently, depending on compressive loading parameters such as loading frequency, magnitude, and waveform, the cartilage can respond either by its "fluid phase", described by the flow of interstitial fluid from high to lower pressure regions through the densely packed extracellular matrix, or by its "solid phase", described by the incompressible nature of matrix constituents grouped together including proteoglycans, collagen, and cells [23].

Creep and stress relaxation regimes performed under settings of confined compression provides compressive properties of compressive modulus and permeability of cartilage. Human femoral articular cartilage exhibits an aggregate modulus of 0.5 – 0.7 MPa and permeability of ~1.1-2.2 m^4/Ns [24]. Poisson's ratio of cartilage is ~0.07-0.10 (lateral expansion relative to axial compression) by unconfined compression and structural stiffness of cartilage in situ is ~10-20 N/m by indentation tests [24, 25].

Human knee cartilage can also be compressed to ~5-20% of the overall thickness with repeated knee bending and running [26, 27]. However, the compressive modulus of cartilage is inhomogeneous at different depths, increasing with increasing

depth from the articular surface [28]. Thus, the superficial (rather than the mid and deep) zone cartilage and chondrocytes are the main structures affected by such amplitudes of compressive strain.

1.4.2 Tribology

Tribology also concerns articulation cartilage, as cartilage surfaces of the femoral condyle and tibial plateau apposes each other during articulation. Factors such as sliding velocity, stroke length, contact stress level, and lubrication can dictate the friction coefficient between cartilage and cartilage or cartilage on hard bearing materials [29]. A higher percentage of interstitial fluid, and articulation with lower sliding velocities and greater stroke lengths that allow for rehydration can help lower the coefficient of friction for the apposing cartilage. On the other hand, the contact stress reduces the coefficient of friction at low amplitudes of load, the friction can increase as the load reaches certain levels and further increases proportionally.

Boundary lubrication is a critical determinant of coefficient of friction in cartilage. Lubricants in synovial fluid such as hyaluronic acid, lubricin/PRG4, and surface active phospholipids all contribute to the extremely low coefficient of friction between apposing cartilage surfaces. The kinetic friction coefficient between two apposing adult bovine osteochondral cores lubricated with synovial fluid is lower, ~0.025 compared to ~0.2, the kinetic friction coefficient for cores not lubricated and instead articulated in saline [30]. The need for lubrication is further emphasized when wear is generated at the cartilage surface, in the absence of appropriate lubrication.

Wear is defined by "*the removal of material from the contact surfaces due to mechanical action between (the surfaces)*" [29]. In cartilage, wear is expected to partake in the development of cartilage lesions and erosions, but is complicated due to the uncertain causative factors that may involve biochemical degradation. When wear is induced experimentally by articulating cartilage against hard bearing materials, it is characterized by the biochemical compositions of the detached particles and by analyzing the surface for roughness.

1.4.3 Shear

The shear properties and behaviors of cartilage can be complex, affected by combined properties that relate to compression and lubrication. Shear properties of articular cartilage have mainly been tested using dynamic simple shear, cylindrical/torsional shear, or surface motion created with continuous rolling of a ball or wheel. Shear moduli measured can be dependent on source of tissue (animal, joint), tissue type (chondral disk with all or different zones, with bone as osteochondral cores), and testing device or setup (interface material roughness). While not completely physiological, a common experimental approach to study steady state cartilage tissue shear properties requires reaching compressive equilibrium to minimize hydrostatic pressure, fluid flow, and transport effects [31].

Relative motions between two apposing cartilage surfaces have been studied to undergo a sequence of 4 main events: adherence, adherence and deformation, detachment, and sliding [32]. When sliding, peak shear strain (and tissue deformation) is maintained with further lateral displacement. However, the actual progression from

one event to the next, is dependent on the frictional properties between the interfaces and the degeneration levels of the tissue, with the shear strain of the superficial zone particularly sensitive to these factors. In instances where cartilage is interfaced against a highly roughened material (rough polysulfone) under high level of compressive strain, without lubrication of synovial fluid, the two apposing surfaces can be in adherence for a greater duration and result in larger tissue shear strain [33].

In human knee cartilage, amplitudes of shear strain ranges from 0.03-0.10 and is dependent on tissue state (normal or degenerated), and lubrication applied at interface (PBS or synovial fluid). Normal human osteochondral cores exhibits 0.030 peak shear strain when apposed in the presence of bSF, and increases to ~0.045 without lubrication [32]. Degenerated cartilage exhibits greater shear strain, ~0.045 and ~0.06 in the presence and absence of lubrication, respectively.

The shear modulus of cartilage is categorized into instantaneous, equilibrium, complex, storage and loss. Shear stress is measured using recorded shear/lateral load, but shear strain is measured by different techniques including microscopically tracking cell location before and after shear and using the applied lateral displacement. Shear modulus of human knee cartilage (using cell tracking techniques for strain) is between 0.1-3.0 MPa and also depth-dependent, increasing from ~0.1 MPa near the articular surface to 2.0-3.0 MPa at the deepest cartilage regions of full-thickness human cartilage [32]. Similar depth-dependent properties are expressed in calf chondral disks, but instead of the surface being deformed the most, a global minimum in shear modulus of 0.07 MPa (relating to large shear strain) was expressed at ~125 μm depth from the articulating surface, to be ~ 0.07 MPa. Whereas, a global plateau in shear

modulus was located at >500 μm depth from the articular surface, with a shear modulus that is nearly 10 fold larger ~0.65 MPa [34]. However, it is unknown whether different approaches to securing the samples can influence the results, between apposing osteochondral blocks against each other and glued ends of a chondral hemi-cylinder.

The shear modulus is species dependent and typically greater in human cartilage compared to other animal species, and greater in bovine calf than smaller animals such as canine and rabbit. Although the methods to determine shear modulus varies, similar ranges of shear modulus are determined per species. Depending on the type of shear modulus and cartilage zone examined, human osteochondral cores is 2.6-4.1 MPa, calf cartilage is 0.18-3.00 MPa, canine is 0.44-0.79 MPa, and rabbit is 0.35 MPa [35-40].

Overall, at the apposing cartilage of the two articulating long bones, the combination of compression and sliding causes tissue deformation at varying degrees, which is dependent on internal factors such as compressive and shear modulus and external factors of counter surface roughness, lubrication, and compressive stress and/or strain amplitudes [33]. External physical forces of compression and shear perceived by extracellular matrix can be transmitted and transduced to become electrical, mechanical, and chemical phenomena experienced by chondrocytes. These forces can modulate the chondrocyte biological behavior and feedback to modify the structure and composition of the matrix, ultimately changing the compressive properties of cartilage.

1.5 MechanoBiology of Articular Cartilage

The biological response of articular cartilage to its environment can vary broadly depending on the combined effect of external factors such as mechanical loading (and associated anatomical structures that result in this loading) and internal factors that can be systemic, biological, chemical.

Shear and sliding transmitted through the interface and then to the matrix micro-environment can cause behavioral or phenotypical changes of chondrocytes, summarized in **Table 1.1**. The biological responses of cells to shear can be categorized into alterations in chondrocyte health status, and cell mediated changes in lubrication and matrix synthesis. Here we will focus on cell death and lubrication.

Table 1.1: Shear stimulation induced biological effects on articular cartilage (AC) and tissue-engineered (TE) cartilage.

Mechanical stimulation	Species	Sample	Biological response	Reference
dynamic compression	Bovine (immature)	AC	↑ total protein & PG syn. ↑ gene exp. of matrix protein ↑ gene exp. of protease ↑ rebound PRG4 secretion ↑ depth of PRG4+ exp. cells	Sah+, *J Orthop Res* 1989 Fitzgerald+, *J Biol Chem* '06 Nugent+, *Biorheology* '06.
Rotation (shear)	Bovine (immature)	AC	↑↑ gene exp. of matrix protein ↑ gene exp. of protease	Jin+, *Arch Biochem Biophys* '01 Fitzgerald+, *J Biol Chem* '06
*Rotation (shear)	Bovine	AC	↑ lubrication ↓ cell apoptosis	Waller+, Proc Natl Acad Sci U S A '13
Simple (shear)	Bovine (immature)	AC	↑ overall PRG4 secretion ↑ depth of PRG4+ exp. cells	Nugent+, *Arthritis Rheum* '06
Simple (shear)	Bovine (immature)	TE	↑ matrix synthesis ↑ mechanical properties	Waldman+, *Eur Cell Mater* '06
Ball-induced (dyn rot.+comp.)	Bovine	TE	↑ COMP mRNA expression	Wimmer+, *Tissue Eng* '04
Ball-induced (dyn rot.+comp.)	Bovine	TE	↑ PRG4,HAS1,HAS2 mRNA exp (sheared surface)	Li+, *Osteoarthritis Cartilage* '07
Wheel-induced (shear+dyn comp.)	Human	TE	↑ GAG, total collgen & type II collagen synthesis	Shahin+, *Biotechnol Bioeng* '11

1.5.1 Proteoglycan 4 (PRG4) Lubrication

The physiological importance of PRG4 is suggested in patients and animals with mutations in the *PRG4* gene [41] that experience early onset joint abnormalities and failure [42-45]. Low concentrations of PRG4 is also associated with increased wear of the cartilage surface after knee injury [46, 47].

cDNA encodes a protein of 1,404 amino acids (human A isoform) with a somatomedin B homology domain, heparin-binding domains, multiple mucin-like repeats, a hemopexin domain, and an aggregation domain (**Fig. 1.3**). There are 3 consensus sequences for N-glycosylation and 1 chondroitin sulfate substitution site.

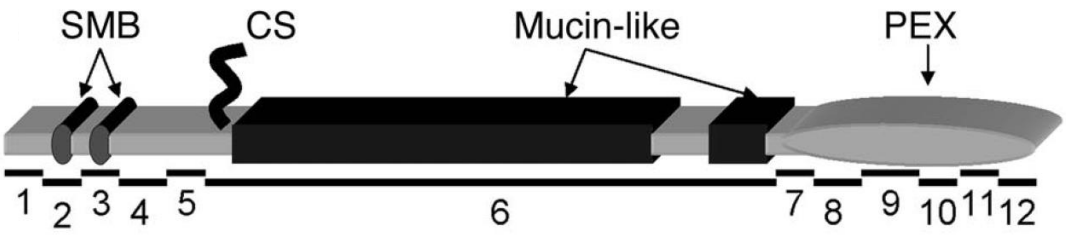

Figure 1.3: PRG4 structure. The *PRG4* gene contains 12 exons (labeled 1 – 12), with the amino-terminus at the left and the carboxyl-terminus at the right. *PRG4* has somatomedin B homology domains (SMB), multiple mucin-like repeats, a hemopexin (PEX) domain, and covalently linked chondroitin sulfate side chain (CS). (Adapted from [44]).

The secretion of PRG4 by chondrocytes can be influenced by chemical and mechanical stimuli. *In vitro*, TGF-β1 stimulates [48-51], while IL-1α [48-51] and TNF-α [48, 51] inhibit cartilage PRG4 secretion. PRG4 secretion by chondrocytes is also modulated by mechanical stimuli of compression, shear, and continuous passive motion in varying manners [52-54]. In calf cartilage, static compression consistently inhibits while dynamic compression inhibits during but promotes PRG4 secretion for a

short duration following stimulation. In contrast, dynamic shear stimulates PRG4 secretion both during and following stimulation.

1.5.2 Cell death-associated pathways

High amplitudes, high rate, or prolonged mechanical stimulations can induce changes in chondrocyte phenotypes to enter pathways that are associated with cell death, such as apoptosis, autophagy, and necrosis [55, 56]. Cell apoptosis is characterized as an energy-dependent cell death pathway orchestrated by caspases that result in downstream biochemical processes of protein cleavage, protein cross-linking, DNA fragmentation, formation of apoptotic bodies, and phagocytosis [55]. Autophagy can induce chondrocyte death with its main function of removing dysfunctional proteins and organelles present in the cell, but such a function enables it a second and apposing role of delaying programmed cell death [57]. Moreover, reduction in autophagy expression due to aging and mechanical injury (single impact of 40% compressive strain in 0.5s) is correlated with an increase in apoptosis, which demonstrates the protective mechanism of autophagy against cell apoptosis [58, 59]. Necrosis, on the other hand, represents the terminal stage of any form of cell death [60]. The rupturing of chondrocyte membrane is a characteristic process of necrosis, which feature allows nuclear markers to diffuse and fluorescently detect necrotic cells [55].

1.6 Aging and Degeneration of Articular Cartilage

Macroscopic and microscopic feature alters with aging and degeneration in the human MFC

Normal aging can affect the homeostasis of articular chondrocytes and indirectly affecting the cartilage matrix, whereas joint injury oftentimes causes direct damage to the cartilage matrix. Cartilage degeneration due to normal aging has been generally described at the gross level with macroscopic grades from 1 to 4 (**Figure 1.4A**): grade 1, cartilage is observed with a glistening white surface, to grade 2, the cartilage surface becomes roughened or fibrillated, grade 3, the cartilage is partially eroded, and grade 4, cartilage is fully eroded to the subchondral plate surface (**Figure 1.4**). The coloration of the cartilage surface also becomes yellow with aging, resulting from the accumulation in advanced glycation end products [61].

Microscopically and histologically, changes occur in the structure and content of cartilage matrix as well as in the metabolism of chondrocytes, with aging, degeneration, and osteoarthritis (OA) (**Figure 1.4B**). Although aging and OA are strongly correlated, aging does not always result in OA. Aging does, however, provide a basis for the initiation of OA, and therefore is of interest to compare the cartilage biology at these different health stages. Surface roughness gradually increases with aging, degeneration, and OA. Glycosaminoglycan or proteoglycan content is typically affected early on, to reach lower levels with aging; while collagen does not degrade substantially with aging, but is degraded with degeneration and OA. Chondrocyte density also decreases with aging and degeneration; however, can be maintained rather than further decrease in OA with cell proliferation compensating for cell loss due to death or tissue loss [13]. Aging-associated changes in chondrocyte phenotype involve reduced prevalence of superficial zone chondrocytes exhibiting progenitor phenotypes such as High Mobility Group Protein 2, attenuated autophagy response which could be

associated with aging-induced mitochondrial damage [62]. The gene expression and protein secretion of PRG4 lubricant is also decreased in old versus young donor cartilage explants [63].

Spatial variation in the human MFC cartilage

The difference in these matrix and chondrocyte features between the different health states serve as a good general guideline to understanding the temporal aspect and progression of cartilage degeneration. However, the spatial variation in these individual health states should be also be considered, particularly to establish baseline measurements for matrix and chondrocyte features. Substantial topographical differences exist in normal human femoral cartilage, of the biochemical and mechanical properties of the MFC and lateral femoral condyles (LFC). With normal aging, MFC typically advances to degeneration earlier than LFC, exhibiting greater surface damage, lower intrinsic fluorescence indicating lower collagen content, and weaker tensile stiffness [13].

At finer resolutions, features can vary across different regions within the MFC. Biologically, PRG4 lubricant secretion is ~10 fold higher in the anterior region relative to the posterior region of the calf knee [54]. Whereas, mechanically, the structural stiffness determined by performing indentation tests across the anterior-posterior direction of the MFC, indicated a steadily increase in stiffness in cartilage moving from the anterior region toward the posterior region [25].

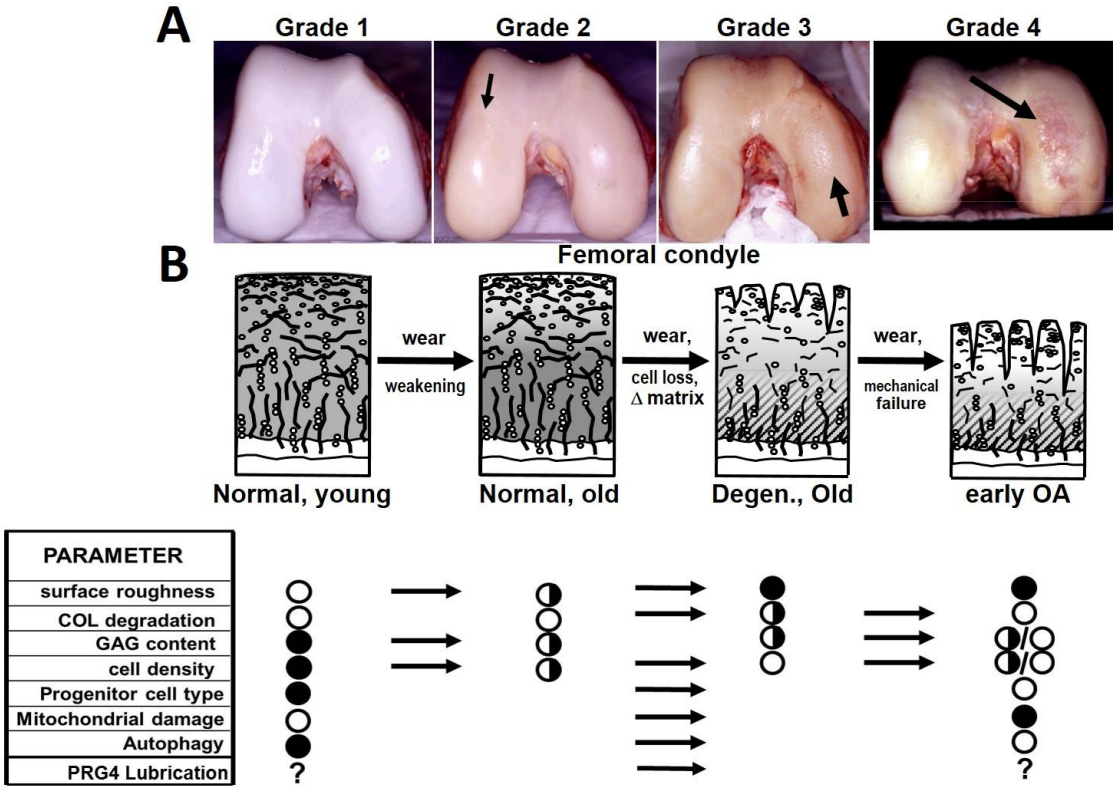

Figure 1.4: (A) Macro- and (B) micro-scale changes in articular cartilage with aging, degeneration, and disease.

1.7 Histopathology of Osteoarthritic Articular Cartilage

Similar as many other biological systems, histological analysis or the study of histopathology has been commonly utilized to assess and describe the condition of deterioration in articular cartilage. The key classical grading systems to osteoarthritic or degenerated cartilage are Collins, Mankin that is also termed Histologic/Histochemical Grading System (HHGS), an array of modified Mankin systems (such as by Shapiro), and a grading system developed by Osteoarthritis Research Society International (**Table 1.2**).

In 1949, Collins established a system for grading of osteoarthritis severity in knee joint that was mainly based on macroscopic observations. About 20 years later, Mankin grading system was developed to evaluate more microscopic histological features, grading 4 main categories of cartilage, cells, tidemark, and Safranin-O staining. In 2006, the Osteoarthritis Research Society International (OARSI) committee created a cartilage grading system using standardized, qualitative approaches to analyze various cartilage characteristics with consideration of feature horizontal extent

These grading systems are generally developed from clinical and experimental observations. Additionally, the Mankin grading system is one of the few systems that validated the feature scores by correlating to biochemical contents [64]. Most other newly developed grading systems are validated by correlating their category (cells, matrix) or accumulated scores to the scores determined from these classical grading systems [65-67]. [68]. Both Mankin and OARSI grading systems have also been tested to be reliable and reproducible for grading of human normal and osteoarthritic knees, and the respective scores from the two systems were highly correlated with each other (Spearman's coefficient 0.883 – 0.980, $P<0.05$) [65-67].

The key principles of an "ideal" histopathological grading system were noted when developing the OARSI grading system were: *simplicity*, *utility* (for both clinical and experimental OA), *scalability* (able to correlate between macroscopic appearance and cartilage histopathology), *extendability* (simple observation to advanced analysis), and *comparability* (assess other types of cartilage such as repair) [69]. However, more fundamentally, establishing a histopathological grading system for human knee cartilage can be difficult, since (1) invasive longitudinal studies could rarely be performed in human subjects, (2) the transition between normal and degenerated articular cartilage is continuous and gradual, normally without clear boundaries in space and (3) the challenge in distinguishing specific zones of cartilage based on morphological features.

Table 1.2: Classical grading systems for osteoarthritic and degenerated cartilage. Mankin or Histologic/histochemical grading system (HHGS) and Shapiro-modified Mankin.

Grading System	Category	Grading Scheme	
		Grade	Description
Mankin (Mankin, Dorfman et al. 1971)	I. Structure	0	Normal
		1	Surface irregularities
		2	Pannus and Surface irregularities
		3	Clefts to transitional zone
		4	Clefts to radial zone
		5	Clefts to calcified zone
		6	Complete disorganization
	II. Cells	0	Normal
		1	Diffuse hypercellularity
		2	Cloning
		3	Hypocellularity
	III. Safranin-O staining	0	Normal
		1	Slight reduction
		2	Moderate reduction
		3	Severe reduction
		4	No dye noted
	IV. Tidemark integrity	0	Intact
		1	Crossed by blood vessels

Grading System	Category	Grading Scheme	
		Grade	Description
Mankin modified by Shapiro (Shapiro and Glimcher 1980)	(Gross Appearance) Glistening Surface Fissures Osteophytes	0 1 2 3	Normal Mild Moderate Severe
	(Histological Appearance – Cartilage structure) Surface irregularities; Vertical clefts into transitional zone; Vertical clefts into radial zone; Transverse clefts Traverse clefts with tissue loss	0 1 2	Normal Mild Advanced
	(Cellularity) Cloning Hypocellularity	0 1 2 3	Normal Mild Moderate Advanced
	Safranin O staining Characteristics	0 1 2 3	Normal Slight decrese Moderate decrease Severe decrease or absence

Table 1.2: Classical grading systems for osteoarthritic and degenerated cartilage. **(cont'd)…** Osteoarthritis Research Society International.

Grading System	Grading Scheme	
	Grade	Description
Osteoarthritis Research Society International (OARSI) (Pritzker, Gay et al, 2006)	0	Matrix: normal architecture Cells: intact, appropriate orientation Key feature: Surface intact, cartilage morphology intact
	1	Matrix: superficial zone intact, oedema and/or superficial fibrillation (abrasion), focal superficial matrix condensation Cells: death, proliferation (clusters), hypertrophy, superficial zone Reaction must be more than superficial fibrillation only Key feature: Surface intact
	2	As above + Matrix discontinuity at superficial zone (deep fibrillation) ± Cationic stain matrix depletion (Safranin O or Toluidine Blue) upper 1/3 of cartilage ±Focal perichondronal increased stain (mid zone) ±Disorientation of chondron columns Cells: death, proliferation (clusters), hypertrophy Key feature: Surface discontinuity
Osteoarthritis Research Society International (OARSI) (Pritzker, Gay et al, 2006)	3	As above. Matrix vertical fissures into mid zone, branched fissures ±Cationic stain depletion (Safranin O orToluidine Blue) into lower 2/3 of cartilage (deep zone) ±New collagen formation (polarized light microscopy, Picro Sirius Red stain) Cells: death, regeneration (clusters), hypertrophy, cartilage domains adjacent to fissures Key feature: vertical fissures (clefts)
	4	Cartilage matrix loss: delamination of superficial layer, mid layer cyst formation Excavation: matrix loss superficial layer and mid zone Key feature: erosion
	5	Surface: sclerotic bone or reparative tissue including fibrocartilage within denuded surface. Microfracture with repair limited to bone surface Key feature: denudation
	6	Bone remodeling (more than osteophyte formation only). Includes: microfracture with fibrocartilaginous and osseous repair extending above the previous surface Key feature: deformation

1.8 Mechanisms of Human Knee Cartilage Degeneration

Degeneration of the human knee is a complex process that could lead to substantial changes in the histology of cartilage matrix, chondrocytes, and subchondral bone plate features. Mechanisms of cartilage degeneration have been proposed to differ between aging and diseases, namely osteoarthritis. Cartilage degeneration can be initiated from the articular surface, involving mechanisms of chondrocyte death [60] or senescence independently or combined with disruption of matrix molecule metabolism and swelling near the cartilage surface (Mankin 1974; Buckwalter and Mankin 1997; Buckwalter and Mankin 1998; Martin, Brown et al. 2004). Early changes also occur at the cartilage and subchondral bone interface, described by increased subchondral bone remodeling activity [70-72] and vascular penetration of into the zone of calcified cartilage [73]. While the mechanisms of age-associated cartilage deterioration remain to be fully established, they likely involve both biomechanical and biochemical factors (Buckwalter and Mankin 1997; Loeser 2006).

1.9 Acknowledgements

The dissertation author was the primary author and thanks to co-authors Alexander Y. Hui, Neil Chang, Michele M. Temple-Wong, and Robert L. Sah. This work was supported by grants from the National Institutes of Health.

CHAPTER 2:

HUMAN MEDIAL FEMORAL CONDYLE CARTILAGE HISTOPATHOLOGY: STANDARDIZED GRADING WITH QUANTITATIVE FEATURE DEFINITIONS

2.1 Abstract

INTRODUCTION. Histopathological grading is a primary research tool used to investigate cartilage degeneration and several systems have been proposed for this purpose. However, quantitative definitions and comprehensive atlases for cartilage histopathology remain lacking. The aims were to develop a standardized, sensitive, and reliable histopathological grading system with quantitative features definitions supplemented with an image atlas.

METHODS. By studying primary literature, histopathological features were identified, feature definitions were made quantitative, and features scores were assigned to characteristics based on degeneration level. Intra- and inter-observer reliability and reproducibility of the grading system was determined by Cronbach's alpha and 95% level of agreement. A histological image atlas with representative

Safranin-O/Fast Green images per score per feature was formulated at standardized resolutions and field-of-views.

RESULTS. A standardized, reliable (Cronbach's alpha ≥0.7) histopathological grading system was developed with quantitative feature definitions (**Table 2.1**) supplemented with an image atlas (**Figure 2.1**) for grading of matrix and chondrocyte features.

DISCUSSION. The development of quantitative definitions and an image atlas for human MFC histopathological features can facilitate comparisons both within and between studies. This grading system can be used to characterize transitions in degenerative states spatially and temporarily with distinct sub-scores assigned per feature to help distinguish tissues states that are in homeostasis versus those that are deteriorating.

2.2 Introduction

Through the years, histological grading systems of cartilage degeneration have been developed from clinical and experimental observations, improved by correlating to biochemical contents [64], and further validated by comparing between grading systems [65-67]. In 1949, Collins established a system for grading of osteoarthritis severity in knee joint that was mainly based on macroscopic observations [74]. About 20 years later, the Mankin grading system, also termed the Histological-Histochemical Grading System (HHGS), was developed to evaluate more microscopic histological features, grading 4 main categories of cartilage, cells, tidemark, and Safranin-O staining [64]. However, several past studies applying HHGS resulted in high intra- and inter-observer variability and concluded that the grading system was unable to differentiate between mild and moderate degrees of OA [75].

To address these concerns, an array of modified versions of HHGS as well as the Osteoarthritis Research Society International (OARSI) grading system were developed [76]. In 2006, the OARSI grading system was created by a committee using more standardized, qualitative approaches to analyze various cartilage characteristics and with consideration of feature horizontal extent [69]. The respective scores from the original HHGS and OARSI have been found to be highly correlated with each other [65-67]. Nevertheless, most current grading systems are focused on summed or most severe scores, comprised of feature definitions that some are semi-quantitative but mostly qualitative, rather than quantitative, and without a comprehensive atlas for visual guidance and/or any proposed digital image parameters for standardization [68].

The advent of imaging modality and digitization methods in combination with accumulated quantitative data on human cartilage and chondrocyte features can enhance the reliability of histopathological scoring. As two-dimensional histological images remain the "gold standard" for clinical diagnosis and researching disease, advances in imaging and digitization modalities has enabled acquisition of large (centimeter-scale) field-of-view (FOV) histology at high (submicron-scale) resolution that could assist in understanding disease [67]. Some grading systems provide histology image examples that magnify the samples 40–400X using conventional microscopy; but few systems standardize these images in a manner to be easily applied to grading [77]. Quantitative measurements of cartilage and chondrocyte features are also constantly being collected from primary literature studying human cartilage, and some have been referenced by grading systems such as OARSI [69]. Even so, quantitative definitions and standardized image atlases for histopathological features are not readily available, which could be the missing components for histopathological analysis by pathologists and researchers to become more objective and translatable [78]. One method to enhance objectivity in grading is by establishing metrics for histological features and applying computer programs for examination. Attempts to automate scoring of human cartilage degeneration were reasonably successful, using metrics derived from the Mankin grading system. The custom image analysis program yielded lower standard deviation between scores (than human) which scores were also consistent with human observer scoring [79].

Overall, quantitative histopathological feature definitions can be formulated by implementing classical grading systems as guidelines to identify features,

summarizing and extrapolating feature characteristics from the primary literature, followed by transforming the feature descriptions to engineering metrics. Additionally, standardization of histology image parameters (resolution and FOV) are important not only for generating images for an atlas to compare samples to, but also for establishing consistent image datasets to be analyzed by a designed set of quantitative definitions. The establishment of these grading procedures are critical to the analysis of early degeneration in human knee MFC. Therefore, the aims of this study were to (1) determine histological features and their quantitative definitions for a human knee MFC histopathology grading system, (2) apply and refine feature definitions to achieve high intra- and inter-observer reliability of the grading system. Then, (3) create a histopathology image atlas of human MFC as visual aide for the grading system.

2.3 Materials and Methods

2.3.1 Study Design for Aim I

To determine histological features and their quantitative definitions for a human knee MFC histopathology grading system. Histopathological features were identified from classical grading systems, and quantitative definitions derived mainly from primary literature; with scores assigned to feature characteristics according to comprehensive review of both sources.

2.3.2 Literature Review and Analysis

Identification of histopathological features from classical grading systems. Classical grading systems for osteoarthritic and degenerated cartilage were reviewed to identify histological features of cartilage matrix and chondrocytes for the current grading system. The classical grading systems reviewed included Collins, Mankin/HHGS, modified Mankin by Shapiro, and OARSI [64, 69, 74, 76] (**Table 1.2**).

Deriving quantitative definitions for histopathological features based on primary literature. For features without quantitative definitions based on classical grading systems, a primary literature search was conducted to obtain empirical data on feature characteristics. Articles were selected from papers referenced by past grading systems or using search terms that include the specific feature name, “cartilage”, “degeneration”, “histology”, “histopathology” on search engines such as Google Scholar and Pubmed.org. From a total of ~100 articles, with ~50 on matrix and ~50 on chondrocytes, measurements of feature characteristics were collected and depending on the specific conditions of cartilage tissue analyzed (ie. normal, mildly degenerated,

severely degenerated), were utilized to establish either the normal and/or the boundary values for feature definitions.

Determining severity of feature characteristic (to assign histopathology score). The level of degeneration represented by a feature characteristic was determined based on the different scores given to the characteristics by classical grading systems (such as grades 0, 1, 2, and 3 for cell characteristics of *normal*, *diffused hypercellularity*, *cloning* and *hypocellularity* in Mankin grading system). Additional literature was referenced if the feature characteristics were not adequately associated with a cartilage degeneration level in past grading systems. For instance, characteristics of cell shape has not been included in grading systems although cartilage degeneration can cause the disappearance of flat cells at the superficial zone [80].

2.3.3 Study Design for Aim II and III.

Aim II: to apply the grading system to donor MFCs spanning all four macroscopic grades and to refine the quantitative feature definitions to achieve high intra- and inter-observer reliability of the grading system.

Portions from whole MFC strips were selected to represent all 4 macroscopic grades of normal, roughened, partially eroded, and fully eroded cartilage samples for grading, to test and refine the grading system under a feedback loop of (1) deriving (or refining) feature definition (Aim I) to (2) grading of selected histology to (3) assessing observer reliability and reproducibility. The feedback loop was set to terminate when adequately high inter-observer reliability was achieved, with all feature scores with Cronbach's Alpha greater than 0.7. After summarizing and processing quantitative results of features from the literature, features that were only described by few or limited measurements without specifying a range, were further assessed quantitatively

using histological images from the human MFC. Specific methods are addressed below.

Aim III: to create a histopathology image atlas of human MFC as visual aide for the grading system. Histopathological features in donor MFCs of a wide range of age and macroscopic grade in the histology of grade 1-2, young and old donor MFCs, and grade 3-4 old donor MFCs (in a total of 180 images from 36 donor MFCs) were screened qualitatively, then analyzed quantitatively using the feature definitions proposed in Aim I (**Table 2.1**), to determine at least 1 representative image per score per feature for the atlas. For certain features that were not precisely defined from past grading systems or literature with evidence, pilot studies (results not shown) were performed to measure the size, percentage, or frequency of the features to be used in formulating novel quantitative definitions. Images with features that were most comparable to the expected mean value were chosen to serve as the representative image of the atlas. Multiple representative images at varying FOVs were also provided if the feature characteristics exhibited a broad range in value.

2.3.4 Histology Processing

A total of 211 human knee MFCs and ~1050 slides (~5 sites per MFC) of osteochondral tissue blocks (between 2009 and 2014) were processed for histology. As described in [67], for each donor knee, sagittal osteochondral slabs (~0.5-1.0 mm wide) were harvested at the central region of the MFC, anteriorly from the medial groove of the MFC to the distal line of the capsular reflection posteriorly (few including a small portion of the medial patellofemoral groove). Immediately following harvest, samples were fixed in Z-Fix (Anatech, Battle Creek, MI) and sequentially decalcified using TBD-2 (Thermo Fisher). Each decalcified osteochondral slab was

further cut in the transverse direction into 5-7 continuous tissue blocks (each ~1.5-2.0 cm in the anterior-posterior direction) and then dehydrated using a series of alcohol, cleared in Pro-Par (Anatech), and infiltrated and embedded using paraffin. Five micron-thick sections were taken in the sagittal/anterior-posterior plane from each block and stained with Safranin-O/Fast Green. Sections were slide-scanned at high resolution (0.25μm/pixel, 40X power) with large field-of-views (FOVs) (75mm X 25mm+) that encompass the entire microscope slide.

2.3.5 Human Donor MFC Selection

Macroscopic gross images and histology of MFCs were examined alongside to confirm the precise locations of histological sampling of MFCs, by cartilage thickness as well as the contour length and shape of cartilage. Low resolution (10μm/pixel, 4X power) histology images across the anterior to posterior extent of the MFCs were assembled first to visualize the overall condyle-scale histology.

For testing and refining quantitative feature definitions (Aim II): to test the reliability and reproducibility of the quantitative grading system, a total of 16 human knee MFCs were selected from 211 donor MFCs (m=4 per macroscopic grade [81]). A minimum of m=4 donor MFCs were included for each dataset that was graded to develop a new iteration of the grading system, with m=1 each representing 1 of the 4 macroscopic grades.

For creating an image atlas (Aim III): to create a comprehensive atlas for human knee MFC, also from the 211 human knee MFCs in the database, a total of m=36 human donor MFCs were selected for feature specific analysis. To establish a baseline of normal cartilage histology examples that is independent of age, m=12 and 12 MFCs with low macroscopic grades of 1-2 were randomly selected from each of

the age groups, young (<40 years old) and old (40+ years old). Then, to encompass the expected variability in histopathological features at different stages of cartilage degeneration, another m=12 old donor MFCs with high macroscopic grades of 3-4 were randomly selected from the database for examination. Since few young donor MFCs exhibit high macroscopic grades of 3-4 in normal aging and was clearly reflected in the rare occurrence of such examples in the 211 donor MFC database, no image examples of this group were utilized in the image atlas. Donors with prior history of knee joint associated injury and disease were also excluded.

2.3.6 Digital Histology Acquisition

Histology images were collected at standardized resolutions of pixel size = 0.25 micrometres^2 and FOVs of 1.2 mm width by full-thickness articular cartilage, comparable to 20X and 10X power images taken using conventional histology. The total number of FOVs digitally acquired depended on the specific aims. For Aim I, a total of n=6-12 consecutive FOVs were taken per MFC which were sufficient to cover a wide variation in features to test their quantitative definitions. Distinctively, for the image atlas (Aim III), discrete images were analyzed quantitatively at the standardized FOV, but presented at 3 different FOVs within the atlas.

Image presentation in atlas (full image atlas not included in this thesis). For presenting images in the atlas, 3 different FOVs were collected of the representative image. Large, 3.0mm by 2.0mm (~4X), medium, 0.6mm by 0.4mm (~10X), and small, 0.3mm by 0.2mm (~20X) FOVs were acquired to provide perspectives of the whole MFC as well as clear views of the specific feature(s). Generally, matrix features were presented at large and medium FOVs, while chondrocyte features were presented at large and small FOVs, with considerations of the individual feature sizes. For features

that were more localized than the given FOV, arrows or dashed boxes were used to indicate the features. Schematics were also provided for some features, to assist with distinguishing the various components of histology and to calibrate visually and quantitatively for easier detection of the features.

2.3.7 Histopathological Grading

Three observers that were familiar with cartilage histopathology but possess different levels of experience were recruited. Each grader was provided with the quantitative definitions for features (**Table 2.1**). To determine inter- and intra-observer reliability and reproducibility, each ROI was graded for all features by 3 observers independently, and repeated following a 2 week period. The observers were blinded regarding donor age, gender and disease state for all specimens as well as to the grades of the other observers.

The grading approach by observers generally entailed steps of object identification (via image segmentation), feature extraction, quantitative measurement/estimation of feature, and classification. Object identification involves determination of major objects in the histology section including cartilage, chondrocytes, and subchondral plate.

Large areas of cartilage (uncalcified cartilage and its superficial and deep layers) were first identified by establishing the regional boundary markers such as the average surface and tidemark lines. Small objects such as cells were located based on color distinctions (to the matrix) and of their expected sizes, while mid sized objects such as fissures were located by examining deflections of the surface contour or edges of void spaces in the matrix.

Characteristics of cartilage erosion, subchondral plate exposure, and Saf-O staining were quantified by measuring cartilage thickness (within 1.2mm width section differences between the average surface and tidemark lines), y-axis value of the cartilage surface and of subchondral plate components, and the areas represented by different predominant colors, respectively. Lengths and orientation (relative to the tidemark) of (1) deflections in the surface contour relative to a smooth surface and (2) the major axes of void spaces in the matrix were measured for fissure characteristics. In terms of cell features, individual cell morphological features were described quantitatively by the absolute and relative lengths of the major and minor axes, whereas chondrons or groups of cells by the direction of its major axes, the total number (in a specific area) and the relative x and y positions of the chondrons or cells (for cell orientation, density, and cloning/clustering, respectively). In addition to assessing the appearance of features, several identified features were graded on their prevalence.

Semi-quantitative grading of features was conducted by comparing the measured values against their quantitative definitions. However, since fine differences distinguish between smooth and rough, non- and fibrillated cartilage surfaces, which were difficult to quantify for each sample, the scores for these features were decided by direct comparisons to an array of representative images in the atlas. The roughness and waviness of the representative images were quantified previously using image processing techniques involving fractal dimension and Fast Fourier Transformation (results not shown).

2.3.8 Statistical Analysis

Intra- and inter-observer reliability and reproducibility of the proposed grading

system were calculated by comparing original and repeated scores by the 3 independent observers. Different methods were utilized to summarize the reliability and reproducibility of the grading system.

Reliability of the system was determined by the Cronbach's alpha that measures the degree of correlation and represents internal consistency of the scores. Cronbach's alpha of ≥0.8 was considered good and ≥0.7 acceptable, while <0.7 was considered as either questionable (≥0.6), poor (<0.6, but ≥0.5), or unacceptable (<0.5) [65, 82, 83].

Reproducibility was assessed using the Bland-Altman limits of agreement (LOA) method [84]. 95% LOA were determined from pairwise comparisons within and among observers and served as intervals within which 95% of differences between the two measurements are expected to be.

2.4 Results

2.4.1 Quantitative histopathological feature definitions and grading scheme was formulated (Aim I).

A total of 16 features for histopathological grading were identified from classical cartilage degeneration grading systems, with 8 each pertaining to cartilage matrix (feature# 1-8) or chondrocytes (feature# 9-16) (**Table 2.1**). In classical cartilage degeneration grading systems examined (Collins, Mankin/HHGS, Shapiro-modified Mankin, OARSI, ICRS, and Outerbridge), all systems discussed and provided grades for most matrix features, but analyzed only limited features of cells (such as density). OARSI was the only system that evaluated more than 1 cell feature. A total of ~100 original articles were identified with extractable quantitative measurements to be incorporated into the definition of histopathological features, with ~50 on matrix- and chondrocyte-associated features each. For grading of each feature, specific regions (such as surface or deep layer) were focused on, with grades of between 1 and 3 or 4 paired with a descriptive term and quantitative definitions for the feature characteristic.

Quantitative feature definitions and associated (degeneration severity) scores. **Table 2.1** summarizes the quantitative definitions for each score of each feature, and the percentage width or frequency of the feature to be examined relative to the width or area of the FOV, or to the total number of cells within a layer. Additionally, the layers for which features are analyzed are specified, which also affects the ranges of the quantitative values for each definition. Scores were assigned to the different types of characteristics for a feature (ie. surface roughness with 3, and cartilage erosion with 4 possible characteristics) arranged so that more degenerative characteristics were

graded with a higher score (ie. surface roughness: grade 1 for a smooth and grade 2 for rough cartilage surface). The association between the characteristics and their assigned scores were supported by concepts from classical grading systems and/or primary literature.

Definitions for *surface roughness* and *fibrillation* both relate to the greatest length of an asperity relative to a representative average line of the surface contour, within a specified sampling width. As features describing the waviness of the cartilage surface, both features are examined across the width of the FOV. *Horizontal and vertical fissures*, on the other hand, are large scaled cracks within cartilage, which orientations are typically along the direction of collagen fibrils. Both extensive fissuring and cartilage erosion could lead to *subchondral plate exposure*, and the absence of stained substance (uncalcified and/or calcified cartilage) resting on calcified cartilage or the subchondral bone. *Cartilage erosion* and *Saf-O staining* are features that evaluate the entirety of cartilage, in terms of thickness and coloration of the stained cartilage area, respectively. The thickness of cartilage is determined by comparing externally to a reference section within the same MFC, while Saf-O staining is assessed by comparing internally between the coloration of different sub-regions.

Chondrocyte feature definitions can generally be distinguished into ones that analyze for individual cells, such as *cell shape* and *size*, and ones that analyze for group cells, such as *cell orientation*, *density*, and *cloning/clustering*. All cell features are examined of the surface layer, which is 0-200µm depth from the representative average line of the surface contour; whereas only group cell features are examined of the deep layer, defined as 200-600µm above the representative average line of the tidemark. This is because superficial zone chondrocytes are commonly described to

exhibit specialized cell morphological characteristics. Different percentage cutoffs (cells expressing characteristic versus total cells) were also decided on, to be lower (10%) for more specialized individual cell features, and to be higher (33%) for features that aim to characterize characteristics of the group of cells.

Table 2.1: Histopathological grading table for human MFC cartilage features. Grading of each feature is focused on a particular layer, with a grade/score between 1 and 3 or 4 that are matched with specific feature characteristics. Characteristics within a feature that correspond to higher grades suggests greater severity in cartilage degeneration. Each score is further described by quantitative definitions and associated frequency of characteristics in the FOV.

#	FEATURE	REGION	GRADE		DEFINITION	FREQ in FOV
1	Macroscopic Grade	FT	normal	1	Surface normal/smooth in appearance	≥ 50%
			roughened	2	Fibrillation to the cartilage surface	≥ 50%
			PtlT erosion	3	Loss of catilage without exposing the underlying bone	≥ 1X in area
			FT erosion	4	Loss of cartilage exposing the underlying bone	≥ 50%
2	Surface Roughness	S	smooth	1	Asperities of **0-5 µm**, within a width of 20 µm	≥ 50% of width
			rough	2	Asperities of **5+ µm**, within a width of 20 µm	
			no AC	3	No articular cartilage	100% of width
3	Fibrillation	S	non-fibrillated	1	Asperities of **0-20 µm**, within a width of 80 µm	≥ 50% of width
			fibrillated	2	Asperities of **20+ µm**, within a width of 80 µm	
			no AC	3	No articular cartilage	100% of width
4	Horizontal Fissures	FT	none	1	Crack(s) with a portion oriented 0–45° to the x-axis that is **0-200µm** in length	100% in area
			horizontal	2	Crack(s) with a portion oriented 0–45° to the x-axis that is **200+µm** in length	≥ 1 / area
			no AC	3	no articular cartilage	100% of width
5	Vertical Fissures	FT	none	1	Crack(s) with a portion oriented 45-90° to the x-axis that is **0-200µm** in length	100% in area
			vertical	2	Crack(s) with a portion oriented 45-90° to the x-axis that is **200+µm** in length	≥ 1 / area
			no AC	3	no articular cartilage	100% of width
6	Cartilage Erosion	FT	none	1	Cartilage surface within **50µm** of the surface for the reference section from the same MFC	100% of width
			SZ	2	Cartilage surface lower by **50-250µm** than that of the reference section from the same MFC	≥ 50% of width
			MZ	3	Cartilage surface lower by **250-450µm** than that of the reference section from the same MFC	≥ 50% of width
			DZ	4	Cartilage surface lower by **450µm** than that of the reference section from the same MFC	≥ 50% of width
7	ScP Exposure	ScP	none	1	No exposure of CC, ScB	100% of width
			CC	2	Exposure of calcified cartilage (CC)	≥ 1 / width
			ScB	3	Exposure of subchondral bone (ScB)	≥ 1 / width

Table 2.1: Histopathological grading table for human MFC cartilage features. (cont'd)…

#	FEATURE	REGION	GRADE		DEFINITION	FREQ in FOV
8	Saf-O Staining	FT	1	normal	Saf-O staining (of red/purple) (**> 90%** area of the total cartilage)	>90% in area
			2	moderate	Saf-O staining (of red/purple) (**50-90%** area of the total cartilage)	50-90% in area
			3	weak	Saf-O staining (of red/purple) (**< 50%** area of the total cartilage)	<50% in area
			4	absent of AC	no articular cartilage	100% of width
9	Cell Shape	S	1	flattened	Cell aspect ratio (minor over major axis length) **≤ 1/3**	≥10% of cells
			2	non-flattened	Cell aspect ratio **> 1/3**	>90% of cells
			3	no AC	no articular cartilage	100% of area
10	Cell Size	S	1	normal	Cell height (in y-axis) **< 10µm**	>90% of cells
			2	hypertrophic	Cell height (in y-axis) **≥ 10µm**	≥10% of cells
			3	no AC	no articular cartilage	100% of area
11,12	Cell Orientation	S,D	1	oriented	Chondrons oriented in expected zonal orientation: Surface parallel and DZ perpendicular to x-axis	≥33% of cells
			2	not oriented	Chondrons not oriented in expected zonal orientation	>67% of cells
			3	no AC	no articular cartilage	100% of area
13,14	Cell Density	S,D	1	normal	(S) **200-500 cells**/mm2; (D) **100-200** cells/mm2	
			2	hypercellular	(S) **> 500 cells**/mm2; (D) **> 200** cells/mm2	
			3	hypocellular	(S) **< 200 cells**/mm2; (D) **< 100** cells/mm2	
			4	no AC	no articular cartilage	100% of area
15,16	Cell Cloning / Clustering	S,D	1	none	(S) **≤ 2 cells**/chondron; (D) **1** independent cell column	≥ 1 / area
			2	cloning	(S) **3-4 cells**/chondron; (D) **2+** associated cell columns or no column and ≤ 8 cells/chondron	≥ 1 / area
			3	clustering	(S) **5+ cells**/chondron; (D) no column and **9+** cells/chondron	≥ 1 / area
			4	no AC	no articular cartilage	100% of area

…

2.4.2 The grading system exhibited high intra- and inter-observer reliability and reproducibility (Aim II).

High intra- and inter-observer reliability and reproducibility were achieved following 3 separate rounds of refinement in the quantitative definitions. The intra- and inter-observer reliability (**Table 2.2**) and reproducibility (**Table 2.3**) of the grading system were high for the grading system following three rounds of refinement in the quantitative feature definitions.

Reliability (**Table 2.2**). Reliability. The Cronbach's alpha for the grades between the three observers (inter-observer) ranged from 0.70–1.00 for all features and overall 0.89 ± 0.08 and 0.89 ± 0.09 for original and repeat scores, respectively (**Table 2.2 B**). In general, the inter-observer Cronbach's alpha was high and above the acceptable range for both matrix- (0.70–1.00; 0.90 ± 0.08 original, 0.92 ± 0.08 repeat) and cell- (0.73–1.00; 0.89 ± 0.07 original, 0.86 ± 0.09 repeat) associated features. The experience of the grader did not appear to have an effect on the reliability of the scores: 0.91 ± 0.06, 0.90 ± 0.08, 0.87 ± 0.09 between the original scores from graders 1 and 2, 2 and 3, 3 and 1, respectively, with graders 1 and 2 being more experienced than grader 3. Surface roughness (0.66 ± 0.06 original, in **Table 2.2 A**, improved to 0.84 ± 0.08 original), and horizontal fissures (0.69 ± 0.13 original, in **Table 2.2 A**, improved to 0.83 ± 0.11 original) were the main features that improved in Cronbach's alpha following refinement in quantitative feature definitions.

Cronbach's alpha for intra-observer was similar to that of inter-observer, ranging from 0.73–1.00 and overall 0.94 ± 0.07. Intra-observer matrix and cell feature Cronbach's alpha were also comparable to or higher than that of inter-observer, calculated to be (0.70–1.00; 0.95 ± 0.07 vs 0.92 ± 0.08 repeat) and (0.73–1.00; 0.92 ± 0.08 vs 0.86 ± 0.09 repeat), respectively. Considering both intra- and inter-observer

results, all 8 matrix and 8 cell-associated features exhibited Cronbach's alpha results that were acceptable (≥0.70 on average) based on internal consistency.

Reproducibility (**Table 2.3**). The 95% LOA for inter-observer differences for the majority of features were within 1 points between observers 1 and 2 (11/16), 1 and 3 (11/16), 2 and 3 (8/16) for repeated scores. While, the 95% LOA for intra-observer differences of features were also mostly within 1 point for observers A (12/16), B (10/16), and C (15/16).

A total of 144 comparisons were made to determine trends in LOA, for the 8 matrix and 8 cell features that were graded by 3 observers repeatedly (**Table 2.3**). Overall, the 95% LOA differences for matrix-associated features for both intra- and inter-observer included fewer points (only 15/72 instances greater than 1 point) than that for cell-associated features (26/72 instances greater than 1 point and 5 instances greater than 2 points). Also, within the cell-associated features, scores that were determined mostly based on individual cells (size, shape, orientation) exhibited few instances of 95% LOA greater than 1 point (3/36; including inter- and intra-observer scores and their repeated scores), while features given based on population of cells (density, cloning/clustering) exhibited 95% LOA mostly greater than 1 point (23/36) and some greater than 2 points (5/36).

Table 2.2: (A) Original and (B) final intra- and inter-observer *reliability* of the histopathological grading system for each feature, analyzed by Cronbach's alpha. Scores for each feature on 30 images were assessed by 3 independent observers. The diagonal cell entries compare the repeated scores of observer A, B, and C while the off-diagonal entries correspond to specific inter-observer comparisons.

Cronbach's alpha	α ≥ 0.9	0.9 > α ≥ 0.8	0.8 > α ≥ 0.7
Internal consistency	Excellent	Good	Acceptable
	0.7 > α ≥ 0.6	0.6 > α ≥ 0.5	0.5 > α
	Questionable	Poor	Unacceptable

Grader	A	B	C
A	Original vs Repeat	A vs B Original	A vs C Original
B	B vs A Repeat	Original vs Repeat	B vs C Original
C	C vs A Repeat	C vs B Repeat	Original vs Repeat

FEATURE	GRADER	A	B	C
Macroscopic Grade	A	0.98	0.94	0.91
	B	0.98	0.96	0.90
	C	0.98	0.97	0.90
Surface Roughness	A	0.94	0.29	0.94
	B	0.72	0.43	0.10
	C	0.68	0.60	0.63
Fibrillation	A	0.91	0.77	0.86
	B	0.80	0.81	0.67
	C	0.85	0.92	0.69
Horizontal Fissures	A	0.90	0.84	0.83
	B	0.83	0.88	0.71
	C	0.66	0.59	0.77
Vertical Fissures	A	0.95	0.97	0.91
	B	0.97	0.95	0.87
	C	0.97	0.97	0.89
Cartilage Erosion	A	0.97	0.96	0.95
	B	0.97	0.97	0.91
	C	0.92	0.93	0.91
ScP Exposure	A	1.00	0.75	0.97
	B	1.00	0.72	0.85
	C	1.00	1.00	0.97
Saf-O Staining	A	0.95	0.78	0.85
	B	0.91	0.91	0.68
	C	0.90	0.84	0.95

CELL FEATURE	Zone	Grader	A	B	C
Shape	S	A	0.99	0.67	0.47
		B	0.94	0.97	0.60
		C	0.88	0.91	0.93
Size	S	A	0.96	0.90	0.78
		B	0.90	0.95	0.76
		C	0.92	0.86	0.92
Orientation	S	A	0.98	0.87	0.56
		B	0.92	0.96	0.43
		C	0.89	0.89	0.89
Orientation	D	A	0.84	0.80	0.56
		B	0.79	0.84	0.66
		C	0.83	0.71	0.92
Density	S	A	0.95	0.91	0.69
		B	0.97	0.93	0.74
		C	0.92	0.93	0.94
Density	D	A	0.86	0.73	0.69
		B	0.77	0.87	0.73
		C	0.72	0.72	0.85
Cloning / Clustering	S	A	0.95	0.59	0.91
		B	0.94	0.97	0.32
		C	0.93	0.92	0.95
Cloning / Clustering	D	A	0.94	0.94	0.91
		B	0.91	0.90	0.91
		C	0.93	0.88	0.87

Table 2.2: (A) Original and (B) final intra- and inter-observer *reliability* of the histopathological grading system for each feature, analyzed by Cronbach's alpha. (cont'd)…

Cronbach's alpha	α ≥ 0.9	0.9 > α ≥ 0.8	0.8 > α ≥ 0.7
Internal consistency	Excellent	Good	Acceptable
	0.7 > α ≥ 0.6	0.6 > α ≥ 0.5	0.5 > α
	Questionable	Poor	Unacceptable

Grader	A	B	C
A	Original vs Repeat	A vs B Original	A vs C Original
B	B vs A Repeat	Original vs Repeat	B vs C Original
C	C vs A Repeat	C vs B Repeat	Original vs Repeat

FEATURE	GRADER	A	B	C
Macroscopic Grade	A	0.98	0.98	0.96
	B	0.97	0.97	0.98
	C	0.98	0.97	0.99
Surface Roughness	A	0.96	0.84	0.92
	B	0.77	0.85	0.77
	C	0.90	0.90	0.98
Fibrillation	A	0.77	0.79	0.70
	B	0.91	0.86	0.84
	C	0.85	0.89	0.98
Horizontal Fissures	A	0.92	0.90	0.89
	B	0.97	0.97	0.70
	C	0.88	0.83	0.97
Vertical Fissures	A	0.88	0.97	0.86
	B	0.97	1.00	0.89
	C	0.97	1.00	1.00
Cartilage Erosion	A	0.91	0.91	0.95
	B	0.97	0.97	0.93
	C	0.97	0.96	0.98
ScP Exposure	A	1.00	1.00	0.92
	B	0.89	1.00	0.92
	C	1.00	0.89	1.00
Saf-O Staining	A	0.93	0.95	0.95
	B	0.91	0.97	0.98
	C	0.91	0.99	0.99

CELL FEATURE	Zone	Grader	A	B	C
Shape	S	A	1.00	0.97	0.97
		B	1.00	0.96	0.93
		C	1.00	1.00	0.98
Size	S	A	0.96	0.97	0.97
		B	1.00	1.00	1.00
		C	0.93	0.93	1.00
Orientation	S	A	0.94	0.94	0.93
		B	0.89	0.98	0.88
		C	0.86	0.73	0.98
Orientation	D	A	1.00	0.92	0.97
		B	0.84	0.85	0.90
		C	0.91	0.73	0.98
Density	S	A	0.91	0.88	0.98
		B	0.77	0.84	0.85
		C	0.77	0.74	0.97
Density	D	A	0.79	0.83	0.81
		B	0.75	0.73	0.78
		C	0.85	0.81	0.86
Cloning / Clustering	S	A	0.96	0.89	0.85
		B	0.94	0.92	0.81
		C	0.94	0.91	0.87
Cloning / Clustering	D	A	0.95	0.86	0.77
		B	0.87	0.77	0.75
		C	0.79	0.73	0.90

Table 2.3: Final intra- and inter-observer *reproducibility* of the histopathological grading system for each feature, analyzed by 95% level of agreement (LOA). The three entries per cell are: lower 95% LOA, average difference, and upper 95% of LOA. Scores for each feature on 30 images were assessed by 3 independent observers. The diagonal cell entries compare the repeated scores of observer A, B, and C while the off-diagonal entries correspond to specific inter-observer comparisons.

95% LOA
1-2 point
2+ point

Grader	A	B	C
A	Original vs Repeat	A vs B Original	A vs C Original
B	B vs A Repeat	Original vs Repeat	B vs C Original
C	C vs A Repeat	C vs B Repeat	Original vs Repeat

Feature \ grader		A	B	C
Macroscopic Grade	A	-0.46 0.07 0.61	-1.06 0.19 1.43	-0.61 0.19 0.98
	B	-0.53 0.11 0.75	-1.06 0.22 1.50	-1.06 0.22 1.50
	C	-0.58 0.15 0.87	-0.53 0.11 0.75	-0.35 0.04 0.42
Surface Roughness	A	-0.35 0.04 0.04	-0.61 0.19 0.98	-0.46 0.07 0.61
	B	-0.58 0.15 0.87	-0.58 0.15 0.87	-0.53 0.11 0.75
	C	-0.46 0.07 0.61	-0.76 0.15 1.06	-0.35 0.04 0.42
Surface Fibrillation	A	-0.30 0.19 0.67	-0.79 0.30 1.38	-0.79 0.26 1.31
	B	-0.53 0.11 0.75	-0.58 0.15 0.87	-0.61 0.19 0.98
	C	-0.74 0.11 0.96	-0.58 0.15 0.87	-0.16 0.04 0.23
Horizontal Fissures	A	-0.21 0.15 0.51	-0.53 0.11 0.75	-0.58 0.15 0.87
	B	-0.35 0.04 0.42	-0.46 0.07 0.61	-0.61 0.19 0.98
	C	-0.58 0.15 0.87	-0.61 0.19 0.98	-0.19 0.07 0.34

Feature \ grader		A	B	C
Vertical Fissures	A	-0.31 0.07 0.46	-0.74 0.11 0.96	-0.74 0.11 0.96
	B	-0.35 0.04 0.42	0.00 0.00 0.00	0.00 0.00 0.00
	C	-0.35 0.04 0.42	0.00 0.00 0.00	0.00 0.00 0.00
Cartilage Erosion	A	-0.12 0.52 1.16	-0.76 0.37 1.50	-0.63 0.30 1.23
	B	-0.63 0.22 1.07	-0.58 0.15 0.87	-0.61 0.37 1.35
	C	-0.63 0.22 1.07	-0.63 0.22 1.07	-0.21 0.15 0.51
ScP Exposure	A	-0.16 0.04 0.23	-0.70 0.07 0.84	-0.35 0.04 0.42
	B	-0.35 0.04 0.42	0.00 0.00 0.00	-0.35 0.04 0.42
	C	0.00 0.00 0.00	-0.35 0.04 0.42	0.00 0.00 0.00
Saf-O Staining	A	-0.12 0.37 0.86	-0.61 0.19 0.98	-0.61 0.19 0.98
	B	-0.54 0.48 1.50	-0.46 0.07 0.61	-0.46 0.07 0.61
	C	-0.50 0.52 1.54	-0.35 0.04 0.42	-0.16 0.04 0.23

Table 2.3: Final intra- and inter-observer *reproducibility* of the histopathological grading system for each feature, analyzed by 95% level of agreement (LOA). (cont'd)…

95% LOA
1-2 point
2+ point

Grader	A	B	C
A	Original vs Repeat	A vs B Original	A vs C Original
B	B vs A Repeat	Original vs Repeat	B vs C Original
C	C vs A Repeat	C vs B Repeat	Original vs Repeat

Feature \ grader		A	B	C
Surface Cell Shape	A	0.00 0.00 0.00	-0.74 0.11 0.96	-0.35 0.04 0.42
	B	0.00 0.00 0.00	-0.35 0.04 0.42	-0.46 0.07 0.61
	C	0.00 0.00 0.00	0.00 0.00 0.00	-0.16 0.04 0.23
Surface Cell Size	A	-0.16 0.04 0.23	-0.35 0.04 0.42	-0.35 0.04 0.42
	B	0.00 0.00 0.00	0.00 0.00 0.00	0.00 0.00 0.00
	C	-0.46 0.07 0.61	-0.46 0.07 0.61	-0.19 0.07 0.34
Surface Cell Orientation	A	-0.19 0.07 0.34	-0.46 0.07 0.61	-0.53 0.11 0.75
	B	-0.53 0.11 0.75	-0.35 0.04 0.42	-0.61 0.19 0.98
	C	-0.58 0.15 0.87	-0.63 0.26 1.15	-0.16 0.04 0.23
Deep Cell Orientation	A	0.00 0.00 0.00	-0.53 0.11 0.75	-0.35 0.04 0.42
	B	-0.61 0.19 0.98	-0.63 0.30 1.23	-0.58 0.15 0.87
	C	-0.46 0.07 0.61	-0.63 0.26 1.15	-0.16 0.04 0.23

Feature \ grader		A	B	C
Surface Cell Density	A	-0.37 0.37 1.11	-1.15 0.30 1.74	-0.35 0.04 0.42
	B	-1.19 0.41 2.00	-1.19 0.41 2.00	-1.13 0.33 1.80
	C	-1.19 0.41 2.00	-1.25 0.44 2.14	-0.31 0.07 0.46
Deep Cell Density	A	0.63 1.37 2.11	-0.93 0.26 1.45	-0.93 0.26 1.45
	B	-0.92 0.30 1.51	-0.78 0.19 1.15	-0.92 0.30 1.51
	C	-0.78 0.19 1.15	-0.79 0.26 1.31	0.24 0.70 1.17
Surface Cell Clone/Cluster	A	-0.21 0.19 0.58	-0.63 0.33 1.29	-0.59 0.41 1.41
	B	-0.58 0.15 0.87	-0.63 0.22 1.07	-0.57 0.44 1.46
	C	-0.58 0.15 0.87	-0.63 0.22 1.07	-0.12 0.37 0.86
Deep Cell Clone/Cluster	A	-0.20 0.22 0.65	-0.59 0.41 1.41	-0.60 0.56 1.71
	B	-0.57 0.44 1.46	-0.78 0.33 1.44	-0.89 0.37 1.63
	C	-0.68 0.48 1.64	-0.79 0.26 1.31	-0.20 0.22 0.65

2.4.3 An image atlas, with at least 1 sample image per score per feature, was created as visual aide for the grading system (Aim III).

Image atlas for histopathology of human knee MFC were created in 2 different formats, with representative images focused on each score/characteristic per feature (not shown here in the thesis) or several scores/characteristics and features annotated per donor MFC histology of different macroscopic grade (**Figure 2.1**).

Since precise grading of surface roughness and fibrillation based on the quantitative definitions had proven to be difficult from pilot analysis, examples of smooth versus rough surfaces and non-fibrillated versus fibrillated are presented in the image atlas for direct comparison to the image of interest (**Figure 2.2**). All 4 different combinations of smooth or rough, and non-fibrillated or fibrillated, are included in images for the two features. Lesions in cartilage are present in some of the images, to help with dissociating lesions from surface examination and direct comparison to images of interest that contain lesions.

Separately, variations of horizontal fissures (Fig. 2.1 J, P) and vertical fissures (Fig 2.1 M, multiple) are presented in the atlas versus images without fissures (Fig 2.1 A, D). In the smaller FOV images (Fig. 2.1 Q and N for horizontal and vertical fissure, respectively) individual examples of fissures were also presented at higher magnifications.

Cartilage erosion and Saf-O staining are recommended to be assessed at large FOVs (and if needed lower resolutions) considering the entirety of the cartilage from the surface to the subchondral bone. Cartilage erosion (Fig 2.1 A, D, G, J, M, P, S, V) is shown by comparing each region of interest to a corresponding reference section, in cartilage thickness measured by aligning their representative average line of the tidemark. Cartilage erosion to the deep zone (Fig 2.1 S) also includes loss of cartilage

to depths of exposing the subchondral plate, further shown in images representing features of subchondral plate exposure. Exposure to the subchondral bone is shown to reach depths of the calcified cartilage (Fig 2.1 S) or subchondral bone (Fig 2.1 V). Safranin-O staining of the cartilage is determined based on the coloration differences within the (remaining) stained cartilage. Normal cartilage is shown with a thin layer of substance unstained by Saf-O due to proteoglycan-poor lamina splenden (Fig 2.1 A), while loss in Saf-O staining can be of varying degrees (Fig 2.1 D, M, J).

Cell morphology of shape and size are examined of each individual cell in the surface layer, either to be flattened (Fig 2.1 B) or non-flattened (Fig 2.1 E, K), and either to be normal sized (Fig 2.1 B, H) or hypertrophic (Fig 2.1 E, N, T). These features are suggested to be analyzed at high resolution (and if needed smaller FOVs) for clear visualization of the features. Additionally, scoring of images to possess flattened and/or hypertrophic cells requires at least 10% of the cells in the surface layer to exhibit such phenotype.

Group cell features of cell orientation, density, and cloning/clustering are evaluated for both surface and deep layers. Cell orientation can be oriented (Fig 2.1 B for surface, I and R for deep) or not oriented (Fig 2.1 K for surface, F for deep); cell density can be normal (Fig 2.1 B and E for surface, C and L for deep), hypercellular (Fig 2.1 K for surface, R for deep) or hypocellular (Fig 2.1 T for surface, U for deep); and for the number of cells per chondron or columns of cells, there can be no cloning nor clustering (Fig 2.1 B for surface, C for deep), cloning (Fig 2.1 K for surface, L for deep), or clustering (Fig 2.1 Q for surface, R for deep). Prior to analyzing for these features, the layer boundaries are to be indicated.

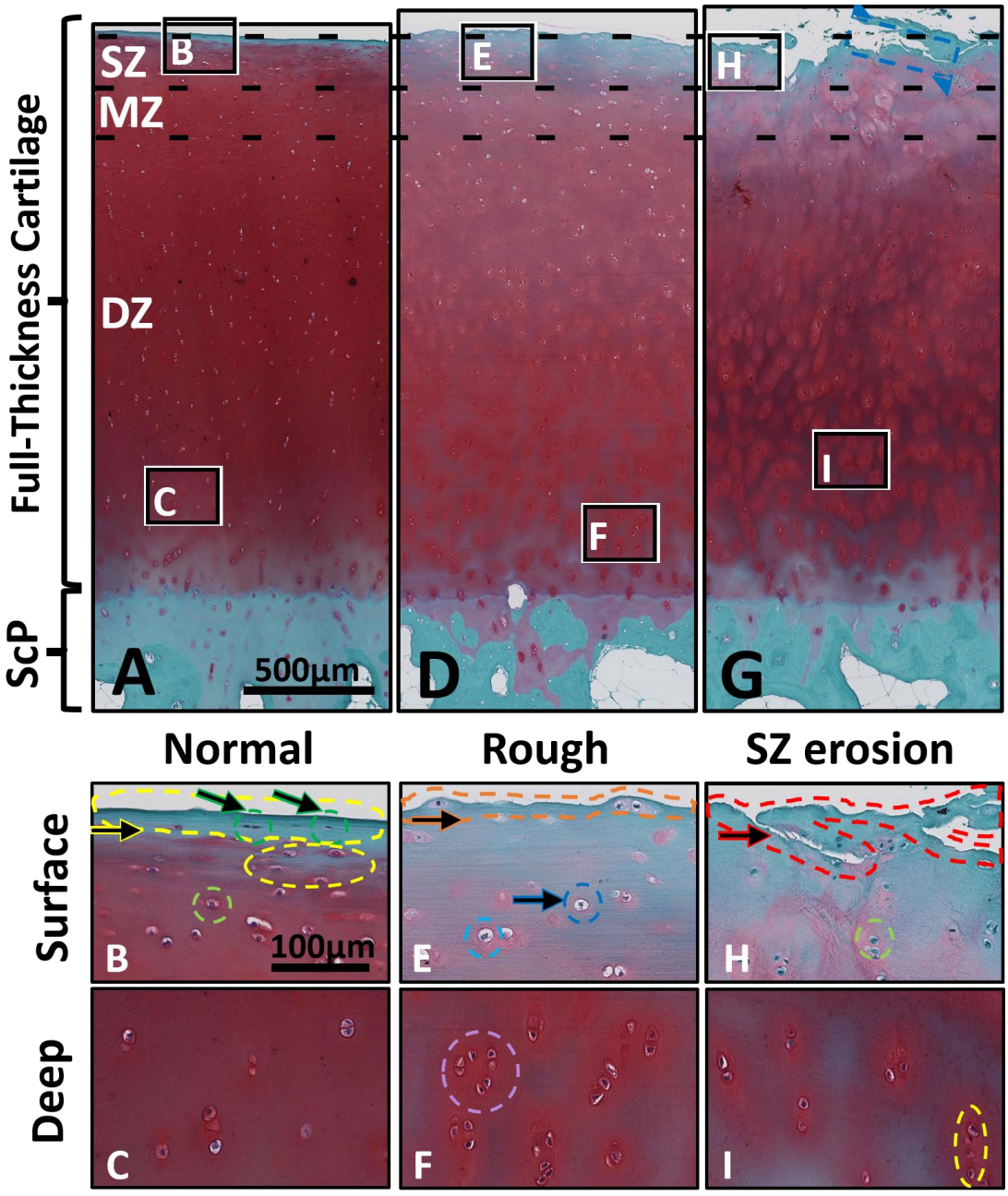

Figure 2.1: Combined atlas with standardized images and corresponding feature annotations, formed by m=7 representative donor MFCs. At least 1 image example per feature per score listed in the table portion is shown in the image portion. Labels consisted of letters and/or colored arrows and/or dotted areas in the table are used to associate specific feature characteristics with their image examples. Normal, roughened, and superficial zone eroded examples. (Table with labels/indices on p.62)

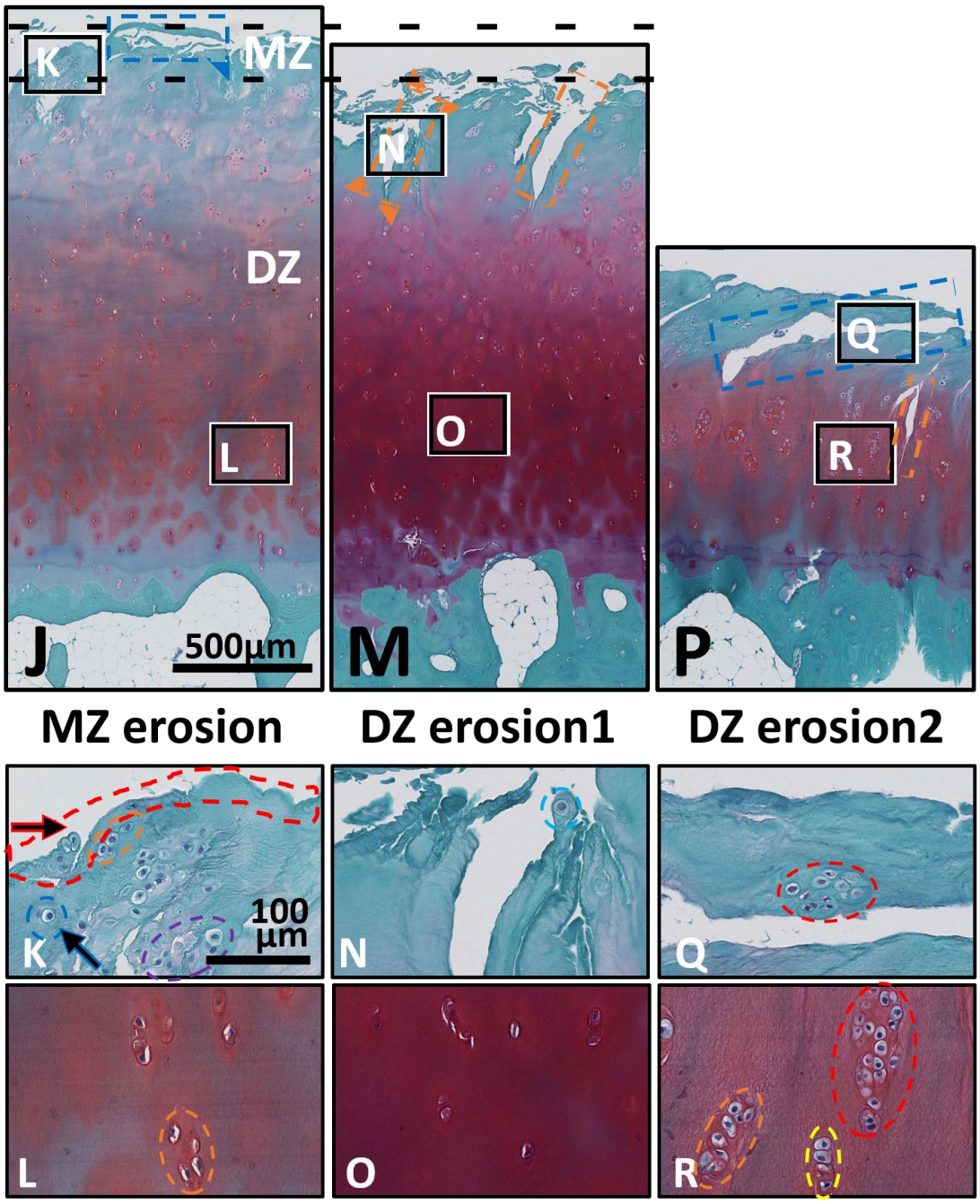

Figure 2.1: Combined atlas with standardized images and corresponding feature annotations, formed by m=7 representative donor MFCs. (cont'd)… Middle and deep zone eroded cartilage examples. (Table with labels/indices on p.62)

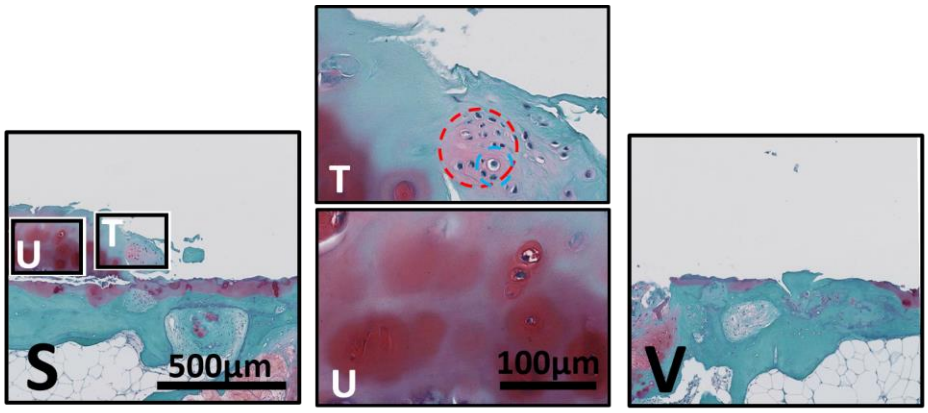

#	FEATURE		ZONE	GRADE					
				1	label	2	label	3/4	label
1		Macro. Grade	FT	normal	A	roughened	D	PtIT/FT eros.	J,P/S,V
2	Matrix	Roughness	S	smooth	B	rough	E		
3		Fibrillation	S	normal	B	fibrillated	H		
4		Hori. Fissures	FT	none	B	horizontal	J,P		
5		Vert. Fissures	FT	none	B	vertical	M		
6		Cart. Erosion	FT	none	A,D	SZ	G	MZ/DZ	I/M,P
7		Saf-O Staining	FT	normal	A	≥ 50% area	D,M	< 50% area	J
8		ScP Exposure	ScP	none	A,G,P	CC	S	ScB	V
9	Chondrocyte	Shape	S	flattened	B	Non-flat	E,K		
10		Size	S	normal	B,H	hypertrophic	E,N,T		
11		Orientation	S	normal	B	not oriented	K		
12		Orientation	D	normal	I,R	not oriented	F		
13		Density	S	normal	B,E	hypercellular	K	hypocellular	T
14		Density	D	normal	C,L	hypercellular	R	hypocellular	U
15		Clone/Cluster	S	none	B,E	cloning	K	clustering	Q,T
16		Clone/Cluster	D	none	C,F,I	cloning	L,R	clustering	R

Figure 2.1: Combined atlas with standardized images and corresponding feature annotations, formed by m=7 representative donor MFCs. (cont'd)… Deep zone and full-thickness eroded cartilage examples.

Figure 2.2: Portion of image atlas with focus on surface roughness and fibrillation features. Feature definitions (left) and multiple examples displaying a range of surface roughness and fibrillation (right), focused at the cartilage surface relative to the larger FOV shown at the bottom left.

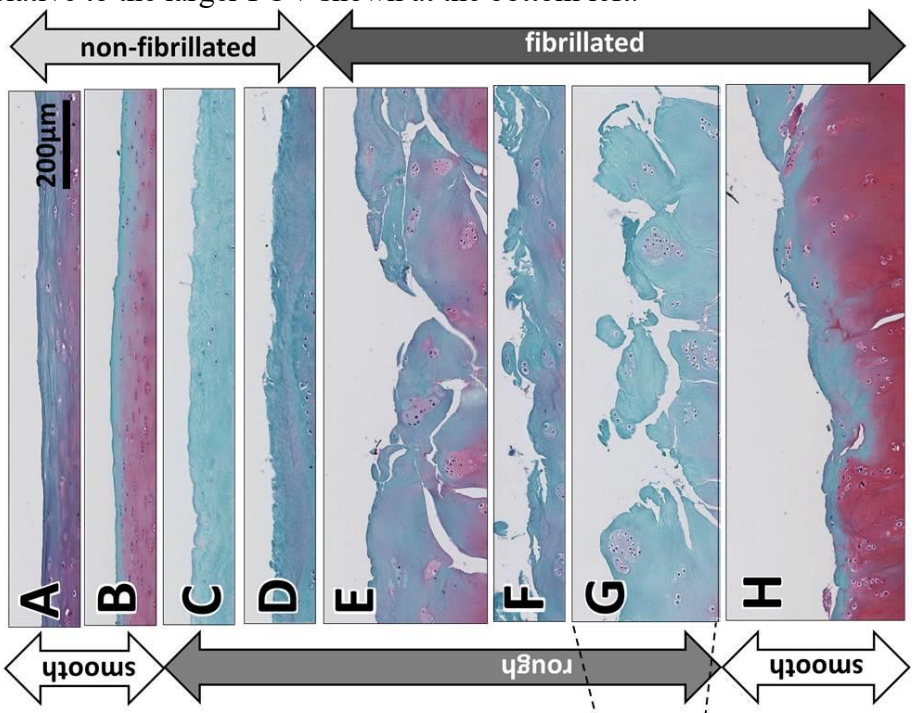

Feat	Grade	Definition
Surface roughness	1 smooth	Asperities of **0-5** μm, (within a width of 20 μm)
	2 rough	Asperities of **5+** μm, (within a width of 20 μm)
Fibrillation	1 non-fibrillated	Asperities of **0-20** μm, (within a width of 80 μm)
	2 fibrillated	Asperities of **20+** μm, (within a width of 80 μm)

2.5 Discussion

A histopathological grading system for human knee MFC was developed based on 16 histological features (8 for matrix and 8 for chondrocyte) compiled from classical grading systems, and quantitative feature definitions analyzed from primary literature. Three separate trials of grading were conducted to achieve high intra- and inter-observer reliability and reproducibility across all features (Cronbach's alpha of 0.7–1.0). An atlas with at least 1 image example per feature per score was created for visual aide, with images acquired from donor MFCs with a wide range in age and macroscopic grade.

Strengths and limitations of the study approach. The systematic approach applied to develop the grading system, including feature identification, derivation of quantitative definitions, and collection of supporting visual examples, allows for consistent grading that can be independent of user experience. Features were identified from summarizing past grading systems, though, a novel categorization was implemented that relied less on associations between matrix and cell features (as in OARSI grading). Since by assigning features into the same category implies the progressive nature from one feature to another during cartilage degeneration, for our system, features were only grouped within the same category if they differed in terms of measured characteristic (size, distribution, and frequency). The ranges of feature characteristic values were adjusted to be mutually exclusive from each other. Unfortunately, few comparisons could be made to validate these definitions as quantitative definitions were rarely provided in other grading systems. Also, to ensure

that user experience did not affect grading results substantially, users of varying experience in grading human cartilage histology were also recruited.

Although attempts were made to balance the total number of each score per feature graded, by balancing the MFCs graded to be 3 donor MFCs per macroscopic grade range (grade 1, grade 1/2-3 and grade 3-4), the frequency of the resultant scores per feature were not always balanced. The imbalance in score frequency can potentially affect the measured reliability of the feature. At the same time, the low occurrences for a certain feature score can indicate the natural rarity of such a feature presentation in vivo. Also, identical to all classical grading systems, scoring of cell density was complicated by the non-linear changes in quantitative definitions for increasing grades from grade 1(normal), to 2 (hypercellular), to 3 (hypocellular). It was important to maintain these levels, however, since they describe the typical pathophysical process of cartilage degeneration, in which cells proliferate for cartilage repair followed by cell loss due to death or cartilage loss. Normal cellularity can also be graded if regional cell proliferation compensates for overall cell loss. Nonetheless, final scores for cell density were examined per donor (rather than as an average) to ensure no trends of higher or lower cellularity were overlooked. (not including subchondral plate features) Furthermore, other than grading for subchondral bone plate exposure, features of the subchondral bone plate relating to vascular channel and tidemark were not assessed in this study. Although important features, the low frequency of these features in the 1.2mm width FOV in combination with feature shapes that differ substantially based on cross-section direction and potential variability in staining, pilot analysis resulted in low inter-observer reliability

(Cronbach's alpha of < 0.5). Consequently, the current grading system was not developed to analyze subchondral bone plate features.

Furthermore, other than grading for subchondral bone plate exposure, features of the subchondral bone plate relating to vascular channel and tidemark were not assessed in this study. Although important features, the low frequency of these features in the 1.2mm width FOV in combination with feature shapes that differ substantially based on cross-section direction and potential variability in staining, pilot analysis resulted in low inter-observer reliability (Cronbach's alpha of 0.10-1.00,). Consequently, the current grading system was not developed to analyze subchondral bone plate features.

Strengths of proposed grading system. The proposed feature-specific grading system addresses some potential limitations of the currently available grading systems by not only defining each histopathological feature quantitatively, but also standardizing the FOV and resolution for grading. Since more features are graded than past grading systems and some features require manual counting, performing the grading procedures for this grading system may be more time consuming and labor intensive than applying past grading systems. On the other hand, this can greatly reduce the time required to train graders to become considerably experienced, and the time needing to convert findings from one study to compare to another.

Observer experience appeared less important when using the OARSI system [65]. The inter-reader variability was good for both Mankin and OARSI, but OARSI was reported to be more difficult to apply by inexperience readers, and depicted by lower inter-class correlation by the inexperienced readers (Pauli, Whiteside et al.

2012). The greater number of parameters in Mankin (than OARSI) has been noted to be more complicated and requires longer duration of analysis, similar comments can be made of the currently proposed grading system. However, as Mankin, we believe that the additional parameters helped with achieving higher intra- and inter-observer reliability and reproducibility.

Precise identification of histopathological features can be facilitated by examples provided by the multi-scale image atlas formed with standardized images. Few grading systems provide histology images to serve as visual examples to assist in grading. While major grading systems of OARSI and ICRSII include histological images to support their system, most images either contain numerous features within a single figure without notating for each feature, or are not standardized in FOV (and/or at unknown resolutions), and could therefore be limited in their utilization. The presence of accurate feature examples for direct comparisons with features observed in histology samples is critical to an effective atlas, which minimizes potential confusion that can be caused by comparing images of different FOV and resolution.

Multi-scale imaging for histopathological analysis. Direct and broad analysis of human knee components by histopathological grading can serve as the foundation to three-dimensional (3-D) histological analysis and potentially contribute to diagnostics of non-invasive imaging modalities. Quantification of histopathological features provides valuable information to dictate the range of the resolution and FOVs for other early cartilage degeneration detection methods. The smallest sized features of matrix and cell morphology in the current grading system approximates single micron scale which would require sub-micron scale resolution of the imaging modality for

precise detection. On the other hand, large scaled features such as erosion can approximate 1-5cm and span the MFC, needing the device to image a large FOV. Consequently, the appropriate image modalities (with pre-determined image parameters) for analysis or diagnostics would depend on the specific size and shape of the targeted histopathological feature. Larger degenerative features of cartilage fissures and erosion can be detected by modalities of lower resolution, using traditional non-invasive imaging techniques such as radiography and morphological magnetic resonance imaging (MRI). However, smaller features such as individual cell morphology and cartilage surface roughness are to be assessed by imaging modalities like physiological MRI that possess sub-micron scale resolution.

Conventional two-dimensional histology can be imaged at sub-micron resolution and with reasonably large FOV of centimeter scale for the analysis of cartilage features at multiple scales. Moreover, although imaged at two-dimension (2-D), histology sections can be analyzed in series to extract three-dimensional (3-D) measurements using stereological methods [11]. Histology can detect small scaled features of single cells in cartilage and subchondral bone plate, as well as deflections from a smooth line at the articular surface and within the tidemark. Large scaled features of propagated matrix fissures and widespread erosion in cartilage can be followed along the joint component, and site variation in cell distribution can also be captured with histology. Consequently, multi-scale analysis by histology enables potential association of features of different scales in addition to precise determination of features and their grades. Nonetheless, small-scaled and low frequency features that are sensitive to the location of histological cross-sections such as surface integrity, cell

morphology, and several subchondral plate features can be difficult to analyze using 2-D histology, indicated by the lower inter-observer reliability, and may be more precisely analyzed by high resolution3-D imaging modalities, such as digital volumetric imaging (DVI).

Depending on the feature shape and whether the feature is isotropic (or anisotropic) in the plane parallel to the surface, observations via histological 2-D cross-sections can differ with the based on the direction of the section. For instance, fissures can appear as slits in three-dimensional views, and appear as a crack when sectioned in a perpendicular plane to the direction of the slit but can be missed when the plane is parallel to the slit direction. Several 3-D imaging modalities like laser scanning confocal imaging, optical coherence and projection tomography, and digital volumetric imaging are capable of detecting small scaled, anisotropic features in cartilage (Youn, Choi et al. 2006). On the other hand, these modalities can be limited in the physical range that can be covered.

Conclusion. A grading system for human MFC cartilage that is composed of quantitative definitions, supported by an image atlas, and tested to be reliable and reproducible can help study spatial variation in histopathological features with progression in cartilage degeneration.

In contrast to longitudinal studies in animal knee joints where cartilage degeneration is induced in a specific manner, studying degeneration patterns in human knee cartilage is most feasible by retroactively analyzing a population of human cadaveric knees or cartilage retrievals from joint replacement surgeries. The degenerative states of these human knees are strongly dependent on the previous joint

histories, prompting analyses that are standardized in order to generate findings that are potentially translatable across different imaging modalities.

While analyses performed at multiple scales can enable identification of subtle variations in early stage human articular cartilage deterioration, standardized histopathological grading methods also need to consider scale-associated effects, especially with the advent of digital histology. More recent analysis of cartilage histology has been improved with the development in high resolution 3-D imaging techniques; and its application should be strongly considered when studying the characteristics of specific small-scaled histopathological features that have anisotropic shapes.

By compiling observations on histopathological features to represent distinctive stages/time points of normal aging across a population of human knee MFC, temporal changes in features can be outlined to gain insight into the progression of human cartilage degeneration. More importantly, these findings can provide a sound basis for the generation of novel scientific hypothesis for future experimentation.

2.6 Acknowledgements

Chapter 2, in full, will be submitted to *Journal of Orthopaedic Research*. The dissertation author was the primary author and thanks co-authors Haoran Qiu, Leening P. Liu, Neil Chang, and Robert L. Sah. This work was supported by grants from the National Institutes of Health.

CHAPTER 3:

TOPOGRAPHICAL VARIATION IN THE HISTOPATHOLOGY OF CARTILAGE LESIONS IN HUMAN KNEE FEMORAL CONDYLE

3.1 Abstract

INTRODUCTION. Mechanical articulation is a potential factor contributing to topographical variation in the histopathology of human knee medial femoral condyle (MFC). The aims were to study spatial variation in the histopathology of cartilage lesions in human MFC, by developing a standardized, sensitive, and reliable histopathological grading system.

METHODS. By studying primary literature, histopathological features were identified, feature definitions were made quantitative, and features scores were assigned to characteristics based on degeneration level. Intra- and inter-observer

reliability and reproducibility of the grading system was determined by Cronbach's alpha and level of agreement. A histological image atlas with representative Saf-O/Fast Green images per score per feature was formulated at standardized resolutions and field-of-views. Lesion macroscopic characteristics and histological feature scores at sites of the lesion were examined, compared between sites, and to normal.

RESULTS. Relative to the posterior transition, the anterior transition region exhibited prevalent fissures, loss of Saf-O, and more cell cloning/clustering, features that resemble "cartilage flow" (**Table 3.1**, **Figure 3.1 & 3.2**).

DISCUSSION. The development of quantitative definitions and an image atlas for human MFC histopathological features can facilitate comparisons both within and between studies. This grading system can be used to characterize transitions in degenerative states spatially and temporarily with distinct sub-scores assigned per feature to help distinguish tissues states that are in homeostasis versus those that are deteriorating.

3.2 Introduction

Degeneration of the human knee is a complex process that could lead to substantial changes in the histology of cartilage matrix, chondrocytes, and subchondral bone plate features. Mechanisms of cartilage degeneration has been proposed to differ between aging and diseases, namely osteoarthritis. Cartilage degeneration can be initiated from the articular surface, involving mechanisms of chondrocyte death [60] or senescence independently or combined with disruption of matrix molecule metabolism and swelling near the cartilage surface [85-88]. Early changes also occur at the cartilage and subchondral bone interface, described by increased subchondral bone remodeling activity [70-72] and vascular penetration of into the zone of calcified cartilage [73]. While the mechanisms of age-associated cartilage deterioration remain to be fully established, they likely involve both biomechanical and biochemical factors (Buckwalter and Mankin 1997; Loeser 2006).

Articulation in the knee joint during daily locomotion involves thousand cycles of a complex combination of compression, rolling, shearing, and sliding [22, 89, 90]. Local regions of articular cartilage on each knee joint surface, such as the femoral condyle, are subjected to specific spatial and temporal loading patterns. Using real-time imaging and skin or bone marker techniques, joint kinematic studies monitored the loading patterns along different phases of the human gait, calculated from relative positions between joint compartments as a function of time [22, 91]. Movements recorded of the femoral condyle relative to the tibial plateau indicated, as expected, substantial rotation in flexion-extension, but also corresponding millimeter scale

anterior-posterior translation during the stance (loaded) phase (Kozanek, Hosseini et al. 2009). Moreover, coordination between anterior-posterior and proximal-distal translations provides information on when femoral cartilage can be subjected to shear and sliding while being compressively loaded.

At the joint scale, particular loading patterns between the different joint compartments (of medial and lateral femoral condyle against the meniscus/tibial plateau, and patella against the patellofemoral groove) can induce topographical variation in the development of cartilage lesions in the femoral cartilage across the different joint compartments (patella, medial and lateral femoral condyles) [92]. Within the human medial femoral condyle (MFC), which is also the most commonly affected femoral compartment by load bearing, clustering analysis of lesion locations and size suggest possible pathways of small lesions progressing towards the anteromedial direction in becoming larger lesions with degeneration [92, 93]. Effects of in vivo, local mechanical environments on cartilage degeneration have been investigated at the tissue scale in rabbit MFC. In normal rabbit knee MFC, high weight bearing sites possessed thicker cartilage, larger sized chondrocytes, and fewer cell profiles in the superficial zone cartilage compared to low weight bearing sites [94]. With early degeneration in rabbit knees, relative to less weight bearing sites of the MFC, high weight bearing sites possessed greater cartilage thickness but decreased proteoglycan content up to 28% depth from the tissue surface [95]. Further progression in degeneration resulted in site-dependent matrix damage of fibrillation, fissures, and even cartilage erosion that were focalized at the anteromedial aspect of the MFC [96]. The effects of loading on pre-damaged cartilage were further examined

by experimentally inducing full-thickness lesions at weight-bearing areas of rabbit MFC [97]. With *in vivo* loading to the defected MFC, the phenomenon of cartilage flow was observed and described as original cartilage sliding and flowing over the edge and into the center of the defect. Therefore, biomechanical factors play an important role in shaping topographical variation in cartilage degeneration, and the analysis of spatial patterns in human MFC histology can reflect local mechanical environments in vivo. A standardized, sensitive, and reliable grading system for histopathological features was previously developed with quantitative feature definitions supplemented with an image atlas. The possessed characteristics of this grading procedure is crucial to the analysis of topographical variation in cartilage lesions of human knee MFC, which can be difficult to detect using other grading systems. *The hypothesis for this study is that cartilage lesions exhibit spatially oriented histopathology in the anterior-posterior direction of human knee MFCs, implicating mechanobiologically-driven cartilage degeneration*. Therefore, the aim of this study was to investigate if the macroscopic features and histological scores of cartilage lesions vary spatially depending on the location within the cartilage lesion, and relative to normal MFC controls.

3.3 Materials and Methods

3.3.1 Study Design

To determine if histopathological scores for features varied spatially in the proximal-distal direction within the cartilage lesion of human knee MFC. MFCs with lesions (m=6) and normal (m=6) MFCs were graded at multiple distinctive sites of the cartilage lesions and at corresponding control sites on the normal MFCs, to assess the effect of lesion and location on histopathological feature scores. The anterior-posterior position of the 5 lesion sites (anterior end, anterior transition, lesion base, posterior transition, and posterior end) on the MFC were determined based on absolute and relative differences in cartilage thickness. The normal and lesion MFCs were matched first by sex then by age, and on the normal MFC, control sites to the 5 lesion sites were selected by the same angles to the line connecting the anterior and posterior ends of each MFC. Spatial trends in microscopic/histological feature score were assessed by comparing the different sites within the lesion, using spatial trends in the normal sites as control. Macroscopic characteristics specific to the lesion MFC such as lesion width and depth were measured, and more general characteristics of MFCs such as MFC size and cartilage thickness were compared between normal and lesion MFCs.

3.3.2 Histology Processing

A total of 211 human knee MFCs and ~1050 slides (~5 sites per MFC) of osteochondral tissue blocks (between 2009 and 2014) were processed for histology. As described in [67], for each donor knee, sagittal osteochondral slabs (~0.5-1.0 mm

wide) were harvested at the central region of the MFC, anteriorly from the medial groove of the MFC to the distal line of the capsular reflection posteriorly (few including a small portion of the medial patellofemoral groove). Immediately following harvest, samples were fixed in Z-Fix (Anatech, Battle Creek, MI) and sequentially decalcified using TBD-2 (Thermo Fisher). Each decalcified osteochondral slab was further cut in the transverse direction into 5-7 continuous tissue blocks (each ~1.5-2.0 cm in the anterior-posterior direction) and then dehydrated using a series of alcohol, cleared in Pro-Par (Anatech), and infiltrated and embedded using paraffin. Five micron-thick sections were taken in the sagittal/anterior-posterior plane from each block and stained with Safranin-O/Fast Green. Sections were slide-scanned at high resolution (0.25μm/pixel, 40X power) with large field-of-views (FOVs) (75mm X 25mm+) that encompass the entire microscope slide.

3.3.3 Human Donor MFC Selection

Macroscopic gross images and histology of MFCs were examined alongside to confirm the precise locations of histological sampling of MFCs, by cartilage thickness as well as the contour length and shape of cartilage. Low resolution (10μm/pixel, 4X power) histology images across the anterior to posterior extent of the MFCs were assembled first to visualize the overall condyle-scale histology.

For spatial analysis of MFC lesions: to study topographical variation in cartilage lesions (versus normal), a total of m=12 donor knees, m=6 normal, grade 1 MFCs and m=6 MFCs exhibiting partial thickness lesions in the weight-bearing area were identified from the 211 human knee MFC database. Overall sample population

was from donors of age 76 ± 11 years (mean±SD, range 64-91 year, 6M/6F; normal: 77 ± 13 years, range 57-91 years, 3M/3F; lesion: 76 ± 10 years, range 64-87 years, 3M/3F).

3.3.4 Digital Histology Acquisition

Histology images were collected at standardized resolutions of pixel size = 0.25 micrometres^2 and FOVs of 1.2 mm width by full-thickness articular cartilage, comparable to 20X and 10X power images taken using conventional histology.

n=50-80 FOVs were taken from the MFC to include all regions of cartilage lesions.

3.3.5 Histopathological Grading

To analyze the histopathology of cartilage lesions, the histopathology grading system (developed in the Aim 1 of the thesis) with quantitative definitions supplemented by an image atlas was utilized.

3.3.6 Normal and Lesion MFC Site Determination

Macroscale characteristics of condyle length and cartilage thickness were measured using the compiled sagittal osteochondral histology slabs (**Figure 3.1 C**) , while sites of the lesion were also determined based on comparisons of cartilage thicknesses between adjacent 1.2mm width FOVs (**Figure 3.1 E**). The (uncalcified) cartilage thicknesses for each FOV were determined by measuring the height (vertical) differences between the average straight lines representing the surface and the tidemark. Characteristics of the lesion were determined based on the articular cartilage thickness. The (uncalcified) cartilage thicknesses for each FOV were determined by measuring the height (vertical) differences between the average straight lines representing the surface and the tidemark.

The lesion base was determined by the minimum cartilage thickness within the MFC histology slab, and the 2 FOVs (1.2mm width) representing the lesion **base** for histological analysis were centered at this point. The "slope" between adjacent FOVs were defined by the cartilage thickness difference between adjacent sections normalized by 1.2mm width, and used to identify the other sites of the lesion. The **ant**erior and **post**erior **trans**itional regions were identified each as the 2 FOVs central to the greatest cartilage slope, between the lesion base and the anterior and posterior ends of the MFC, respectively. By extending further anteriorly and posteriorly from these two sites, respectively, the anterior and posterior border regions of the lesion were determined as the horizontal extent where 3-5 consecutive slopes were <10% different from the more proximal FOV (=0.12 mm difference between adjacent sections). Two FOVs at the center of these regions were used to represent the **ant**erior

and **post**erior **bord**er. The lesion width at half-max depth were measured by the horizontal distance between the 2 points on the lesion representing 50% height difference between the **base** and **antbord** or **postbord**.

The specific sites of normal MFCs were also determined independently by angle to the anterior and posterior extents. Normal MFCs were dissected into 5 equal portions of 36 degrees each (**Figure 3.2 A, B**) based on the angle to the line connecting the medial groove of the MFC (0 degrees) and the distal line of the capsular reflection (180 degrees). A standardized field-of-view (FOV), high resolution microscopic image (1.2mm wide, with height encompassing full-thickness articular cartilage, 0.5µm/pixel) was collected from the center of each pie portion (**Sites 1, 2, 3, 4, 5** at 18, 54, 90, 126, 162 degrees, respectively).

For the normal MFC to site-match with regions within the cartilage lesion, the angles of the lesion anterior border, posterior border, and lesion base, as well as that of 2 transitional regions between each border and the base were measured in the lesion MFC (**Figure 3.2 C**). By superimposing these angles onto a normal MFC, the final lesion site-matched sites in the normal MFC were annotated as sections **A** (to anterior border), **B** (to anterior transition), **C** (to base), **D** (to posterior transition), and **E** (to posterior border) (**Figure 3.2 D**).

Separately, to assess the orientation of "cartilage flow" (bending cartilage projections) at FOVs of **anttrans**, **base**, and **posttrans**, the articular surface, fissures enveloping regions of cartilage, and tidemark were traced, and analyzed with ImageJ.

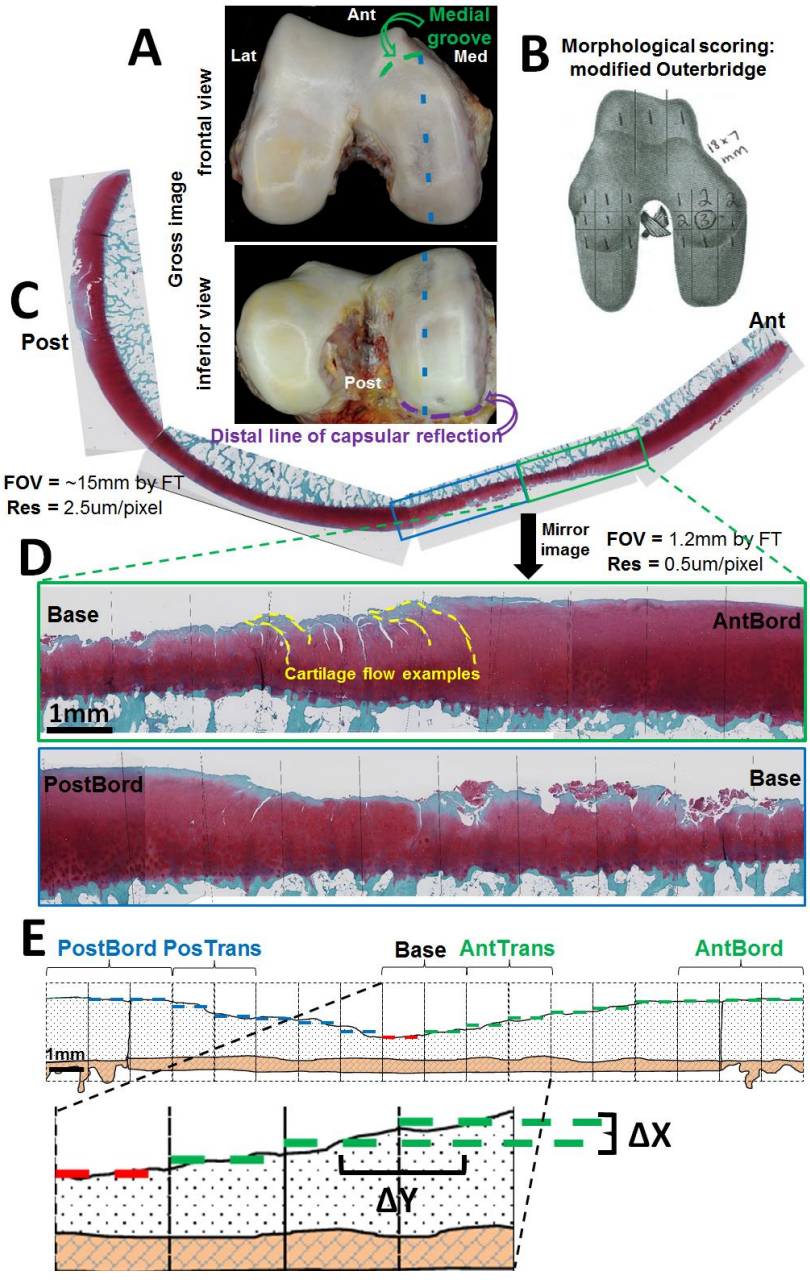

Figure 3.1: Macro- and micro-scale characteristics of MFC lesions and approaches to analysis. (A) Gross image and (C) reconstructed histology image from an osteochondral slab estimated at the blue dotted line in (A). (D) Large magnification of histology to examine specific features such as the "cartilage flow". (E) Schematic presentation of the lesion site showing how "cartilage slopes" were determined (=$\Delta x/\Delta y$).

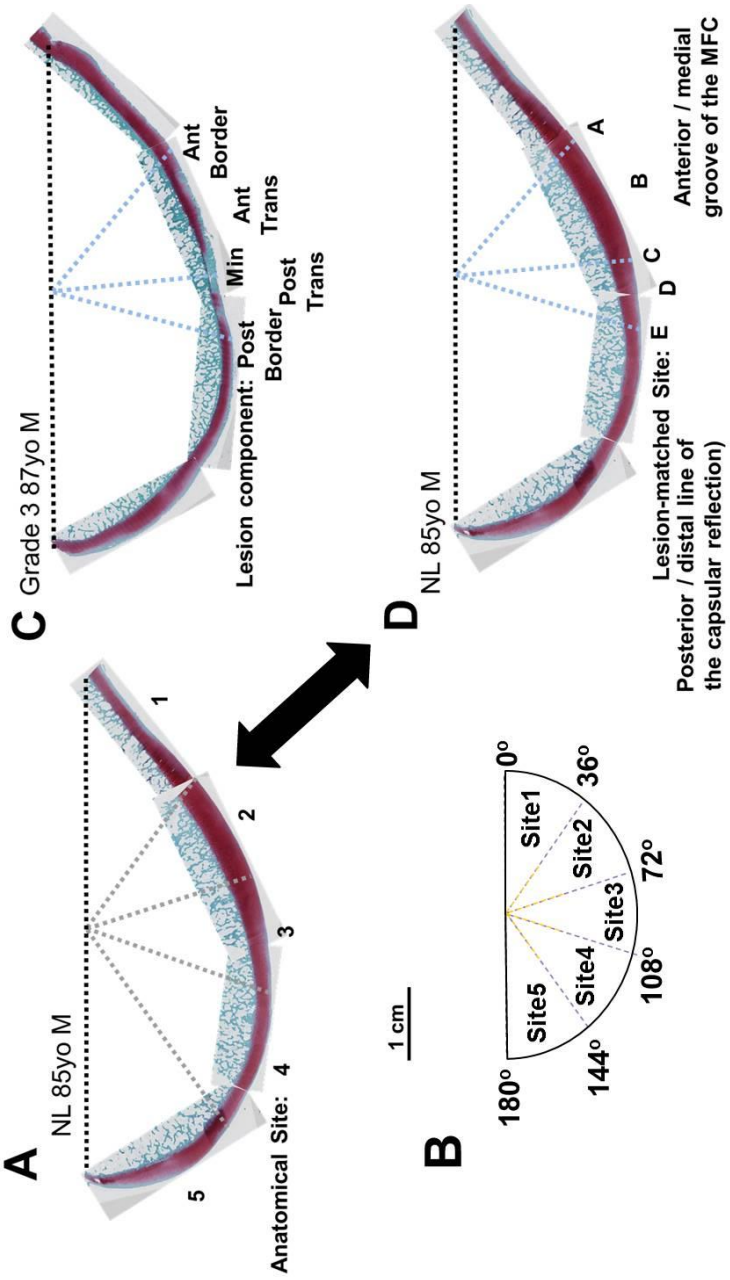

Figure 3.2: Approach to determine sites on a normal MFC, and in the cartilage lesion of a damaged MFC, as well as corresponding sites to the lesion in a normal MFC. (A) is a normal MFC sliced digitally into 5 sites based on angles defined as in (B). The 5 lesion component/sites in (C) were determined base on cartilage thickness differences, where sites in (D) correspond to in normal MFC, based on angle to the anterior-posterior extents.

3.3.7 Statistical Analysis

Histopathological scores were presented as mean ± standard deviation. Lesion characteristics of angles for and widths between lesion components (anttrans, base, and posttrans) were analyzed by 1-way repeated measures ANOVA with post-hoc Bonferroni test and paired t-test, respectively. Percentage data were arcsine transformed to improve normality prior to statistical analysis. The effects of anatomical site (sections 1-5) and lesion site-matched sites (sections A-E) in normal MFC, and regions within lesion (sections antbord, anttrans, base, posttrans, postbord) of lesion MFC, on feature scores were assessed using Friedman test (1-way repeated measures ANOVA for ordinal data), followed by a Wilcoxon test (two treatment repeated measures for ordinal data) for specific group comparisons. The effects of the presence of lesion on feature scores were examined by comparing site-matched regions between lesion and normal MFCs using Fligner-Wolfe.

3.4 Results

3.4.1 *Cartilage lesions exhibited specific macroscopic characteristics in cartilage flow*.

In normal donor MFC, the articular cartilage thickness was 2.05 ± 0.28 mm and the total length of the MFCs was 72.6±9.0 mm. In lesion MFC, the articular cartilage thickness at the *lesion base* was 1.17 ± 0.21 mm, and the total length of the MFCs was 79.4±14.8 mm. Cartilage thickness of lesion base was smaller than that of the anterior and posterior borders of the lesion ($p < 0.005$ and $p < 0.05$, respectively). Relative to the corresponding site B in normal MFC, the depth of the lesion was 43%, with about 60% of the cartilage remaining in height. Lesion width defined by horizontal distance between 50% heights of anterior or posterior borders and lesion base was 16.6±2.7 mm, which corresponds to 20% of the total MFC length. Lesion widths defined by the horizontal distance between anterior and posterior transition sites were 21.0±8.7 mm, which approximates 1/4 of the total MFC. Within this range, the anterior portion (anterior transition to lesion base) and posterior portion (posterior transition to lesion base) were each 11.6±6.2 and 9.4±4.8 mm.

Cartilage flow: there was an effect of location relative to lesion on the directionality of cartilage projections ($p<0.001$). The periphery of cartilage lesions were polarized toward the lesion center. Cartilage orientation in the lesion base were normal (88^o) to the tidemark, and different from the directionality of anterior and posterior borders, which were oriented toward the posterior (131^o, $p<0.01$) and toward the anterior (37^o, $p<0.05$), respectively.

3.4.2 Normal MFCs exhibited anterior-posterior histopathological feature variation

In normal donor knees, several histological features varied by anterior-posterior anatomical site within the MFC. Overall, Saf-O staining, surface cell size and surface cell cloning and clustering were site-dependent ($p<0.05$, $p<0.05$, and $p<0.01$, respectively), and deep cell orientation tended to be site-dependent ($p=0.11$). Relative to posterior sites 4 and 5, anterior sites 1 and 2 exhibited stronger Saf-O staining ($p<0.05$ for all 4 comparisons). Relative to site 4, sites 1 and 2 possessed larger sized surface cells (both $p<0.05$). Compared to site 5, sites 1 and 2 expressed more surface cell cloning and clustering (both $p<0.05$) while site 1 received higher grades than site 4 for this feature ($p<0.05$). Compared to site 5, site 2 deep layer cells were oriented more vertically to the articular surface ($p<0.05$).

3.4.3 Histopathology varied in the transitional regions of cartilage lesions

Lesion components spanned a large angle of the MFC (there was an effect of lesion component on angle): postbord (114±24 degrees) was at a greater angle than both the min (87±23 degrees) and antbord (37±7 degrees) ($p<0.005$ and $p<0.005$), while the Min was also at a greater angle than the ant bord ($p<0.01$).

Histopathological features of fissures, Saf-O staining, surface cell size, and cell cloning and clustering exhibited varying spatial patterns across normal and lesion MFCs (**Table 3.1**). Similar (absolute) anterior-posterior site-variation in feature scores observed in normal MFC, were examined in lesion site-matched regions of normal MFCs (results not shown). In lesion-site matched regions of normal MFCs, Saf-O staining, surface cell size, and surface cell cloning and clustering were site-dependent (each $p<0.05$), and deep cell cloning and clustering tended to be site-

dependent ($p=0.09$). Specifically, relative to site D (matching to PostTrans), site B (matching to AntTrans) possessed stronger Saf-O staining, larger surface cell size, and greater surface cell cloning and clustering (each $p<0.05$). Also, site C (matching to LesBase) exhibited greater deep cell cloning and clustering than site D ($p<0.05$).

Several features varied across the different components/spatial regions of the lesion. Some feature scores varied with site when comparing between the AntTrans, Base, and PostTrans regions. Horizontal and vertical fissures, cartilage erosion, Saf-O staining and deep cell cloning and clustering were site-dependent (each $p<0.05$). Relative to the PostTrans region, AntTrans expressed a higher prevalence of horizontal and vertical fissures, weaker Saf-O staining, more deep layer cell cloning and clustering (each $p<0.05$). Relative to the Base, AntTrans region was also less eroded ($p<0.05$), and Saf-O staining tended to be weaker ($p=0.06$). On the other hand, the Base and PostTrans region mostly expressed comparable feature scores.

Some trends were also delineated when comparing spatial trends in normal MFC and MFCs with lesions. 3 main types of trends were observed in differences of histopathological features, (1) from no difference in normal MFCs to difference in lesion MFCs, (2) from difference in normal MFCs to no difference in lesion MFCs, and (3) from one difference in normal MFCs to another in lesion MFCs. For instance, no differences were observed in the 3 sites (B, C, and D) of normal MFCs for fissures and cartilage erosion, mainly due to the absence of these features. With lesion, horizontal and vertical fissures were differentially present in all three regions, being more prevalent in the AntTrans relative to PostTrans for both horizontal and vertical fissures (both $p<0.05$) and horizontal fissures tended to be more in LesBase versus PostTrans. Similarly, in lesion MFC, cartilage erosion was greater at LesBase relative

to the PostTrans ($p<0.05$), while the PostTrans trended to be more eroded than AntTrans ($p=0.07$).

A few of the histology score differed at baseline (in normal MFC), but were rather comparable in MFCs with lesion. As described, Saf-O staining, surface cell size, surface and deep cell cloning and clustering were features that differed between sites B, C, and D of normal MFCs. However, in lesion MFCs, AntTrans surface cell size was not larger than PostTrans ($p=0.48$; but larger in site B versus site D, $p<0.05$), and AntTrans did not exhibit more surface cloning and clustering than PostTrans ($p=0.82$; but more in site B versus site D, $p<0.05$).

Normal versus lesion MFC differences in deep cell cloning and clustering were site-dependent. In normal MFCs, site D deep cell cloning and clustering was less than site B ($p<0.05$) while not different from site B ($p=0.16$). With lesion, deep cell cloning and clustering scores were higher, particularly when comparing PostTrans and AntTrans to sites D and B, respectively ($p<0.001$). As a consequence, PostTrans were comparable to LesBase ($p=0.10$) while AntTrans was greater than LesBase ($p=0.04$) in deep cell cloning and clustering.

Although rare, differences in feature score could also be trending towards apposite directions in lesion versus normal MFC, exemplified in histopathological feature of Saf-O staining. In normal MFCs, relative to site D, site B exhibited stronger Saf-O staining ($p<0.05$). On the other hand, in lesion MFCs, AntTrans was stained weaker than PostTrans ($p<0.05$) while also tended to be weaker than LesBase ($p=0.59$).

Table 3.1: Effect of site on cartilage lesions on histopathological feature scores in human MFC. Histopathological feature scores are presented for sites AntTrans, LesBase, and PostTrans from lesion MFC and corresponding sites (B, C, D) in normal MFC. Letters (a, b, c, d) designate significantly different groups ($p<0.05$), with a shared letter indicating no difference. (Top) panel indicates the different color codes and characteristic for each feature score, (bottom) panel with color coded scores for each site examined. Data = mean ± standard deviation, calculated from m=6 normal and m=6 lesion MFCs.

#		FEATURE	ZONE	GRADE			
				1	2	3	4
1		Macroscopic Grade	FT	normal	roughened	PtlT erosion	FT erosion
2	Matrix	Surface Integrity	Sur	smooth	rough	no AC	---
3	Matrix	Fibrillation	Sur	non-fibrillated	fibrillated	no AC	---
4	Matrix	Horizontal Fissures	FT	none	horizontal	no AC	---
5	Matrix	Vertical Fissures	FT	none	vertical	no AC	---
6	Matrix	Cartilage Erosion	FT	none	SZ	MZ	DZ
7	Matrix	Saf-O Staining	FT	normal	moderate	weak	no AC
8		ScP Exposure	ScBP	none	CC	ScB	---
9	Chondrocyte	Shape	Sur	Flattened	non-flattened	no AC	---
10	Chondrocyte	Size	Sur	normal	hypertrophic	no AC	---
11	Chondrocyte	Orientation	Sur	oriented	not oriented	no AC	---
12	Chondrocyte	Density	Sur	normal	hypercellular	hypocellular	no AC
13	Chondrocyte	Cloning / Clustering	Sur	none	cloning	clustering	no AC
14	Chondrocyte	Orientation	D	oriented	not oriented	no AC	---
15	Chondrocyte	Density	D	normal	hypercellular	hypocellular	no AC
16	Chondrocyte	Cloning / Clustering	D	none	cloning	clustering	no AC

#		FEATURE	Posterior Transition				Lesion Base				Anterior Transition			
			Normal		Lesion		Normal		Lesion		Normal		Lesion	
1		Macroscopic Grade	1.0 ± 0.0		3.0 ± 0.0		1.0 ± 0.0		3.0 ± 0.0		1.0 ± 0.0		2.8 ± 0.4	
2	Matrix	Surface Integrity	1.3 ± 0.5		1.9 ± 0.2		1.2 ± 0.4		1.9 ± 0.2		1.5 ± 0.5		1.9 ± 0.2	
3	Matrix	Fibrillation	1.2 ± 0.4		1.9 ± 0.2		1.0 ± 0.0		1.8 ± 0.3		1.0 ± 0.0		1.8 ± 0.3	
4	Matrix	Horizontal Fissures	1.0 ± 0.0	a	1.3 ± 0.3	b	1.0 ± 0.0	a	1.6 ± 0.2	c	1.0 ± 0.0	a	2.0 ± 0.0	d
5	Matrix	Vertical Fissures	1.0 ± 0.0	a	1.3 ± 0.4	b	1.0 ± 0.0	a	1.7 ± 0.4	c	1.0 ± 0.0	a	1.8 ± 0.3	c
6	Matrix	Cartilage Erosion	1.0 ± 0.0	a	3.3 ± 0.8	c	1.0 ± 0.0	a	4.0 ± 0.0	d	1.0 ± 0.0	a	2.5 ± 0.5	b
7	Matrix	Saf-O Staining	1.7 ± 0.5	b,c	1.9 ± 0.2	c	1.3 ± 0.5	a,b	1.8 ± 0.6	b,c	1.0 ± 0.0	a	2.8 ± 0.4	d
8		ScP Exposure	1.0 ± 0.0		1.0 ± 0.0		1.0 ± 0.0		1.0 ± 0.0		1.0 ± 0.0		1.0 ± 0.0	
9	Chondrocyte	Shape	1.5 ± 0.5		1.9 ± 0.2		1.2 ± 0.4		2.0 ± 0.0		1.3 ± 0.5		1.8 ± 0.4	
10	Chondrocyte	Size	1.5 ± 0.5	a	2.0 ± 0.0	b	1.7 ± 0.5	a,b	2.0 ± 0.0	b	2.0 ± 0.0	b	1.9 ± 0.2	b
11	Chondrocyte	Orientation	1.3 ± 0.5		1.9 ± 0.2		1.0 ± 0.0		2.0 ± 0.0		1.2 ± 0.4		2.0 ± 0.0	
12	Chondrocyte	Density	1.0 ± 0.0		1.3 ± 0.3		1.2 ± 0.4		1.4 ± 0.4		1.0 ± 0.0		1.3 ± 0.4	
13	Chondrocyte	Cloning / Clustering	1.3 ± 0.8	a	1.8 ± 0.8	b	1.0 ± 0.0	a	1.7 ± 0.8	b	1.3 ± 0.5	b	1.6 ± 0.8	b
14	Chondrocyte	Orientation	2.0 ± 0.9		1.0 ± 0.0		1.5 ± 0.5		1.3 ± 0.4		1.3 ± 0.5		1.2 ± 0.4	
15	Chondrocyte	Density	1.5 ± 0.5		2.6 ± 0.8		1.8 ± 0.8		2.8 ± 0.4		2.3 ± 0.5		2.5 ± 0.8	
16	Chondrocyte	Cloning / Clustering	1.0 ± 0.0	a	2.2 ± 0.5	b	1.7 ± 0.5	a	2.5 ± 0.4	b,c	1.3 ± 0.5	a	2.8 ± 0.3	c

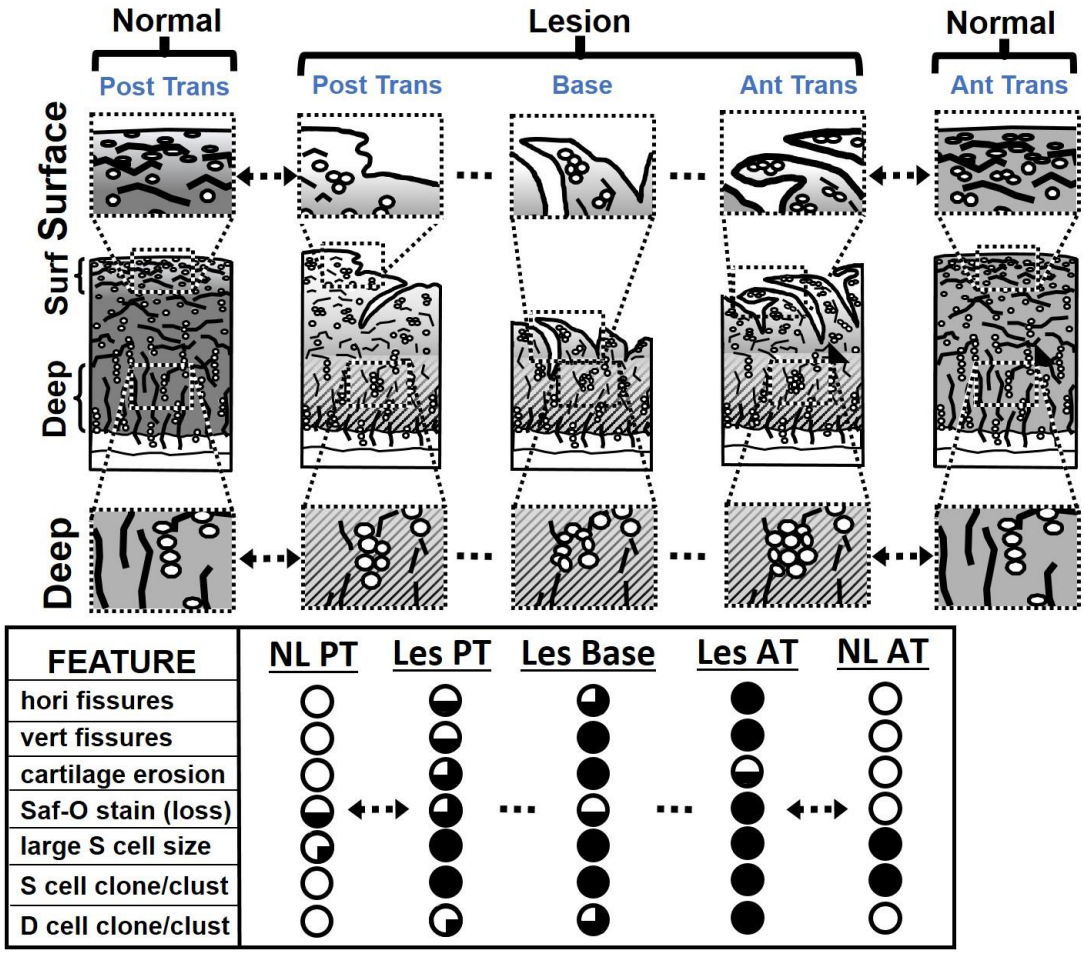

Figure 3.3: Schematic summary of histopathological feature spatial trends in lesions, also compared to corresponding (anterior and posterior transition) sites in normal MFCs. Circles filled with quarter, half, three quarters, and full indicate prevalent, severity, or frequency of respective features.

3.5 Discussion

Cartilage lesions in human knee MFCs exhibited specific anterior-posteriorly oriented histopathological feature trends (**Figure 3.3**) examined by a systematic grading approach consisted of quantitative feature definitions and an image atlas. Relative to their respective control sites in normal MFC, the PostTrans in lesion MFC exhibited greater surface cell size and enhanced surface and deep cell cloning and clustering. Within the lesion, relative to PostTrans, AntTrans displayed more prevalent horizontal and vertical fissures (than PostTrans), weaker Saf-O staining, greater degrees of deep layer cell cloning and clustering, but comparable large sized surface cells, and high levels of surface cell cloning and clustering.

Strengths and limitations of the study approach. Although the final scores were semi-quantitative, the previously developed grading system appeared robust in detecting differences in features across sites of lesion transition. However, the sample size, m=6 normal MFCs and m=6 MFCs with lesion can be further increased, to determine whether features that were trending are significantly different. Also, since the donor selection filtered for MFCs with naturally occurring lesions at the expected high-weight bearing, anterior regions, only a specific type of cartilage lesion was assessed. Lesions that are located at other sites of the MFC, such as the less-weight bearing regions, could potentially result in different spatial variation in histopathology. Though, even if these results differ, they may further support the concept that a different loading micro-environment shapes the cartilage hi to appear differently.

Mechanobiologically-driven histopathological presentation of degeneration in human knee MFC. Histopathological analysis of human MFCs can be applied to understand the mechanism of cartilage degeneration for the purpose of stimulating new scientific hypothesis. Features of cartilage flow were observed only in the anterior and not the posterior transition site of the lesion, implicating different mechanical micro-environments at work. Normal MFC exhibited site variation in feature scores in the anterior-posterior direction, at regions expected to vary in weight bearing amplitudes, high in the anterior and low in the posterior MFC, respectively. Relative to the posterior MFC, the high weight bearing anterior MFC exhibited stronger Saf-O staining, larger surface cell size was larger, and with more surface cell cloning and clustering. In contrast, Saf-O staining was much weaker in the anterior transitional sites of lesion MFC, relative to all other sites analyzed in the lesion. Variation in Saf-O staining within and between normal and lesion MFCs, may point to effects that are mechanobiologically-driven. In the high weight bearing sites of normal MFC that is subjected to moderate mechanical loading, proteoglycan content is high; whereas, with the formation of lesion, overloading at the anterior transition site can diminish glycosaminoglycan (GAG) content.

Formation of fissures, both horizontal and vertical, were also predominantly in the anterior transitional relative to the posterior transition site of the lesion. Development of cartilage lesions in human knees is related to the cleavage of collagen by collagenase and decreased type II collagen levels by degradation (as well as increased GAG release) [98]. Fissures can therefore represent detached, or partially cleaved collagen sheets and fibrils induced by both biochemical and mechanical

factors. Cartilage lesions induced experimentally in animal models exhibited cartilage flow (bending of collagen fibrils into the defect) phenomena following few 3-4 weeks of in vivo recovery [97, 99]. Histopathologically, these incidences of collagen fibril bending are graded as horizontal or vertical fissures, and provide information on the collagen network orientations. Shear stress to the superficial layer and rim of the defect has been proposed as the main biomechanical stimulus leading to cartilage flow, with more prevalent cartilage flow in weight bearing versus non-weight bearing regions [99]; however, spatial variation within a cartilage lesion has not been examined. High prevalence of fissures, and particularly horizontal fissures, at the anterior transition site (compared to the posterior transition site) of lesion could indicate localized shear stress at the anterior region of the lesion.

Surface cell sizes were enlarged in the high weight bearing regions compared to the less weight bearing regions (with normal, smaller sized surface cells) in normal MFC, similar to observations made in the rabbit MFCs [94]. With cartilage degeneration and generation of lesion, the prevalence of large surface cells were comparable between the different sites. Mechanical effects on cell hypertrophy has not been examined extensively; but other factors potentially involved include changes in surrounding environment to be hypotonic [100], to have less physical restriction with matrix breakdown, and/or intracellular accumulation of advanced glycation end product [101]. Some of these factors can be driven by mechanotransduction pathways. Cell proliferation, observed histologically in forms of cell clones and clusters were observed in lesioned MFC cartilage. Cell cloning and clustering can be induced by anabolic and mitogenic growth factors released from neighboring cells or from

enzymatic degradation of surrounding matrix during cartilage repair [87]. Along with more prevalent fissures in the anterior transition region, deep cell cloning and clustering was greater than the posterior transition region, both which are described characteristics of cartilage flow [99]. Cell clusters are often localized around fissures, where diffusion of nutrients and cell mediators are faster with the shorter diffusion distance [102].

Conclusion. The human knee MFC experiences anterior-posterior site-dependent variation in mechanical micro-environments during daily articulation that can lead to varying degrees of cartilage damage spatially. With a standardized, reliable histopathological grading system supplemented with an image atlas, early degeneration in cartilage can be detected *in vitro*, which information can help establish baseline feature measurements useful for the advancement in clinical diagnostic imaging. Moreover, the suggestive effects of articulation *in vivo* on cartilage damage and progression of disease can be further studied by recapitulating such an effect *in vitro*. Advanced understanding of the mechanical environments that can initiate cartilage degeneration is critical to the development of preventive therapies for osteoarthritis.

3.6 Acknowledgements

Chapter 3, in full, will be submitted to *Journal of Orthopaedic Research*. The dissertation author was the primary author and thanks co-authors Haoran Qiu, Leening P. Liu, Neil Chang, and Robert L. Sah. This work was supported by grants from the National Institutes of Health.

CHAPTER 4:

ARTICULATION-INDUCED RESPONSES OF SUPERFICIAL ZONE CHONDROCYTE IN HUMAN KNEE ARTICULAR CARTILAGE: EFFECTS OF COMPRESSION AND SHEAR

4.1 Abstract

Introduction: Daily activities require the human knee joint articular cartilage to undergo complex combinations of shear and sliding. With impact loading and disease, articular cartilage can alter in matrix biomechanics as well as be subjected to a wide range of lateral loading; resulting in excessive tissue deformation that can cause chondrocyte death and expression of catabolic phenotypes, while prompting cellular mechanisms that repair or prevent further damage. The objective of this study is to determine the age-dependent biomechanics of human cartilage and biological responses of the superficial zone (SZ) chondrocytes to articulation of shear and sliding.

Methods: To achieve this, explants from macroscopically normal human cartilage patellofemoral grooves of donors (n=16, ranging from 19 – 66 yr) were subjected to 3 different amplitudes of articulation or left free-swelling. The

biomechanics of cartilage were determined by mechanical data and video microscopy obtained during stimulation. Biological outcomes of cell viability were assessed by live/dead staining and imaging analysis, PRG4 secretion into medium by ELISA, and PARP-p85 and LC3 protein localization and quantification by IHC and manual counting.

Results: Multi-axial articulation biomechanics showed characteristic amplitude-dependent features, but were not modulated by age. With high oscillation, lateral stiffness amplitude was higher, lateral stiffness phase was lower, and Lissajous stiffness plots were shaped resembling a parallelogram rather than an oval, compared to that of low oscillation. Chondrocytes within superficial zone cartilage exhibited cell death, PRG4 secretion, apoptosis (by PARP-p85), and autophagy (by LC3) responses to articulation. High articulation caused SZ chondrocyte death (20-25%) and SZ LC3 expression in both young and old human cartilage, but only higher PRG4 secretion (+4.4 μg/(cm2•day)) in young cartilage. By correlating biological chondrocyte response to cartilage matrix behavior, in young cartilage, positive correlations were found between SZ cell death and either max shear stress ($p<0.005$) or bulk shear strain and sliding ($p<0.005$), and PRG4 secretion only to the latter ($p<0.05$). Moreover, SZ chondrocyte death tended to positively correlate with PARP-p85-positive expression ($p=0.11$), while PRG4 secretion positively correlated with SZ LC3-positive expression ($p<0.01$).

Conclusion: High amplitudes of articulation when lubrication is deficient and/or tissue asperities are present can lead to substantial sliding and energy dissipation as well as the stick-slip phenomenon human knee cartilage. The resultant

high levels of tissue shear stress and strain can induce amplitude-dependent biological responses in cell death, but also ones that are age-dependent such as lubricant secretion and autophagy. This may represent a feedback response by the SZ cells to injury, which may be absent in older human cartilage due to aging-associated decreased responsiveness of chondrocytes and contributed to the increased incident of osteoarthritis with aging.

4.2 Introduction

During daily activities, the articular surface and superficial zone of human knee joint cartilage undergoes a complex combination of compression, shear, and sliding. In vivo imaging studies have found that joint articulation results in 3-10% compression in its overall thickness and relative rotational and translational motions between the femoral condyle and tibia cartilage at least at the millimeter scale [22, 103]. The macroscale motions in the joint which translates to microscale tissue lateral deformation have been assessed in vitro to range from 2.8 to 41.0% depending on the tissue state and lubrication [32]. In general, in vitro analyses have also focused on cartilage biomechanics in response to relative surface movement at a constant velocity after startup; however, joint movement typically involves variability in the relative surface velocity.

Cartilage also exhibits a variety of biological responses to mechanical stimulation (such as shear and articulation) that upregulates matrix and lubricant secretion at low and moderate amplitudes. Proteoglycan 4 (PRG4), a mucinous glycoprotein product that functions to mediate boundary lubrication at the articular surface cartilage, is synthesized mainly by superficial zone (SZ) chondrocytes [18, 104]. Several proteoglycan products are encoded by the PRG4 gene, such as PRG4, lubricin, and superficial zone protein (SZP), which will be collectively referred to in this paper as PRG4 [14, 15, 50]. Low PRG4 concentrations and genetic mutations in the PRG4 gene (disease termed camptodactylyarthropathy-coxa vara-pericarditis syndrome) can lead to substantial wear of cartilage following knee injury and an early

onset of joint failure [42, 46, 47]. PRG4 secretion from the cartilage articular surface can be dependent on the cellularity as well as phenotypical expressions (PRG4-positive or negative) of SZ chondrocytes. While topographical variation in PRG4 secretion has been described in calf knee joints [54, 105], regional differences in cellularity also occurs with aging in human knee femoral condyles, most likely a consequence of cell death [13].

On the other hand, high amplitudes of mechanical stimulation can result in excessive tissue deformation leading to alterations in cell phenotypes associated with repair and degeneration. Even though autophagy, apoptosis, and necrosis are categorized as cell death associated pathways, the specific mechanisms and effects have been found to vary in chondrocytes [106]. In general, cell apoptosis is characterized as an energy-dependent cell death pathway orchestrated by caspases that result in downstream biochemical processes of protein cleavage, protein cross-linking, DNA fragmentation, formation of apoptotic bodies, and phagocytosis [55]. Poly (ADP-ribose) polymerase (PARP) is a nuclear enzyme involved in DNA repair while PARP-p85 antibody possesses specific affinity to the 85-kDa fragment of PARP, allowing for specific detection of apoptosis expression in chondrocytes [58, 107]. Autophagy can induce chondrocyte death with its main function of removing dysfunctional proteins and organelles present in the cell, but such a function enables it a second and apposing role of delaying programmed cell death [57]. Moreover, reduction in autophagy expression due to aging and mechanical injury (single impact of 40% compressive strain in 0.5s) is correlated with an increase in apoptosis, which demonstrates the protective mechanism of autophagy against cell apoptosis [58, 59].

Microtubule-associated protein 1 light chain (LC3) correlates with the autophagosome formation required for autophagy [108]. Necrosis, on the other hand, represents the terminal stage of any form of cell death [106]. The rupturing of chondrocyte membrane is a characteristic process of necrosis, which feature allows nuclear markers to diffuse and fluorescently detect necrotic cells [55].

Mechanical loading is a key factor that regulates SZ chondrocyte health/survival and expression. Mechanical compression (rate of 40 MPa/s, ~50% compressive strain, single impact) caused localized cell death by necrosis at the regions of surface fibrillations or fissures; while torsional shear of (±2 revolutions at 0.3mm/s, for 12 total cycles) induced apoptosis at the SZ in the absence of lubrication [109, 110]. Functionally, static compression (~10% compressive strain) inhibits PRG4 secretion, while dynamic compression at (3-300kPa peak amplitude, ~10-30% compressive strain) (Nugent, Schmidt et al. 2006), continuous passive motion (uncharacterized combination of compression, shear, and sliding) [53], and simple shear (at ±3%) [52] all markedly stimulates PRG4 secretion by bovine cartilage disks following stimulation. However, characterization of tissue behavior and resultant loading (vs applied loading), such as degree of resultant tissue lateral strain and sliding, is complicated with mechanical setups; but are certainly important to relate to the biological outcomes.

Even though various types of surface relative motion shown to stimulate the secretion of PRG4 while some (torsional shear) induce chondrocyte apoptosis expression in calf knee cartilage, little evidence has been provided for similar biological effects of cell survival and lubrication in human knee articular cartilage,

perhaps due to the limited availability of young cadaveric knees and species-associated differences in tissue biomechanics and chondrocyte mechanobiology. Human knee articular cartilage also provides the opportunity to study the effects of aging as an underlying factor for associated alterations in chondrocyte activity and tissue biomechanics.

The hypothesis of this study was that articulation induces age- and amplitude-dependent effects on cartilage superficial zone health and responses, and that the variations in responses are due in part to the extent of tissue biomechanics. Therefore, the objective of the present study was to assess the biomechanics and mechanobiology of human knee articular cartilage when subjected to time-varying articulation in the form of different amplitude oscillations.

4.3 Materials and Methods

4.3.1 Study Design

A total of 384 (24 disks per donor) human articular cartilage disks (2mm diameter, 1.1mm thick) were harvested from the patellofemoral groove of 16 cadaveric knees of donors spanning a wide age range (n=7 **Young**, <35 yrs, 27±5, range 19-34 yrs; n=9 **Old**, >50yrs, 58±5, range 51-66 yrs) without evidence of osteoarthritis; the samples were prepared to include the articular surface, and from regions of tissue with a macroscopically intact articular surface.

N=3 disks per knee were immediately checked for cell viability, to ensure minimal cell death resulting from the harvesting procedures. The remaining n=21 disks were incubated in medium supplemented with 10% FBS and 25 μg/ml ascorbate for 3-5 days. Following pre-culture, disks were randomly distributed to 1 of 3 mechanical treatment groups: left free-swelling (**None**) or else subjected to **Low**, **Mid**, or **High** magnitudes of lateral motion. Another n=3 disks total were checked for cell viability prior to mechanical treatments as a response to serum pre-culture, non-loading treatment (results not shown).

N=6 disks per group underwent mechanical treatment. Immediately after mechanical treatment, some disks (n=2-3 per treatment) were analyzed for chondrocyte viability at the articular surface and some disks (n=1-2 per treatment) fixed with 4% paraformaldehyde in 1X PBS overnight, then stored in 1X PBS at 4°C.
- Other disks (n=2-3 per treatment) returned to free-swelling culture for two additional days and conditioned media collected to assess effects of **Low** and **High** articulation on subsequent PRG4 secretion.

Disks that were analyzed for cell death immediately following None articulation were preserved in proteinase inhibitors at −80°C and later on analyzed mechanically (by video microscopy) to assess the effects of **Low**, **Mid** and **High** articulation on tissue deformation (bulk shear strain) and sliding.

4.3.2 Sample Selection

Cartilage samples were selected from cadaveric knee joints (n=16, 19-66 yrs) that exhibited normal aging and distributed between Young (20–35 yr) and Old (≥51 yr) age groups. Donor knees obtained were approved by Human Subjects Committee, and processed within 72 hours post-modem. Cartilage surfaces across the femoral knee joint were inspected macroscopically and graded based on a modified Outerbridge scoring system [111] and the International Cartilage Repair Society knee map. Joints characterized as osteoarthritic by the presence of osteophytes and subchondral bone exposure were excluded, and only cartilage graded 0-I in the Outerbridge scoring system were used for this study.

4.3.3 Cartilage Explant Harvest

Human articular cartilage disks (2mm diameter, 1.1mm thick) were harvested under sterile techniques to include the articular surface from the patellofemoral groove. All explants were randomly distributed amongst experimental groups.

4.3.4 Tissue Culture

Disks were incubated in basal medium supplemented with 10% FBS (Omega Scientific) and 25 μg/ml ascorbate for 3-5 days at 37 ºC and 5% CO2. Basal medium consisted of Dulbecco's Modified Eagle Medium, 10 mM 4-(2-hydroxyethyl)-1-

piperazineethanesulfonic acid, 0.1 mM MEM non-essential amino acids, 0.4 mM L-proline, 2 mM L-glutamine, 100 units/ml penicillin, 100 μg/ml streptomycin, 0.25 μg/ml amphotericin B, and 25 μg/ml ascorbic acid. Medium conditioned by cartilage discs were collected and then replaced with fresh medium of the same type every 2-3 days. Discs were also transferred to new culture plates of the same type for free-swelling culture following mechanical treatments.

4.3.5 *Mechanical Setup*

Cartilage discs were positioned and calibrated to receive mechanical treatments with a surface-finished polysulfone platen for articulation against the articular surface, and a roughened surface and trough to stabilize the deep cartilage surface. As described previously [33], top polysulfone platen surfaces were roughened with 80 grit sand. During mechanical treatment, a clean counter-surface platen that was adapted to a load cell was mounted to the vertical actuator of the mechanical tester (Mach-1TM V500, Biosyntech Canada, Montreal) and in direct apposition to the articular cartilage surface. To minimize relative motion/slippage between deeper disc and the chamber, discs were affixed to the base of the chamber with components sandwiched by a customized metal ring, including multiple troughs (d= 2.0-2.1mm) created within a 0.01” thick Teflon sheet (McMaster, Santa Fe Springs, CA) (to restrict lateral motion of the deeper cartilage) that is positioned upon a super-small-particle filtering stainless steel porous disc (pore size = 10 μm; McMaster). During articulation, the chamber was mounted to the horizontal actuator of the benchtop mechanical tester.

4.3.6 Mechanical Stimulation

Articulation was implemented at sliding amplitudes of ±100μm, ±500μm, or ±1,000μm using a sinusoidal 1Hz waveform in order to simulate effects of Low, Mid, or High levels, respectively. The articulation was imposed for 400 cycles and superimposed upon 20% static compression using a Mach-1 mechanical tester (Biomomentum).

More specifically, under displacement mode of control of the mechanical tester, discs were compressed initially to 20% of the measured thickness (~0.22 mm = 1.10 mm x 20%) with the roughened surface platen at 0.5 μm/s and allowed to stress relax for 1000s while axial forces were recorded. Preliminary tests indicated that for 2 mm diameter cartilage disks, axial load can reach 95% of its equilibrium value after this period. At compressive equilibrium, 400 cycles of sinusoidal, simple lateral displacement with amplitudes of ±100μm (Low), ±500μm (Mid), or ±1000μm (High) were applied at a frequency of 1 Hz while lateral position and force were recorded. Lateral displacement amplitudes were selected such that sliding would occur as maximum resultant tissue shear strain of the discs was achieved, since physiologically, large amplitudes of lateral displacement occur between joint surfaces during articulation.

4.3.7 Biomechanics

Lateral stiffness properties (magnitude and phase) were calculated and Lissajous curves plotted of cartilage disks. Axial and lateral displacement and load were recorded, fit using Fast Fourier Transforms, and total harmonic distortion (THD) were computed. Lateral stiffness magnitude and phase were computed and Lissajous curves were plotted [52]. The total harmonic distortion (calculated as 100% times the

ratio of a, the square root of the sum of the squares of the powers of all higher harmonic frequencies, to b, the power of the fundamental frequency) of the load waveforms was determined as a measure of the quality of the sinusoidal shear stress imparted to the cartilage [52].

4.3.8 Biomechanical Analysis of Tissue Shear Deformation

Biomechanical properties (bulk shear strain and sliding) of the disk was determined by video microscopy. (a subgroup of, from m=5 young and m=5 old donors,) cartilage discs was then assessed by video analysis. Videos were recorded with a Nikon D90 SLR digital camera, fitted with a macro lens, and frames analyzed for disk and platen position to determine shear deformation during imposed articulation. Bulk shear strain was determined from the average of the differences between the largest apparent horizontal distance (on each lagging end) of the cartilage surface from the zero point (defined by the horizontal distance of the corners of the articulating surface and the deep cartilage surface after compressive stress relaxation) normalized to the apparent vertical distance.

4.3.9 Superficial Zone Cell Viability Analysis

Chondrocyte viability at the cartilage surface (post-harvest, following pre-culture, and post-mechanical treatment) were assessed by Live/Dead assay. Disks were stained with Live/Dead® (Invitrogen) immediately after mechanical treatment, and en face images of the disks were taken at 10x magnification with a fluorescent microscope. The resulting live and dead images were analyzed using a custom image-processing program to determine the number and percentages of live and dead cells.

4.3.10 PRG4 Protein Secretion

PRG4 secreted by cartilage disks 48 hours following mechanical stimulation was assessed. Conditioned medium was quantified by PRG4 ELISA. Conditioned medium was diluted serially, adsorbed to ELISA plates, reacted with polyclonal goat antibody E-19 (Santa Cruz Biotechnology) to human PRG4, and quantified by peroxidase-based detection. PRG4 secretion was expressed normalized to cartilage surface area and number of days of incubation [$\mu g/(cm^2 \bullet day)$].

4.3.11 Immunolocalization and Quantification of PARP-p85 and LC3 Positive Cells

PARP-85 and LC3-II expressions as a response to mechanical treatment for superficial zones were determined by manual counting of cells that were positively versus negatively expressed. Discs were fixed with paraformaldehyde immediately after articulation, and following dehydration in an alcohol series and clearing in Pro-Par (Anatech), the tissue blocks were infiltrated and embedded in paraffin [67]. Sections were cut serially with a microtome (at 4 μm) normal to the articular surface, and then deparaffinized in xylene substitute Pro-Par Clearant and rehydrated in graded ethanol and water [59]. Prior to specific staining, sections were treated with (sodium citrate buffer for antigen unmasking and) hydrogen peroxide (to reduce endogenous peroxidase activity), washed with PBS, and blocked with serum [59]. Sections were reacted with the primary antibodies of polyclonal rabbit antibodies LC3 (1:100) and PARP-p85 (1:200) and secondary antibodies of HRP or biotinylated-conjugated anti-rabbit IgG [58]. Sections probed with non-specific rabbit IgG antibody served as negative controls. Sections were detected via a peroxidase-based system, and digitized at 40X (pixel size of $0.25 \mu m^2$). The resultant digital images were analyzed manually

for positive and negative staining cells as a function of depth from the articular surface. The percentage of positive cells was determined only for the top 200μm, the superficial zone (SZ) of cartilage.

4.3.12 Statistical Analysis

Summary statistics are presented as mean ± SEM, with n = # of cartilage disks per experimental condition per donor knee, and m = # of donors, so that n*m = total cartilage disks per condition. Percentage data were arc sine transformed prior to statistical analyses to improve normality and homoscedasticity. The effects of mechanical treatment on SZ cell death was assessed by 2-way ANOVA (with age group as a between-subject factor and articulation amplitude as a within-subject factor) and post-hoc Student's t-test. For measures fitted to regression models, percent change per decade was determined from slopes of regression lines. Linear regression were performed on several parameters to compare mechanical to biological response as well as between biological responses. The effects of age and mechanical stimulus on cartilage PRG4 secretion were assessed by 2-way ANOVA with donor as a random factor. The effects of mechanical stimulus (amplitude) and/or age were assessed by t-test or repeated measures ANOVA.

4.4 Results

4.4.1 Multi-axial articulation biomechanics showed characteristic amplitude-dependent features (Figure 4.1).

Lateral stiffness amplitude was higher at Low than High oscillation ($p < 0.005$, **Fig. 4.1 A**), while stiffness phase was lower ($p < 0.001$, **Fig. 4.1 B**); neither varied with age. Lissajous stiffness plots for Low oscillation were symmetrical steep ovals, while those for High oscillation were irregular shapes, with steep ascending and descending components just after the reversal of movement, and flattened regions during sustained movement associated with increased THD (Fig. 4.1 C).

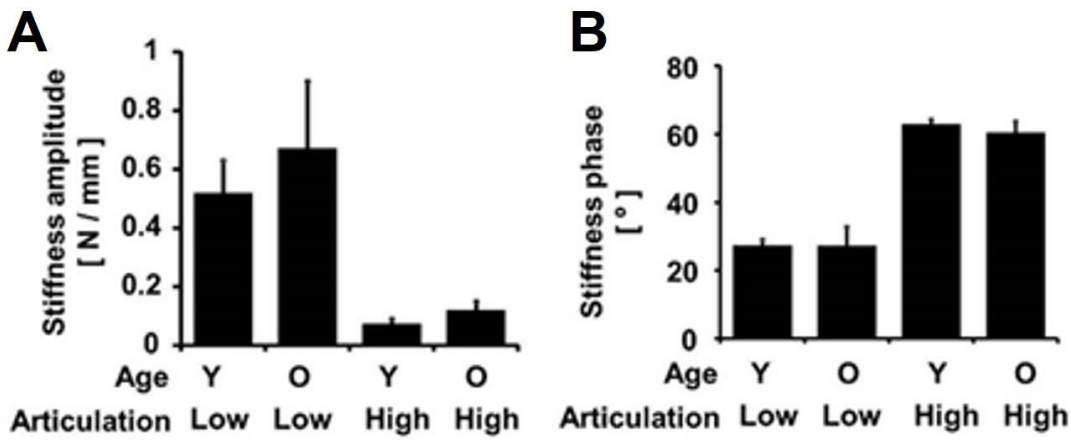

Figure 4.1: The effects of oscillation amplitude and age on articulation biomechanics. Lateral stiffness **(A)** amplitude and **(B)** phase, mean ± SEM, n=5 donors per group, repeated within each age group for low and high articulation. **(C)** Lateral load versus displacement for representative samples, n=1 donor per group, repeated donor for low and high articulation.

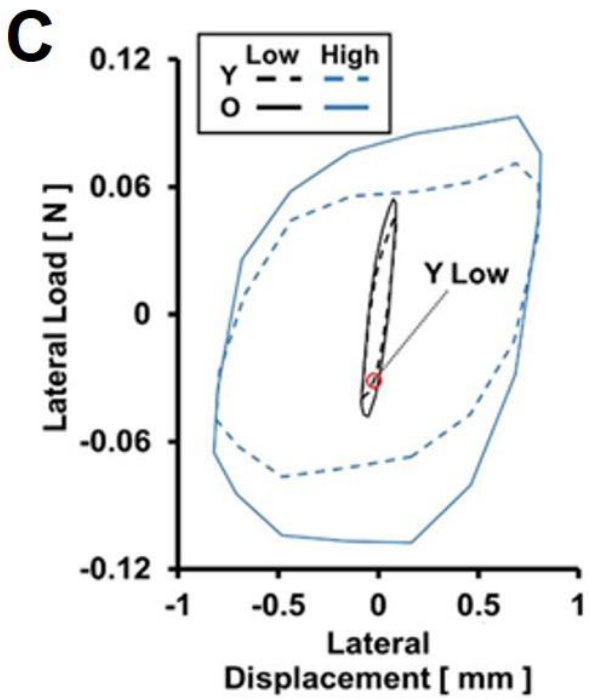

Figure 4.1: The effects of oscillation amplitude and age on articulation biomechanics. (cont'd)… (C) Lateral load versus displacement for representative samples, n=1 donor per group, repeated donor for low and high articulation.

4.4.2 SZ chondrocyte viability was regulated by articulation amplitude

Overall, SZ chondrocyte viability was regulated by articulation amplitude ($p<0.00001$), but not by age ($p=0.09$), or interactively ($p=0.70$) (**Fig. 4.2 B**). Articulation induced cell death in amplitude-dependent manners in both young (**Fig. 4.2 A**, $p<0.0005$) and old ($p<0.00005$) cartilage.

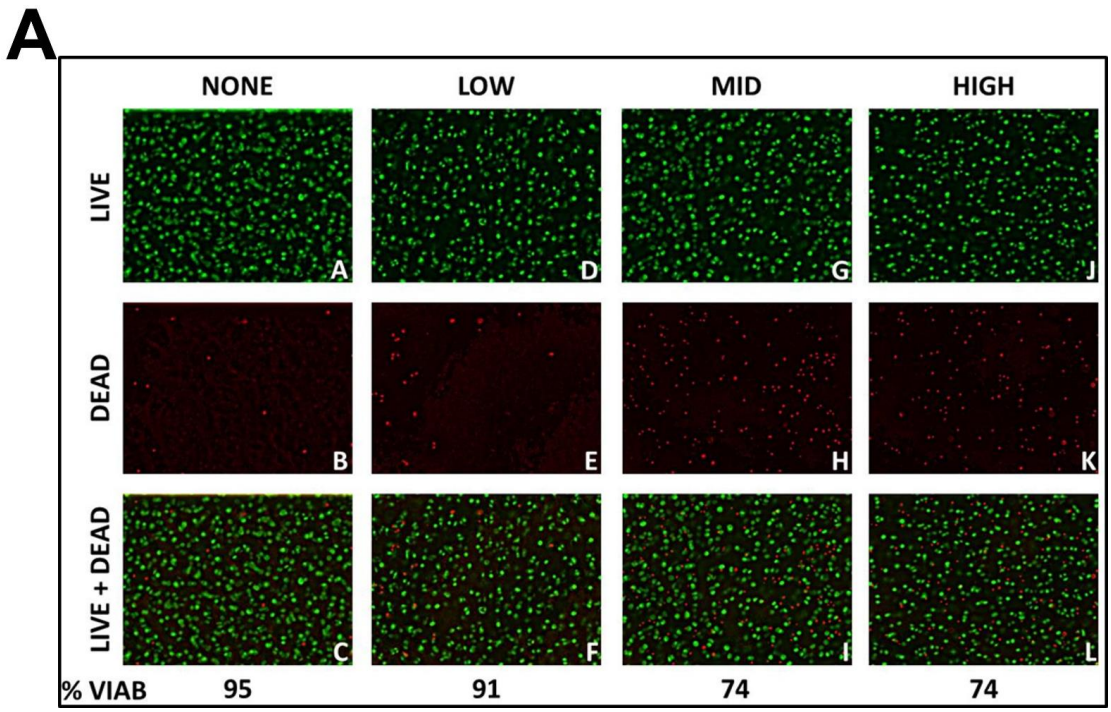

Figure 4.2: Effect of mechanical stimulus on SZ chondrocyte viability. (A) Representative en face image of chondrocyte viability at the articular surface of **Young** donor cartilage discs as a response to mechanical treatments, as analyzed by LIVE/DEAD fluorescent staining. Non-articulated controls (panels A-C), and discs treated at low (D-F), mid (G-I), and high (J-L) magnitudes of articulation. Images of live cells (green fluorescence) (A,D,G,J), dead cells (red fluorescence) (B,E,H,K), and merged live + dead cells (C,F,I,L).

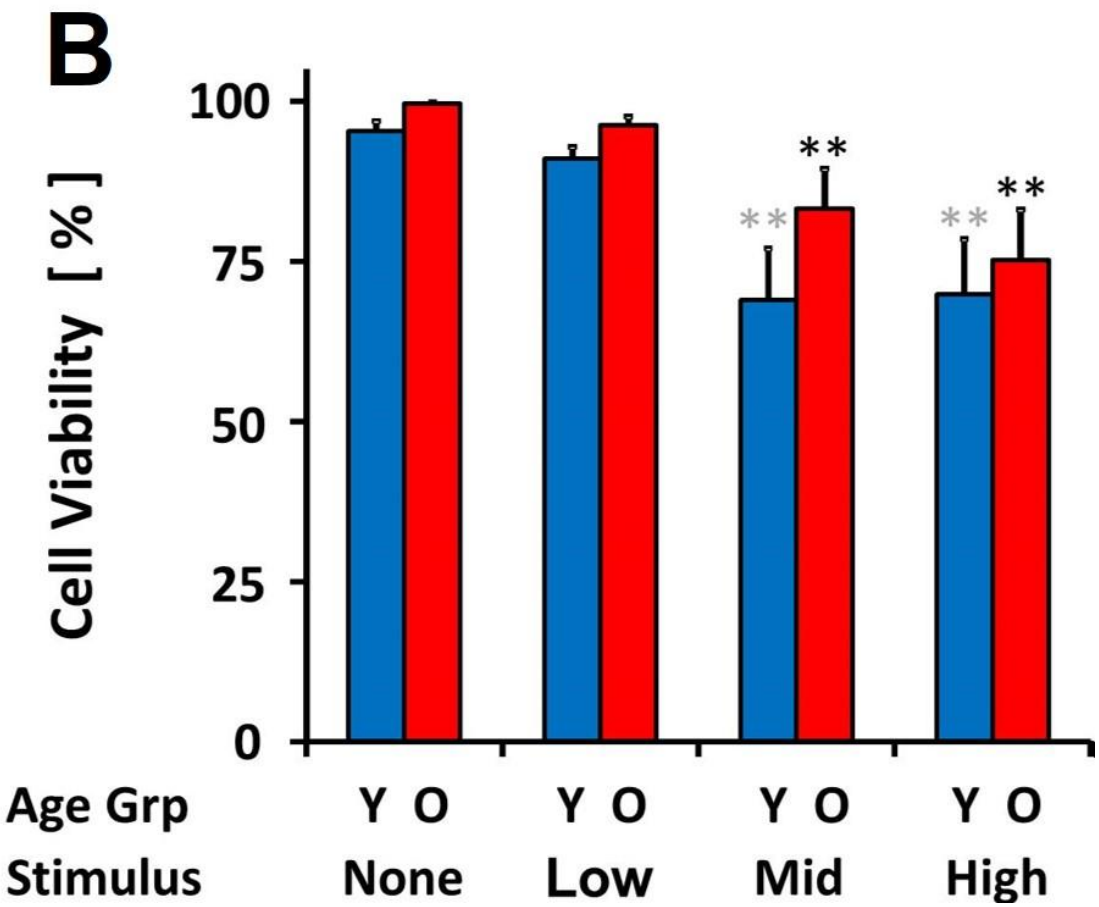

Figure 4.2: Effect of mechanical stimulus on SZ chondrocyte viability. (cont'd)… (B) Percentage viable cell by n=3 disks per group from m=12 donors, from m=6 young (Y) and 6 old (O) donors, in the absence of mechanical stimulus or under low, middle, or high articulation. Data presented as mean ± SEM. **p<0.01, relative to corresponding non-articulated control.

4.4.3 Cartilage PRG4 secretion was modulated by age group ($p < 0.005$) and articulation stimulus ($p < 0.001$) with an interactive effect ($p < 0.05$, Fig. 4.3).

High amplitudes of articulation induced higher PRG4 secretion in human cartilage than none ($p < 0.01$) and low amplitude ($p < 0.05$) articulations. With mechanical stimulation, higher articulation resulted in higher PRG4 secretion (+1.4 and +4.4 µg/(cm2•day), respectively, for low and high ($p < 0.05$) articulation) in **Young** donors. However, high articulation did not have a discernible effect on cartilage from Old donors (–0.1 and +0.9 µg/(cm2•day), for low and high shear, respectively).

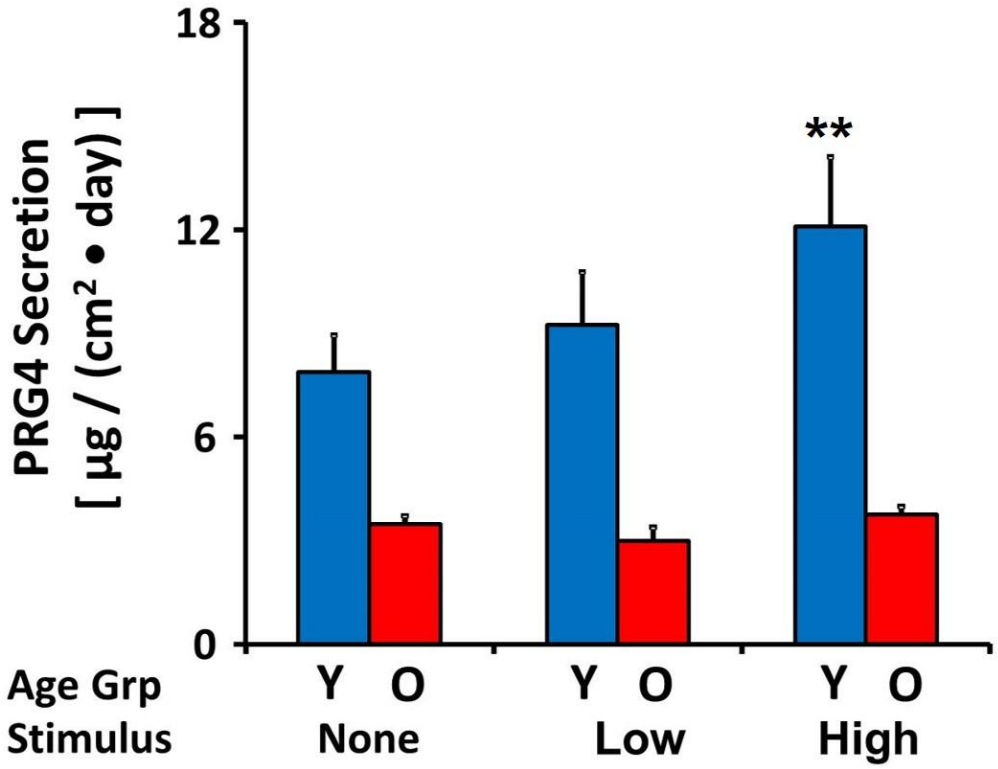

Figure 4.3: Age-dependent effect of mechanical stimulus on cartilage PRG4 secretion. PRG4 secretion by cartilage explants from m=6 young (Y) and 6 old (O) donors, in the absence of applied mechanical stimulation, or stimulated with low or high articulation. Data presented as mean ± SEM.

4.4.4 SZ cell death responses were associated with donor-specific tissue mechanics (Fig. 4.4)

In young cartilage, SZ cell death was positively correlated with both maximum shear stress (**Fig 4.4 A**) and bulk shear strain and sliding (**Fig 4.4 B**) (both $p<0.005$ and $p<0.005$); while in old cartilage, SZ cell death was positively correlated to maximum shear stress ($p<0.05$) but not bulk shear strain and sliding ($p=0.20$).

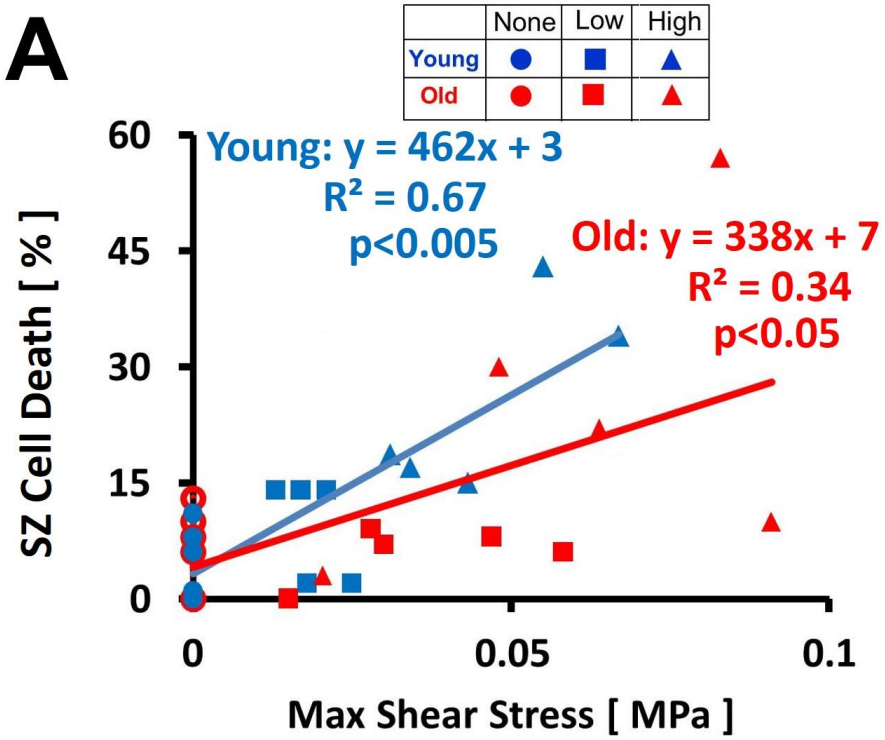

Figure 4.4: Correlation between (A) max shear stress and SZ cell death and (B) bulk shear strain and sliding and SZ cell death. (A) Percentage of SZ cell death from disks of m=10 donors, m=5 young (blue) and 5 old (red), as a function of max shear stress, when stimulated under low (square) and high (triangle) articulation, and left free-swelling (circle). p values are determined relative to slope 0.

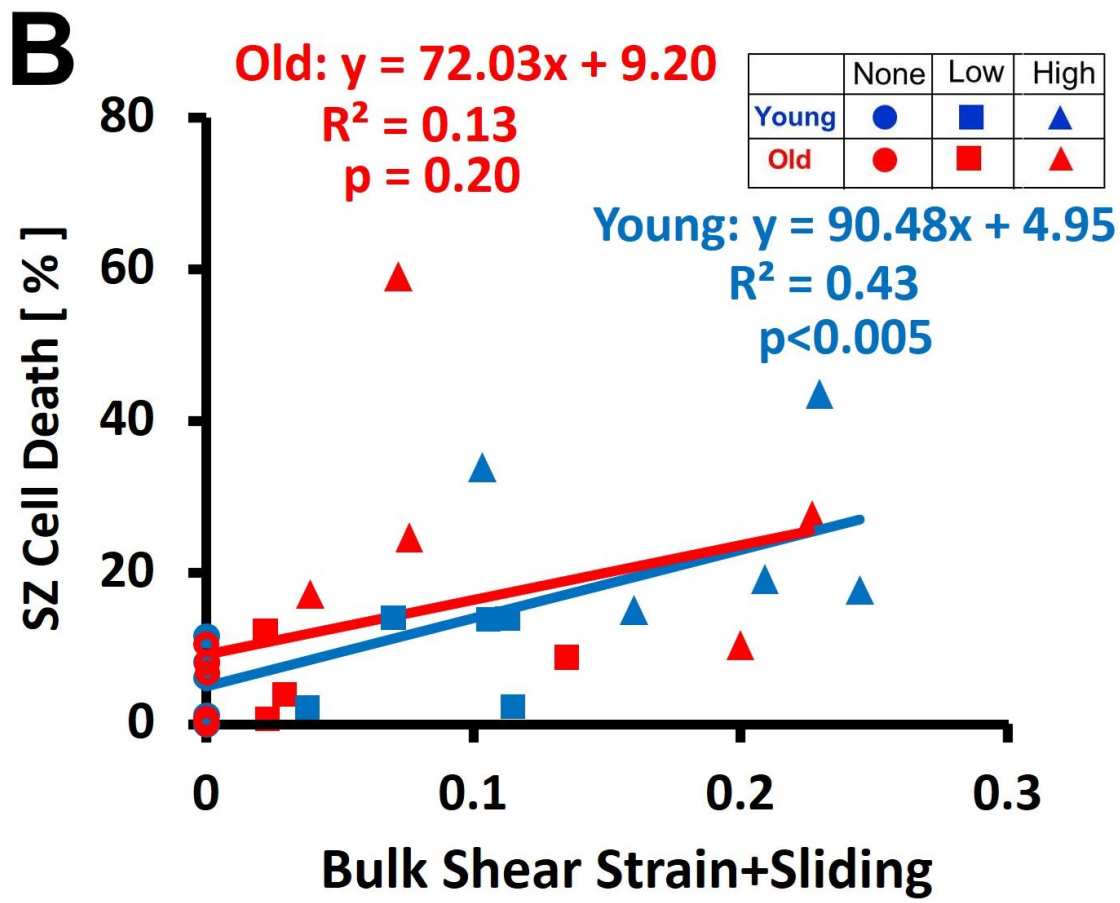

Figure 4.4: Correlation between (A) max shear stress and SZ cell death and (B) bulk shear strain and sliding and SZ cell death. (cont'd)… (B) Percentage of SZ cell death from disks of m=10 donors, m=5 young (blue) and 5 old (red), as a function of bulk shear strain and sliding, when stimulated under low (square) and high (triangle) articulation, and left free-swelling (circle). p values are determined relative to slope 0.

4.4.5 Cartilage PRG4 secretion responses were also associated with donor-specific tissue mechanics (Fig. 4.4)

PRG4 secretion and maximum shear stress were not linearly correlated, for either young or old cartilage (p=0.95 and 0.11, respectively) (**Fig 4.5 A**). However, significant positive correlations were found between PRG4 secretion and bulk shear strain and sliding in young (p<0.05) (**Fig 4.5 B**). On the other hand, a non-significant correlation was found in old (p=0.47) cartilage.

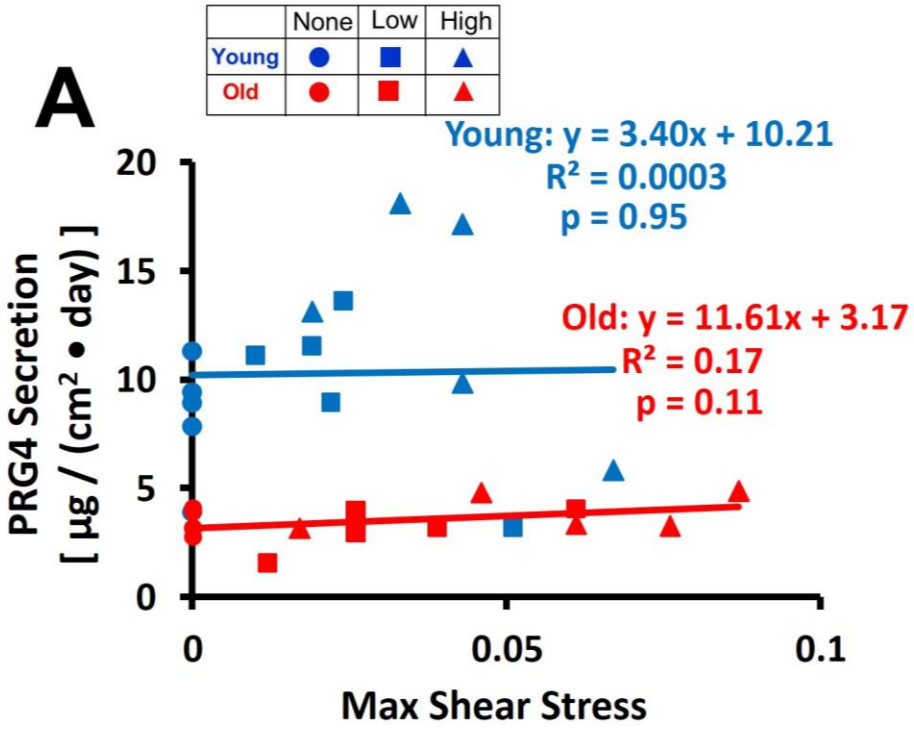

Figure 4.5: Correlation between (A) max shear stress and PRG4 secretion, and (B) bulk shear strain and sliding and PRG4 secretion. (A) PRG4 secretion from disks of m=10 donors, m=5 young (blue) and 5 old (red), as a function of max shear stress, when stimulated under low (square) and high (triangle) articulation, and left free-swelling (circle). p values are determined relative to slope 0.

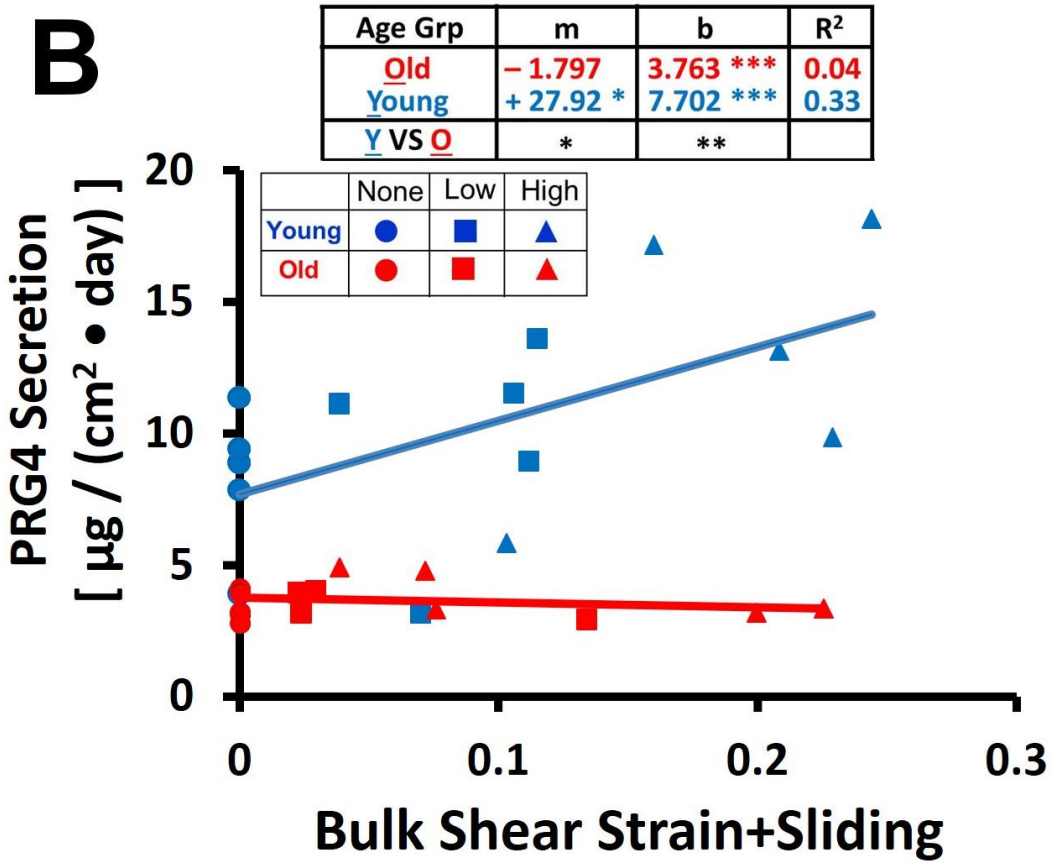

Figure 4.5: Correlation between (A) max shear stress and PRG4 secretion, and (B) bulk shear strain and sliding and PRG4 secretion. (cont'd)… (B) PRG4 secretion from disks of m=10 donors, m=5 young (blue) and 5 old (red), as a function of max shear stress, when stimulated under low (square) and high (triangle) articulation, and left free-swelling (circle). *p<0.05, **p<0.01, ***p<0.001, relative to slope 0 or between young and old cartilage.

The induction of PRG4 secretion associated with higher bulk shear strain and sliding was substantially greater in Young than in Old cartilage (**Fig 4.5 B**), indicated by the difference in slopes ($p<0.001$) and intercepts ($p<0.001$) of the two regression lines.

4.4.6 Chondrocytes within cartilage exhibited apoptosis and autophagy responses to articulation (Figure 4.6).

In the absence of articulation, PARP-p85 expression in the SZ of young cartilage was low (28±3%) but not different from old cartilage (**Fig 4.6 B, C**). Overall, PARP-p85 expression tended ($p=0.06$) to be stimulated by articulation (**Fig 4.6 F**). With high articulation, PARP-p85 expression was stimulated in the SZ of young cartilage ($p<0.05$), but not of old cartilage ($p=0.19$).

In the absence of articulation, LC3 expression was higher in the SZ of young relative to old cartilage ($p<0.05$) (**Fig 4.6 H, J**). LC3 expression was stimulated by high articulation in the SZ ($p<0.001$) overall (**Fig 4.6 L**). However, only old (and not young) cartilage exhibited higher LC3 expression with articulation ($p<0.05$).

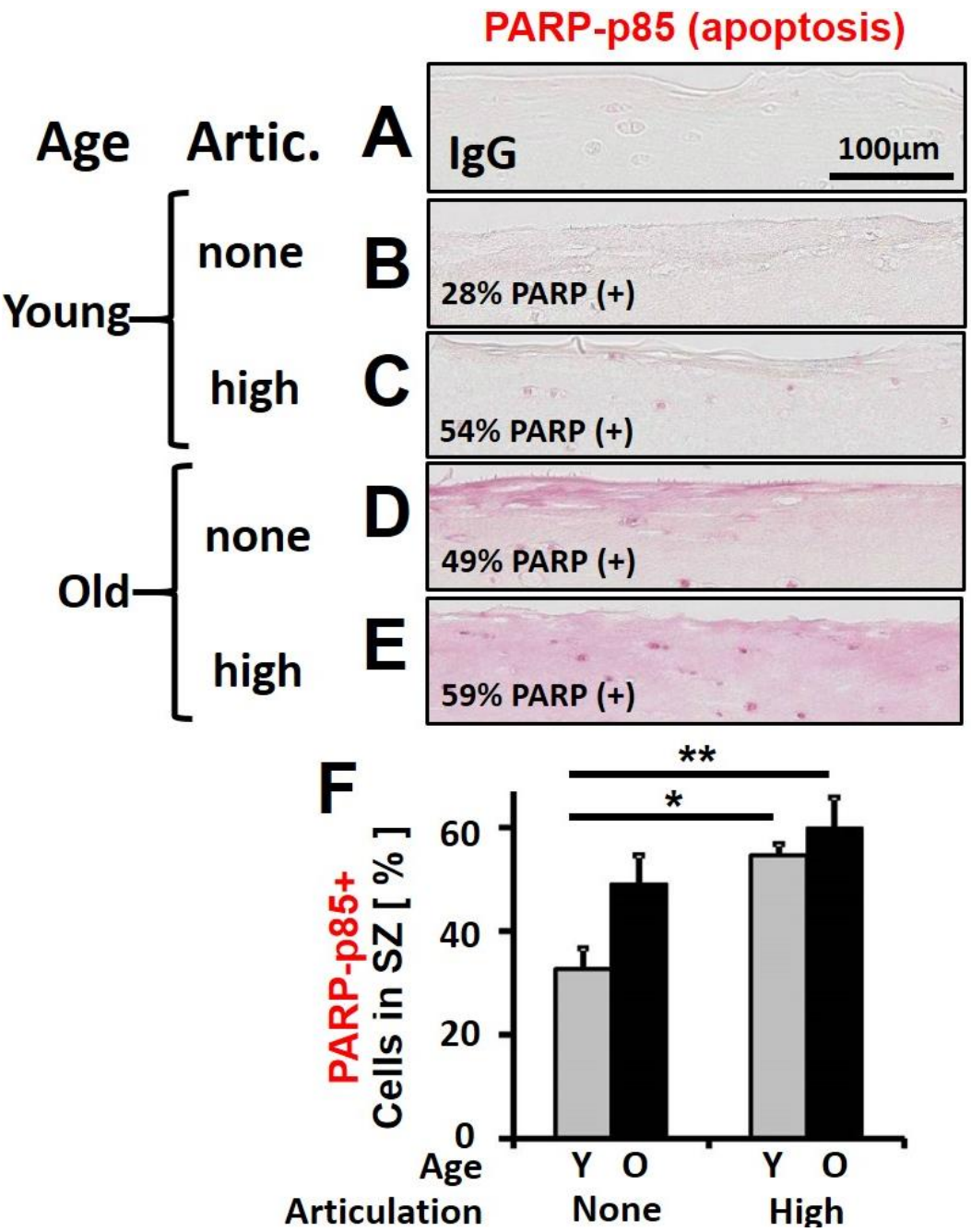

Figure 4.6: Age-dependent effects of high articulation on PARP-p85 and LC3-II expression in human knee articular cartilage. PARP-p85 immunostained sections (B-E) of young and old cartilage, following the absence of mechanical stimulation (B,D) or presence of high articulation (C,E) (IgG control in section A) . Quantitative analysis of PARP-p85-positive expression are shown in individual sections and also summarized (F) and presented as mean±SD of n=4 sections per bar from m=8 human donors, m=4 young and old, respectively.

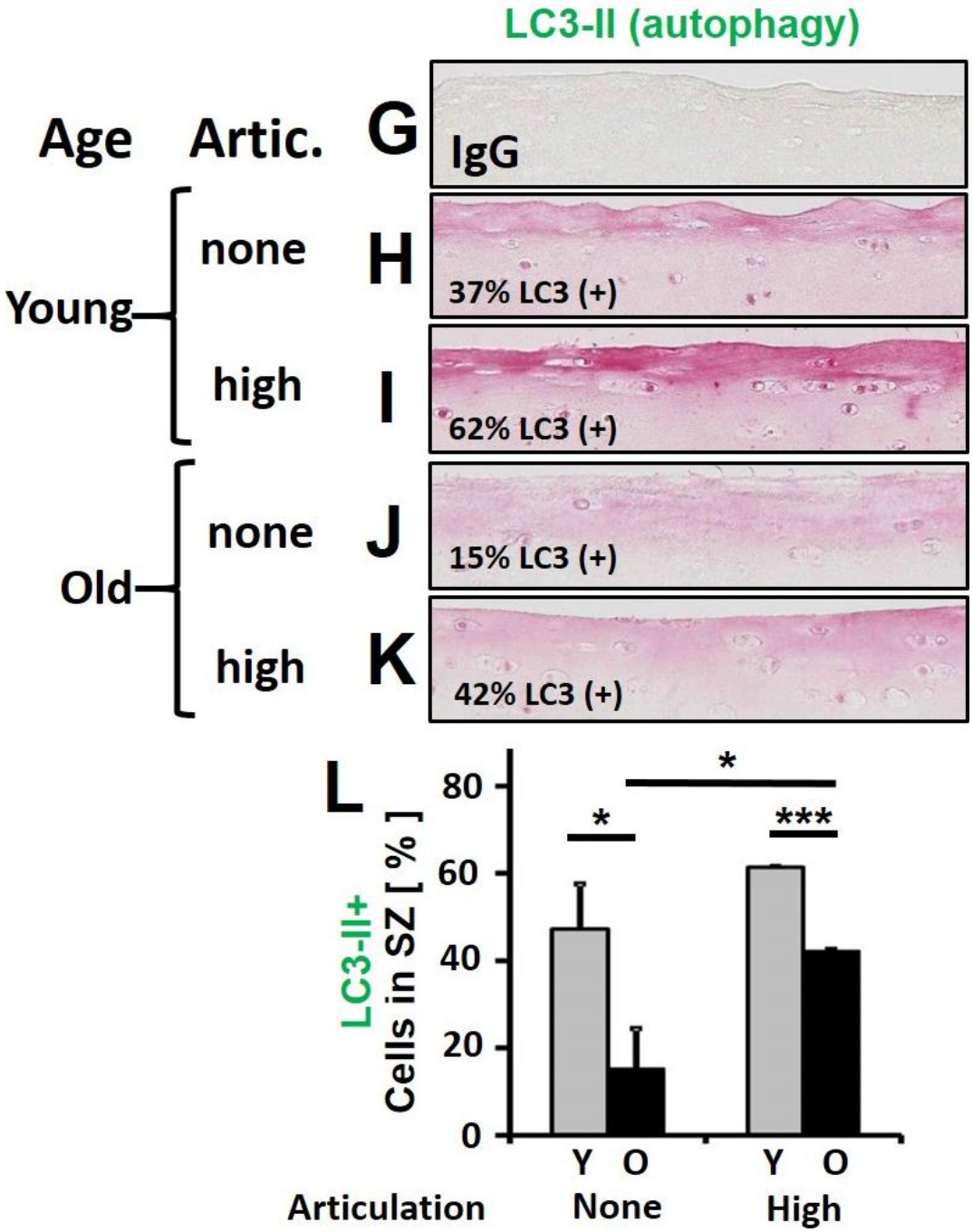

Figure 4.6: Age-dependent effects of high articulation on LC3 expression in human knee articular cartilage. **(cont'd)…** LC3 immunostained sections (H-K) of young and old cartilage, following the absence of mechanical stimulation (H,J) or presence of high articulation (I,K). Quantitative analysis of LC3-positive expression are shown in individual sections and also summarized (L) and presented as mean±SD of n=4 sections per bar from m=8 human donors, m=4 young and old, respectively.

4.4.7 In young donors, PARP-p85 expression tended to correlate with cell death, while LC3 expression was positively correlated with PRG4 secretion.

In young donor cartilage, SZ cell death tended correlate positively ($p=0.10$) with PARP-p85 expression (**Fig 4.7 A**) while cartilage PRG4 secretion positively correlated with LC3 expression ($p<0.001$) (**Fig 4.7 B**). The same correlations were not found in old donor cartilage. PRG4 correlation to LC3 expression was not plotted here, since little difference was found in PRG4 secretion across all articulation conditions on old donor cartilage (**Fig 4.3**). On the other hand, although there was an effect of high level articulation causing greater percentages of cell death in the SZ (**Fig 4.2 B**), there was also no correlation between SZ cell death and PARP-p85 expression.

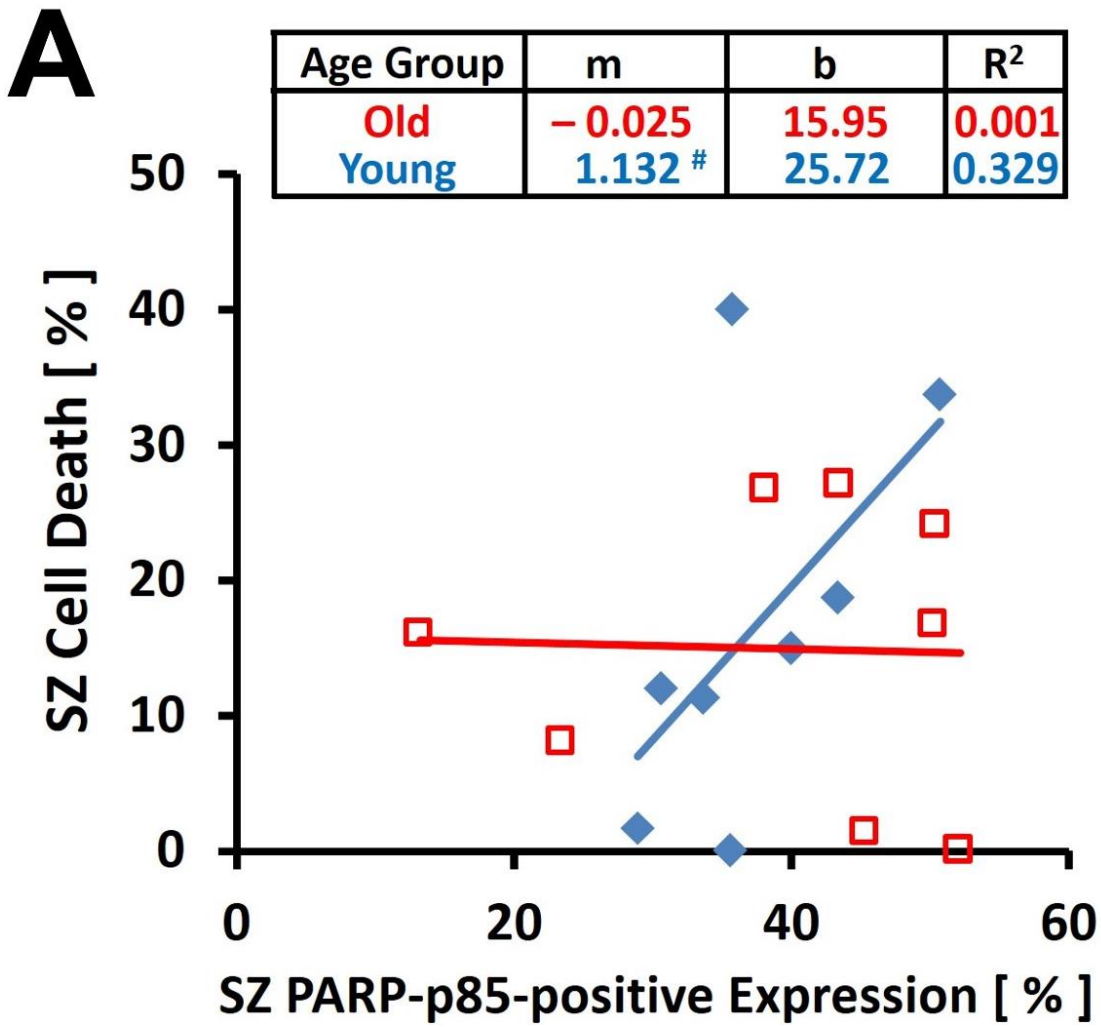

Figure 4.7: Correlations between (A) SZ chondrocyte death and apoptosis expression, and (B) PRG4 secretion and autophagy expression. Data obtained from m=4 young (blue) and m=4 old (red) donor explants, both in the absence and presence of high articulation. A linear trend ($^{\#}p=0.11$, relative to slope 0) of positive correlation was found between cell death and PARP-p85-positive expression in SZ chondrocytes, but only in Young cartilage.

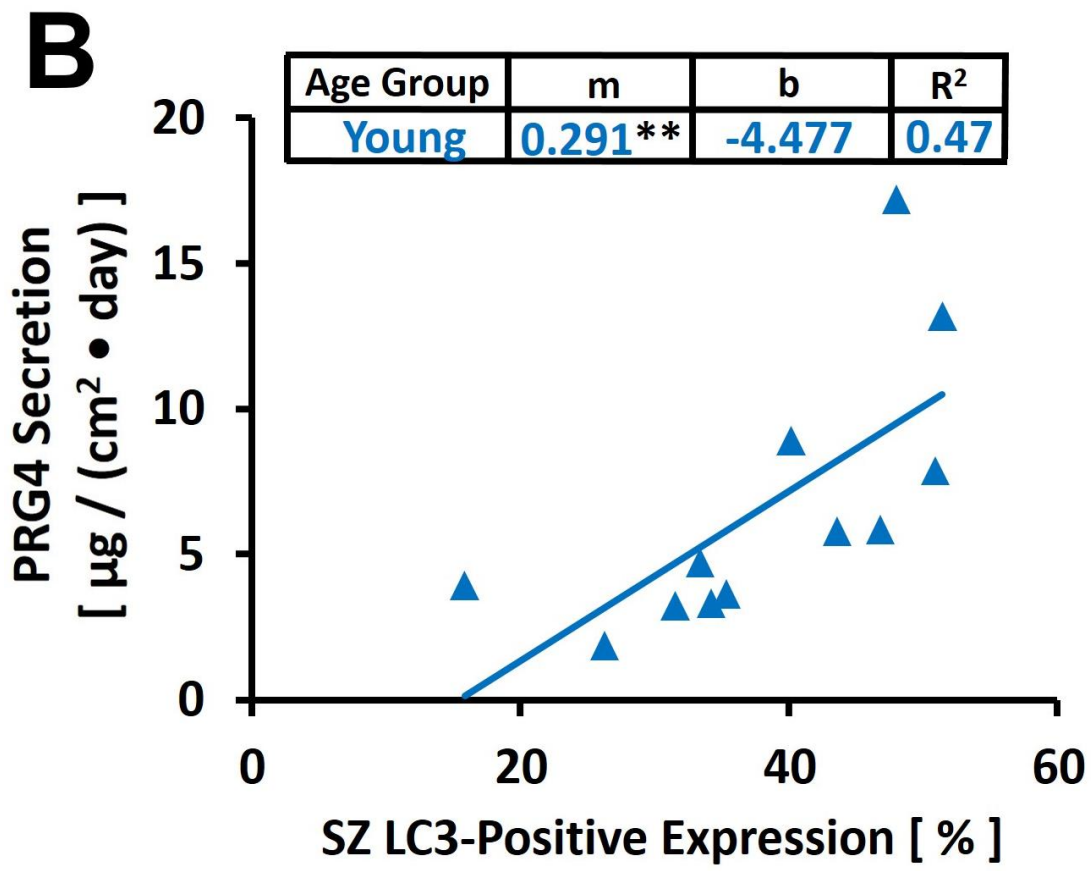

Figure 4.7: Correlations between (A) SZ chondrocyte death and apoptosis expression, and (B) PRG4 secretion and autophagy expression. (cont'd)… Data obtained from m=4 young donor explants, both in the absence and presence of high articulation. Cartilage PRG4 secretion was positively correlated with LC3-positive expression in SZ chondrocytes. **p<0.01 relative to slope 0.

4.5 Discussion

In vivo joint kinematics typically involves variability in the relative surface velocity, but in vitro analysis has yet to examine under a time-varying mechanical articulation, the potential age-dependencies of the biomechanics and mechanobiological responses of human knee cartilage. This study demonstrates that aging in normal human knee articular cartilage results in attenuated biological responses from superficial zone chondrocytes to time-varying mechanical articulation that is excessive in the absence of externally supplemented lubrication. Additionally, the biological outcome measurements of SZ cell viability and phenotypical changes can be attributed to differences in the donor-specific biomechanics of lateral stress and strain.

High amplitudes of time-varying lateral displacement results in biomechanics that are consistent with shearing and then sliding with substantial energy dissipation (**Fig. 4.1 A, B**) and the representation of a slick-slip phenomena, associated with increased friction at lower sliding velocities (**Fig. 4.1 C**). The resultant high levels of cartilage shear stress and/or strain can lead to SZ chondrocyte death (necrosis) (**Fig. 4.2**) and upregulated expressions of apoptosis and autophagy (**Fig. 4.6**), suggesting the susceptibility of cartilage to states when lubrication is deficient. Only young cartilage counteracted by exhibiting anabolic feedback responses, with heightened LC3 expression, and stimulation of PRG4 secretion (**Fig. 4.3**) in its attempt to counter further degeneration by excessive shear.

Strengths and limitations. A number of potential issues were considered when designing the experiment, some that may affect the interpretation of the results. Site-associated variation in PRG4 secretion is described with differences in secretion of the medial and lateral femoral condyles but for both condyles, anterior secreting more than the posterior region [112, 113], and with comparably high secretion in the trochlear as the anterior region in calf knee cartilage [54]. For this study, to minimize potential variations in PRG4 secretion by human cartilage, disc samples were harvested from only the lateral trochlear groove, a region with relatively high and consistent secretion values. Also, to focus on age-related rather than OA-associated variations, the knees studied were screened to be non-OA, and only articular cartilage without macroscopic erosion was used. Such sample selection does not preclude mild histological alterations of the articular surface.

The mechanical setup for articulation was developed by combining previous designs to study the effects of shear stimulation on cartilage PRG4 secretion (Nugent, Schmidt et al. 2006) and shear and sliding biomechanics of human talus cartilage (Nguyen, Wong et al. 2010), but further adapted to facilitate maximal lateral strain (rather than sliding) near the articular surface and within the SZ cartilage of the discs by creating lateral restraints at the deeper end and limiting relative movement laterally at the superficial end with a roughened platen surface. Additionally, contrary to calf cartilage explants, human cartilage discs did not appear to swelling substantially when cultured in serum supplemented media [114].

Although the resultant bulk shear strain may be excessive (due to the high frictional counter loading surface) compared to physiological conditions, the range of

axial strain and absolute amplitudes of lateral displacement discs are subjected to occur during joint articulation in vivo [22, 115]. Slip between the platen and the articular surface (sliding) was also shown at high amplitudes of articulation, supported by the high THD.

Known for its boundary lubrication properties as a sacrificial layer, PRG4 is suggested to be detached from the cartilage articular surface and released into the conditioned media by 5 mins of torsional shear (Chan, Neu et al. 2012). Mechanical stimulation of 400 cycles/7.6 mins was applied and all discs (including none articulation) were rinsed briefly following stimulation with media to prevent residual, partially attached PRG4 adhered to the tissue. This allowed for the PRG4 quantification from the conditioned media to represent newly synthesized and secreted PRG4 by the discs. The effect of the designed articulation regime on SZ matrix structure appears minimal as well. In contrary to short duration (<1s) compressive impact loading with associated, localized cell death to surface and SZ cartilage damage, short periods (<500s in this study) of high articulation did not appear to create noticeable damage to the matrix, resulting in more diffused rather than localized cell death patterns [109]. Lastly, the biological responses of cartilage may vary as a function of time after loading (as some expressions are transient and others progress to different phenotypes rapidly). It is critical to examine cell expressions of apoptosis and autophagy immediate following stimulation in vitro, as the cell death pathways may progress to secondary necrosis [116]. While, necrosis caused by the rupturing of membrane, should occur immediately as well. Alternatively, fluctuations in PRG4 secretion regulated by chemical or mechanical factors have been generally observed

day increments, with the most significant effects at 1-2 days following mechanical effects [52, 53]. Consequently, SZ chondrocyte death features were analyzed at 1-2 hours and PRG4 secretion determined at 1-2 days after mechanical treatment.

Nonetheless, a more detailed and combined understanding of mechanical articulation in tissue behavior and associated biological pathways and responses may be needed to further clarify mechanisms of aging-associated deterioration of human articular cartilage.

Biomechanics. Articulation against roughened platen without supplementation of lubricants resulted in bulk shear deformation amplitudes (0.10-0.20) that are higher or at the high range of prior in vitro shear studies articulating talus cartilage against the same roughened platen (~0.05) [33] and normal (versus degenerated) femoral cartilage-on-cartilage (0.05-0.12) [32]. However, specific biomechanical properties have been noted to differ remarkably across joints, with the higher glycosaminoglycan content in talar cartilage potentially associated with lower shear deformation [117]. The estimated bulk shear modulus was also within range (0.18-1.00) of previous findings though shear modulus is strongly dependent on sample thickness, as substantial increases in shear modulus are observed (Wong, Bae et al. 2008).

Mechanobiology. PRG4 secretion as a function of different media compositions has not been fully characterized in human knee cartilage, however, preliminary experiments have shown a slow attenuation (range of decrease) of PRG4 secretion with time when human cartilage discs are incubated in 10% serum supplemented media. The presence of high articulation-induced shear strain helps prevent this decline (**Fig. 4.3**), even though, killing (causing necrosis in) a portion of

SZ chondrocytes (**Fig. 4.2**) during the process.

Other modes of cell death and repair were detected also, with upregulated apoptosis and autophagy response by articulation (**Fig. 4.6**), pointing to potential hyperactivity of chondrocytes. Similar apoptosis expressions have been reported in calf cartilage, and similar age-dependent baseline autophagy expressions in human cartilage (young = ~50% LC3-positive > ~15% LC3-positive = old with mild osteoarthritic) [58]; but discrepancies exist between mechanical-induced autophagy expression (stimulated by articulation but decreased with impact loading), which most likely suggests the activation of a different downstream mechanism.

Mechanical simple shear similarly upregulated PRG4 secretion in calf and human cartilage discs, but by subjecting calf discs to much lower amplitudes (of ±26 μm) to that of human discs (of ±1000 μm) (an increase of 2.5 fold in calf versus 1.75 fold in human). This can be rationalized by the fact that baseline values of human cartilage PRG4 secretion is typically lower than calf, as well as the density of SZ cells that sustains the secretion; moreover, lateral stiffness at the SZ of human cartilage has been typically described to be higher than calf cartilage, suggesting a higher magnitude of lateral strain required to achieve the same amount of lateral stress.

The viability of and the secretion of PRG4 by SZ chondrocytes may be regulated by different mechanisms, indicated by the difference in governing tissue biomechanical property. PRG4 secretion was correlated with bulk shear strain and sliding but not maximum shear stress. This relationship can be further examined in detail by introducing different concentrations of lubrication (ie. synovial fluid) into the articulation setup, to determine whether the gradient of resultant tissue deformation in

tissue explants from the same donor is correlated with a gradient of PRG4 secretion. Other counter surfaces can also be applied to achieve similar purposes. Nevertheless, to precisely determine the secretion rate per cell, the cell viability has to be better preserved.

In conclusion, this study shows that the multi-axial biomechanics of cartilage articulation can be analyzed using oscillatory signals with consideration and interpretation of magnitude, phase, and harmonic distortion. Moreover, the lack of mechanical responsiveness (due to changes in tissue biomechanics and/or chondrocyte phenotype) of human articular cartilage with aging may contribute to the increased incidence of osteoarthritis with aging.

The mechanobiology of cartilage articulation at high amplitude involves age-associated apoptosis and autophagy responses that are substantially different than those involved in impact-associated damage. Regardless, the susceptibility of articular cartilage to shear-induced cell death, apoptosis, or autophagy suggests that mechanical protection strategies may be helpful to prevent subsequent development of osteoarthritis.

Further understanding of the mechanobiological alteration of human cartilage with aging may involve both mechanical properties of the tissue matrix as well as biological variations in the chondrocytes.

3.6 Acknowledgements

Chapter 4, in full, will be submitted to *Journal of Orthopaedic Research*. The dissertation author was the primary author and thanks co-authors Alexander Y. Hui, Eloy Alonso, Albert C. Chen, and Robert L. Sah. This work was supported by grants from the National Institutes of Health.

CHAPTER 5:

CONCLUSIONS

5.1 Summary of Findings

The objective of this work was to further the understanding of the role mechanical articulation plays in the initiation of early degeneration of human knee articular cartilage. To study naturally occurring early degeneration in human knee MFCs, a reliable, sensitive, and standardized histopathology grading system was created, with quantitative feature definitions supplemented by an image atlas with examples for each score of each feature. Improvement in the inter-observer reliability was achieved by 2 stages of refinement that includes additional details in the feature definitions (**Table 2.1** Feature #2 surface roughness) or providing additional image examples in the atlas to enable direct comparison for scoring (**Figure 2.2**).

Using this histopathology grading system, spatial variation in the anterior-posterior direction of cartilage lesions were identified, specifically when comparing the anterior and posterior transitional regions between the near full-thickness regions and lesion base. Prevalent horizontal and vertical fissures, weaker Saf-O staining, and more cell cloning and clustering were the main features that distinguished the anterior from the posterior transitional regions (**Figure 3.3**). These findings combined with angular measurements of cartilage (finger like) projections (**Figure 3.1 D**) provides further evidence and semi-quantitative details on of “cartilage flow”, described

previously by bending of collagen fibrils/networks [97, 99, 118]. High prevalence of cartilage flow in the anterior transitional region of cartilage lesions can implicate specific mechanobiologically-driven cartilage degeneration.

To recapitulate similar responses as detected by histopathological analysis of cartilage lesions, and focusing on early changes at the cartilage surface/superficial zone(SZ), articulation was applied to SZ cartilage discs explanted from the human knee (**Chapter 4**). The effect of aging was also investigated by separating donors into 2 age groups, young (<35 years old) versus old (50+ years old). The applied high amplitudes of lateral displacement was consistent with shear and sliding with substantial energy dissipation and the slick-slip phenomena, but neither lateral stiffness amplitude or phase varied with age (**Figure 4.1**). This articulation regime resulted in an array of biological response by SZ chondrocytes, including increased cell death (**Figure 4.2**, similar between age groups), PRG4 secretion (**Figure 4.3**, only in young cartilage), and apoptosis and autophagy expressions (**Figure 4.6**, age-dependent changes but reflecting substantial differences at baseline). Certain tissue mechanics were correlated with biological responses (ie. bulk shear strain and sliding with PRG4 secretion in young cartilage, **Figure 4.5 B**) providing insights into direct, upstream regulatory mechanotransduction pathways. Whereas, biological responses were also correlated such as autophagy and PRG4 secretion (**Figure 4.7**), suggesting downstream signal transduction pathways that may partially overlap.

In summary, these studies demonstrate that articulation contributes to cartilage degeneration in the human knee articular cartilage in a spatially-oriented manner, and affects SZ chondrocyte health and repair responses as well as matrix properties via generating shear stress and strain with sliding on the cartilage tissue. When subjected to the same articulation regime in the absence of lubrication, the tissue shear

mechanics differs slightly (at a macroscale) but SZ chondrocyte biological response substantially with aging. Young SZ chondrocytes can exhibit a feedback response, to counter the excessive shear and potential loss of chondrocytes; whereas aged chondrocytes lack this mechanical responsiveness which may contribute to the increased incidence of osteoarthritis with aging

5.2 Discussion

The major contributions of this work includes (1) a thorough analysis of classical grading systems for osteoarthritic and degenerated cartilage and based on the acquired knowledge, a standardized and reliable histopathological grading system for more detailed understanding of cartilage degeneration in the human knee MFC, (2) an in depth examination of spatial variation in the histopathology of naturally occurring cartilage lesions in human knee MFCs, which can stimulate future work in testing concepts relating to mechanical articulation-driven cartilage deterioration, and (3) insight into how a physiological loading pattern of articulation (but resultant excessive tissue shear stress and strain due to the absence of lubrication and rough countersurface) can induce catabolic effects in SZ chondrocytes and matrix, which counteracting feedback responses are attenuated with aging.

Although current grading systems are capable of detecting different stages of degeneration and osteoarthritis, the sensitivity and resolution of the grading systems have been reported to be limiting [68]. Classical grading systems (ie Collins, OARSI, Mankin) generally examine for features that represent the most severe degree of degeneration without specified field-of-views, which can be appropriate for clinical diagnosis purposes. However, to study the early stages of cartilage degeneration in a research setting, the development of a more standardized and sensitive grading system was required.

A thorough review of classical grading systems indicated that the majority of features are graded using qualitative feature definitions. Other primary literature, on

the other hand, has accumulated additional information on measurements of matrix and chondrocyte features particularly since early 2000s. During the same period, the advent of imaging modalities has enabled acquisition of large field-of-view (FOV), high resolution histological images. Conventionally, microscopic imaging has been performed under the microscope with standardized eye piece (10X) and objective lens (4, 10, 20, 40X) and images reported at the multiplied magnifications of these two components (40, 100, 200, 400X). As the FOV and resolution can be determined as separate parameters for each image, image in the literature are typically of varying FOV and resolutions. For similar reasons, even though some histological images have been proposed as examples or guidelines to potentially serve as an atlas, they are difficult to apply and may only help with conceptual understanding of the features.

Therefore, when developing our histopathological grading system for the purpose of studying early degeneration in human knee cartilage (**Chapter 2**), the goals were to identify features from classical grading systems and transform the definitions to become quantitative. It was found that the frequency of the quantitative definitions are dependent on the FOV of the images examined. A standardized image FOV and resolution for images under examination were thus defined to be comparable to 100X (1.2mm width) and 200X (pixel size of 0.25μm^2) magnifications in conventional microscopy. An atlas for human knee MFC was also created based on the quantitative feature definitions with at least 1 image per feature per score, at high resolution (pixel size of 0.25μm^2) and different but specified FOVs (3mm X 2mm, equivalent to 4X, or 0.3mm X 0.2mm, equivalent to 40X) that are easily comparable to the standardized images (1.2mm by full-thickness cartilage, with pixel sizes of 0.25μm^2).

Even with quantitative definitions for each feature, the pilot grading results suggested that graders were required to make interpretations when actually grading the histology. These judgements are user dependent and resulted in low inter-observer reliability of the system (**Table 2.2 A**, Cronbach's alpha of 0.10-1.00, 0.79 ± 0.19). Differences in the specific grading approaches were found between graders and feature definitions were adjusted accordingly to minimize this variation. After 3 separate trials of grading with a total of 2 refinement periods in between, the inter-observer reliability improved substantially (**Table 2.2 B**, Cronbach's alpha of 0.70-1.00, 0.89 ± 0.09).

Computer-assisted grading can be developed to avoid the opportunity for observer bias, but the algorithm is also written based on human knowledge and experience, and limited in making precise measurements for certain features such as cellularity and tidemark invasion [119]. Nonetheless, by establishing quantitative feature definitions and acquiring representative images for an image atlas, one can possibly create a training dataset for machine learning and ultimately develop an automated grading system that is accurate.

The proposed grading system detected spatial variation in naturally occurring cartilage lesions located at the weight-bearing regions of the MFC. Human knee cartilage lesions also occur in the other femoral compartments, such as the patellofemoral groove and lateral femoral condyle [92]. These locations are under different mechanical environments *in vivo* and should display different types of histopathology spatial trends as describe in **Chapter 3**. Since the patellofemoral groove cartilage predominantly experiences shear by sliding against patellar cartilage,

similar patterns in histopathology as ones examined in the anterior transitional regions depicted in **Figure 3.3** can be expected. Relating to this, although our quantitative feature definition and image atlas were designed for the human MFC, it would be useful to determine whether the grading system is applicable for grading of cartilage in other femoral components. Some component-dependent variation in histopathology is expected, even in normal human knees, since mechanical and biological properties differ across these locations [13], but the characteristics of some basic biological unit such as the length of a matrix crack/fissure and chondrocyte size should be comparable. Moreover, specific immunostaining was not performed on the neighbor sections, likely due to the large area of the sections (~15mm by full-thickness), but can be done to associate biological activity of the cells (such as cell hypertrophic expression indicated by Type X collagen and matrix metalloproteinase 13) to observed chondrocyte morphology (enlarged SZ cells) and distribution in Saf-O/fast green histology.

Chondrocyte metabolism and the cartilage matrix macromolecule framework alters at early stages of degeneration in cartilage [120]. Several histological observations are frequently found, but underlying mechanisms suspected and not yet confirmed. For instance, chondrocytes near the articular surface can be shaped flat or non-flat to round. It remains unknown whether this phenomena represents the enlargement of flattened cells in the vertical direction to become round, or the removal of the surface layer containing flattened cells, exposing the middle zone cells that are typically round. Support for the first scenario includes the concept of disruptions occurring in the matrix macromolecule network causing decreased concentration and

length of proteoglycans, and leading to increased water content and a more hypotonic microenvironment as well as increased space for cells to enlarge. Mechanisms underlying changes in cell organization such as cloning and clustering are better studied, which features are induced by a combination of anabolic and mitogenic growth factors for cell proliferation and enzymatic degradation of surrounding matrix for space.

Articulation-induced biological responses of SZ chondrocytes in **Chapter 4** can also be associated with specific histological presentations. SZ cell death or necrosis can cause cells to disintegrate and result in a lower cellularity at the SZ; while many cells that express apoptosis are also presented with a “blebbing” morphology, protrusion of the plasma membrane, when examined under high resolution. PRG4 lubricant protein is localized at the SZ and regulated by SZ chondrocytes, which many are described to be morphologically flat. Whether the prevalence of flattened shape cells in histology can infer specific cell phenotypes such as PRG4 secretion, however, remains to be investigated.

Another approach to study mechanical effects on cell in a biological system is to isolate the cell and apply direct, controlled mechanical forces to the cell. Fluid flow-induced shear stress causes changes in the intracellular calcium levels of monolayer chondrocytes, suggesting active responses of mechanosensitive calcium channels [121]. The ability to test isolated cells individually under different mechanical stimulations can help clarify the association between the types of forces perceived by the chondroctyes and the resultant biological response. Unfortunately, chondrocytes

can dedifferentiate fairly quickly following monolayer culture and may still be best examined in its native environment packed within its pericellular matrix.

This dissertation has studied spatial patterns of cartilage lesions that implicated mechanically-driven cartilage degeneration and then tested the effects of articulation on tissue mechanics and SZ chondrocyte biological response. Taken together, the results from this dissertation contributed to our understanding of mechanically-induced mechanisms of early stage cartilage degeneration.

5.3 Future Work

The current work could be expanded in a number of ways. The research aims altogether strongly imply that excessive levels of articulation can induce damage in cartilage, possibly initiated at the surface and progresses to deeper layers. (Even in the absence of lubrication, minimal cartilage damage created in Chapter 4 may be due to insufficient articulation amplitude and/or duration of loading). The rational next step to take would be to articulate apposing osteochondral cores from the human knee MFC (or against a tibial cartilage ± meniscus core?) at large amplitudes (of 3-10 MPa, slightly above physiological range) and for long total durations (at least 4+ hours per stimulation, and could perform multiple stimulations), also in the absence of lubrication. Ideally, this can be done sterilely to also investigate mechanobiological responses of cartilage, but challenges may exist in long term cultures of cartilage with bone. Bone can secret catabolic factors, which are normally restrained by diffusion through the cartilage *in vivo*, but is free to reach the cartilage in osteochondral core culture. A similar experiment can also be conducted by subjecting whole knee joints of small animals to excessive articulation, conducted either *in vivo* or *in vitro*.

There are also substantial advantages in three- versus two-dimensional characterization/histological imaging of *in vitro* wear and degeneration of cartilage. With 3-D imaging, one could potentially estimate volume of cracks/fissures in cartilage, obtain more precise measurements on chondrocyte number, shape, and size (similar to reasons of using stereological approaches in histology), and study spatial variation not only in a single cross section. Digital volumetric imaging (DVI) is capable of creating 3-

D histology blocks to be analyzed for matrix and cell morphology. However, specific staining using antibodies has not been possible with the DVI, since these molecules are unable to diffuse through the intact cartilage. Moreover, specific procedures for embedding the cartilage requires the antibody to undergo high temperatures, which is likely to degrade the protein leaving no signals even if all components were bound to each other.

During the development of the histopathology feature definitions in **Chapter 2**, it was noted that primary literature does not currently possess clear, standardized definitions to separate the different zones of cartilage, namely superficial, middle, and deep. Although zone-specific gene expression patterns are described in literature [122], there are few zone-specific antibodies available now to distinguish them from each other. The specific concept that can be tested with zone-specific antibody development would be whether (1) the phenotype of the SZ chondroycte is altered with degeneration or (2) instead of SZ cells, MZ chondrocytes are at the cartilage surface with cartilage wear and erosion. Since antibodies that are designed to detect normal SZ chondrocytes, such as anti-lubricin antibodies, may not detect the altered or abnormal SZ cells following phenotypical changes, the approach would be to assess whether MZ/DZ cells are found at the cartilage surface/superficial layer. This could potentially work under the assumption that SZ chondrocytes do not alter to express similar phenotypes as MZ or DZ chondrocytes.

Under a broader perspective, understanding the mechanisms to which cartilage degenerates with articulation, or mechanical loading in general, will provide researchers with opportunities to develop preventive treatments. At the cellular level, SZ

chondrocytes appear to immediately respond to articulation-induced cell death (necrosis) by enhancing PRG4 secretion while maintaining high levels of autophagy, which two factors are positively correlated (**Figure 4.7 B**). It is possible that these represent downstream effects of the same upstream mechanotransduction pathway. Here, we also observed a cartilage flow phenotype at the anterior transition region of lesions, which is believed to be a consequence of loading rather than a protective mechanism in covering the cartilage defect to prevent further damage [97, 99].

Overall, effects of articulation can be further studied at larger amplitudes and for longer durations, to induce substantial (spatially-oriented) damage in human knee articular cartilage. This is ideally studied with live cartilage where biological responses of chondrocytes can be characterized and potential underlying mechanisms elucidated.

5.4 References

1. Ateshian GA, Mow VC. Friction, lubrication, and wear of articular cartilage and diarthrodial joints. In: Basic Orthopaedic Biomechanics and Mechano-Biology, Mow VC, Huiskes R Eds. Philadelphia: Lippincott Williams & Wilkins 2005:447-494.

2. Mow V, Rosenwasser M. Articular cartilage: biomechanics. In: Injury and Repair of the Musculoskeletal Soft Tissues, Woo SL-Y, Buckwalter JA Eds. Park Ridge, IL: American Academy of Orthopaedic Surgeons 1988:427-463.

3. Buckwalter JA, Mankin HJ. Articular cartilage. Part I: tissue design and chondrocyte-matrix interactions. J Bone Joint Surg Am 1997; 79-A: 600-611.

4. Mow VC, Setton LA, Ratcliffe A. Mechanical factors in articular cartilage and their role in osteoarthritis. In: Osteoarthritic Disorders, Kuettner KE, Goldberg VM Eds. Rosemont, IL: American Academy of Orthopaedic Surgeons 1995:147-171.

5. Altman R, Asch E, Bloch D, Bole G, Borenstein D, Brandt K, Christy W, Cooke TD, Greenwald R, Hochberg M, Howell D, Kaplan D, Koopman W, Longley III S, Mankin H, McShane DJ, Medsger Jr. T, Meenan R, Mikkelsen W, Moskowitz R, Murphy W, Rothschild B, Segal M, Sokoloff L, Wolfe F. Development of criteria for the classification and reporting of osteoarthritis. Classification of osteoarthritis of the knee. Diagnostic and Therapeutic Criteria Committee of the American Rheumatism Association. Arthritis Rheum 1986; 29: 1039-1049.

6. Neogi T, Aletaha D, Silman AJ, Naden RL, Felson DT, Aggarwal R, Bingham CO, 3rd, Birnbaum NS, Burmester GR, Bykerk VP, Cohen MD, Combe B, Costenbader KH, Dougados M, Emery P, Ferraccioli G, Hazes JM, Hobbs K, Huizinga TW, Kavanaugh A, Kay J, Khanna D, Kvien TK, Laing T, Liao K, Mease P, Menard HA, Moreland LW, Nair R, Pincus T, Ringold S, Smolen JS, Stanislawska-Biernat E, Symmons D, Tak PP, Upchurch KS, Vencovsky J, Wolfe F, Hawker G. The 2010 American College of Rheumatology/European League Against Rheumatism classification criteria for rheumatoid arthritis: Phase 2 methodological report. Arthritis Rheum 2010; 62: 2582-2591.

7. Lotz MK, Kraus VB. New developments in osteoarthritis. Posttraumatic osteoarthritis: pathogenesis and pharmacological treatment options. Arthritis Res Ther 2010; 12: 211.

8. Furman BD, Olson SA, Guilak F. The development of posttraumatic arthritis after articular fracture. J Orthop Trauma 2006; 20: 719-725.

9. Anderson DD, Chubinskaya S, Guilak F, Martin JA, Oegema TR, Olson SA, Buckwalter JA. Post-traumatic osteoarthritis: Improved understanding and opportunities for early intervention. J Orthop Res 2011; 29: 802-809.

10. Jadin K, Schumacher BL, Price JH, Sah RL. 3-D analysis of chondrocyte organization in articular cartilage during growth. Int Cart Repair Soc 2004; 5: 673.
11. Hunziker E, Quinn T, Shimaoka E, Hauselmann H. Quantitative structural organization of the normal adult human articular cartilage. Trans Orthop Res Soc 2002; 27: 357.

12. Dowthwaite GP, Bishop JC, Redman SN, Khan IM, Rooney P, Evans DJ, Haughton L, Bayram Z, Boyer S, Thomson B, Wolfe MS, Archer CW. The surface of articular cartilage contains a progenitor cell population. J Cell Sci 2004; 117: 889-897.

13. Temple-Wong MM, Bae WC, Chen MQ, Bugbee WD, Amiel D, Coutts RD, Lotz M, Sah RL. Biomechanical, structural, and biochemical indices of degenerative and osteoarthritic deterioration of adult human articular cartilage of the femoral condyle. Osteoarthritis Cartilage 2009; 17: 1469-1476.

14. Swann DA, Sotman S, Dixon M, Brooks C. The isolation and partial characterization of the major glycoprotein (LGP-I) from the articular lubricating fraction from bovine synovial fluid. Biochem J 1977; 161: 473-485.

15. Swann DA, Slayter HS, Silver FH. The molecular structure of lubricating glycoprotein-I, the boundary lubricant for articular cartilage. J Biol Chem 1981; 256: 5921-5925.

16. Ogston AG, Stanier JE. The physiological function of hyaluronic acid in synovial fluid: viscous, elastic and lubricant properties. J Phys 1953; 119: 244-252.

17. Wright V, Dowson D. Lubrication and cartilage. J Anat 1976; 121: 107-118.

18. Schumacher BL, Block JA, Schmid TM, Aydelotte MB, Kuettner KE. A novel proteoglycan synthesized and secreted by chondrocytes of the superficial zone of articular cartilage. Arch Biochem Biophys 1994; 311: 144-152.

19. Jay GD, Britt DE, Cha CJ. Lubricin is a product of megakaryocyte stimulating factor gene expression by human synovial fibroblasts. J Rheumatol 2000; 27: 594-600.

20. Meyer K, Smyth EM, Dawson MH. The isolation of a mucopolysaccharide from synovial fluid. J Biol Chem 1939; 128: 319-327.

21. Jay GD, Harris DA, Cha CJ. Boundary lubrication by lubricin is mediated by O-linked beta(1-3)Gal-GalNAc oligosaccharides. Glycoconj J 2001; 18: 807-815.

22. Kozanek M, Hosseini A, Liu F, Van de Velde SK, Gill TJ, Rubash HE, Li G. Tibiofemoral kinematics and condylar motion during the stance phase of gait. J Biomech 2009; 42: 1877-1884.

23. Mow VC, Holmes MH, Lai WM. Fluid transport and mechanical properties of articular cartilage: a review. J Biomech 1984; 17: 377-394.

24. Athanasiou KA, Rosenwasser MP, Buckwalter JA, Malinin TI, Mow VC. Interspecies comparisons of in situ intrinsic mechanical properties of distal femoral cartilage. J Orthop Res 1991; 9: 330-340.

25. Chang N, Cory E, Chen AC, Raub CB, Chan EF, Urbina AM, Otsuki S, Hasegawa A, Lotz MK, Sah RL. Spatial variation in indentation properties of human femoral articular cartilage. Trans Orthop Res Soc 2011; 36: 2137.

26. Eckstein F, Lemberger B, Stammberger T, Englmeier KH, Reiser M. Patellar cartilage deformation in vivo after static versus dynamic loading. J Biomech 2000; 33: 819-825.

27. Kersting UG, Stubendorff JJ, Schmidt MC, Bruggemann GP. Changes in knee cartilage volume and serum COMP concentration after running exercise. Osteoarthritis Cartilage 2005; 13: 925-934.

28. Schinagl RM, Gurskis D, Chen AC, Sah RL. Depth-dependent confined compression modulus of full-thickness bovine articular cartilage. J Orthop Res 1997; 15: 499-506.

29. Katta J, Jin Z, Ingham E, Fisher J. Biotribology of articular cartilage - A review of the recent advances. Med Eng Phys 2008; 30: 1349-1363.

30. Schmidt TA, Gastelum NS, Nguyen QT, Schumacher BL, Sah RL. Boundary lubrication of articular cartilage: role of synovial fluid constituents. Arthritis Rheum 2007; 56: 882-891.

31. Fitzgerald JB, Jin M, Grodzinsky AJ. Shear and compression differentially regulate clusters of functionally related temporal transcription patterns in cartilage tissue. J Biol Chem 2006; 281: 24095-24103.

32. Wong BL, Bae WC, Chun J, Gratz KR, Lotz M, Sah RL. Biomechanics of cartilage articulation: effects of lubrication and degeneration on shear deformation. Arthritis Rheum 2008; 58: 2065-2074.

33. Nguyen QT, Wong BL, Chun J, Yoon YC, Talke FE, Sah RL. Macroscopic assessment of cartilage shear: effects of counter-surface roughness, synovial fluid lubricant, and compression offset. J Biomech 2010; 43: 1787-1793.

34. Buckley MR, Gleghorn JP, Bonassar LJ, Cohen I. Mapping the depth dependence of shear properties in articular cartilage. J Biomech 2008; 41: 2430-2437.

35. Hayes WC, Mockros LF. Viscoelastic properties of human articular cartilage. J Appl Physiol 1971; 31: 562-568.

36. Spirt AA, Mak AF, Wassell RP. Nonlinear viscoelastic properties of articular cartilage in shear. J Orthop Res 1989; 7: 43-49.

37. Zhu W, Mow VC, Koob TJ, Eyre DR. Viscoelastic shear properties of articular cartilage and the effects of glycosidase treatments. J Orthop Res 1993; 11: 771-781.

38. Jin M, Frank EH, Quinn TM, Hunziker EB, Grodzinsky AJ. Tissue shear deformation stimulates proteoglycan and protein biosynthesis in bovine cartilage explants. Arch Biochem Biophys 2001; 395: 41-48.

39. Woo SL-Y, Kwan MK, Lee TQ, Field FP, Kleiner JB, Coutts RD. Perichondrial autograft for articular cartilage: shear modulus of neocartilage studied in rabbits. Acta Orthop Scand 1987; 58: 510-515.

40. Setton LA, Mow VC, Howell DS. Mechanical behavior of articular cartilage in shear is altered by transection of the anterior cruciate ligament. J Orthop Res 1995; 13: 473-482.

41. Ikegawa S, Sano M, Koshizuka Y, Nakamura Y. Isolation, characterization and mapping of the mouse and human PRG4 (proteoglycan 4) genes. Cytogenet Cell Genet 2000; 90: 291-297.

42. Marcelino J, Carpten JD, Suwairi WM, Gutierrez OM, Schwartz S, Robbins C, Sood R, Makalowska I, Baxevanis A, Johnstone B, Laxer RM, Zemel L, Kim CA, Herd JK, Ihle J, Williams C, Johnson M, Raman V, Alonso LG, Brunoni D, Gerstein A, Papadopoulos N, Bahabri SA, Trent JM, Warman ML. CACP, encoding a secreted proteoglycan, is mutated in camptodactyly-arthropathy-coxa vara-pericarditis syndrome. Nat Genet 1999; 23: 319-322.

43. Coles JM, Zhang L, Blum JJ, Warman ML, Jay GD, Guilak F, Zauscher S. Loss of cartilage structure, stiffness, and frictional properties in mice lacking PRG4. Arthritis Rheum 2010; 62: 1666-1674.

44. Rhee DK, Marcelino J, Baker M, Gong Y, Smits P, Lefebvre V, Jay GD, Stewart M, Wang H, Warman ML, Carpten JD. The secreted glycoprotein lubricin protects cartilage surfaces and inhibits synovial cell overgrowth. J Clin Invest 2005; 115: 622-631.

45. Jay GD, Torres JR, Rhee DK, Helminen HJ, Hytinnen MM, Cha CJ, Elsaid K, Kim KS, Cui Y, Warman ML. Association between friction and wear in diarthrodial joints lacking lubricin. Arthritis Rheum 2007; 56: 3662-3669.

46. Elsaid KA, Fleming BC, Oksendahl HL, Machan JT, Fadale PD, Hulstyn MJ, Shalvoy R, Jay GD. Decreased lubricin concentrations and markers of joint inflammation in the synovial fluid of patients with anterior cruciate ligament injury. Arthritis Rheum 2008; 58: 1707-1715.

47. Elsaid KA, Jay GD, Warman ML, Rhee DK, Chichester CO. Association of articular cartilage degradation and loss of boundary-lubricating ability of synovial fluid following injury and inflammatory arthritis. Arthritis Rheum 2005; 52: 1746-1755.

48. Khalafi A, Schmid TM, Neu C, Reddi AH. Increased accumulation of superficial zone protein (SZP) in articular cartilage in response to bone morphogenetic protein-7 and growth factors. J Orthop Res 2007; 25: 293-303.

49. Schmidt TA, Gastelum NS, Han EH, Nugent-Derfus GE, Schumacher BL, Sah RL. Differential regulation of proteoglycan 4 metabolism in cartilage by IL-1alpha, IGF-I, and TGF-beta1. Osteoarthritis Cartilage 2008; 16: 90-97.

50. Flannery CR, Hughes CE, Schumacher BL, Tudor D, Aydelotte MB, Kuettner KE, Caterson B. Articular cartilage superficial zone protein (SZP) is homologous to megakaryocyte stimulating factor precursor and Is a multifunctional proteoglycan with potential growth-promoting, cytoprotective, and lubricating properties in cartilage metabolism. Biochem Biophys Res Commun 1999; 254: 535-541.

51. Jones AR, Flannery CR. Bioregulation of lubricin expression by growth factors and cytokines. Eur Cell Mater 2007; 13: 40-45; discussion 45.

52. Nugent GE, Aneloski NM, Schmidt TA, Schumacher BL, Voegtline MS, Sah RL. Dynamic shear stimulation of bovine cartilage biosynthesis of proteoglycan 4 (PRG4). Arthritis Rheum 2006; 54: 1888-1896.

53. Nugent GE, Schmidt TA, Schumacher BL, Voegtline MS, Bae WC, Jadin KD, Sah RL. Static and dynamic compression regulate cartilage metabolism of proteoglycan 4 (PRG4). Biorheology 2006; 43: 191-200.

54. Nugent-Derfus GE, Takara T, O'Neill JK, Cahill SB, Gortz S, Pong T, Inoue H, Aneloski NM, Wang WW, Vega KI, Klein TJ, Hsieh-Bonassera ND, Bae WC, Burke JD, Bugbee WD, Sah RL. Continuous passive motion applied to whole joints stimulates chondrocyte biosynthesis of PRG4. Osteoarthritis Cartilage 2007; 15: 566-574.

55. Elmore S. Apoptosis: a review of programmed cell death. Toxicologic pathology 2007; 35: 495-516.

56. Duprez L, Wirawan E, Vanden Berghe T, Vandenabeele P. Major cell death pathways at a glance. Microbes and infection 2009; 11: 1050-1062.

57. Maiuri MC, Zalckvar E, Kimchi A, Kroemer G. Self-eating and self-killing: crosstalk between autophagy and apoptosis. Nature reviews. Molecular cell biology 2007; 8: 741-752.

58. Carames B, Taniguchi N, Otsuki S, Blanco FJ, Lotz M. Autophagy is a protective mechanism in normal cartilage, and its aging-related loss is linked with cell death and osteoarthritis. Arthritis Rheum 2010; 62: 791-801.

59. Carames B, Taniguchi N, Seino D, Blanco FJ, D'Lima D, Lotz M. Mechanical injury suppresses autophagy regulators and pharmacologic activation of autophagy results in chondroprotection. Arthritis Rheum 2012; 64: 1182-1192.

60. Grogan SP, D'Lima DD. Joint aging and chondrocyte cell death. International journal of clinical rheumatology 2010; 5: 199-214.

61. Chen AC, Temple MM, Ng DM, Verzijl N, DeGroot J, TeKoppele JM, Sah RL. Induction of advanced glycation end products and alterations of the tensile properties of articular cartilage. Arthritis Rheum 2002; 46: 3212-3217.

62. Lotz M, Loeser RF. Effects of aging on articular cartilage homeostasis. Bone 2012; 51: 241-248.

63. Hui AY, Hsu FH, Noori NB, Hung LV, Pichika R, Schumacher BL, Ching AM, Lotz MK, Masuda K, Sah RL. Age-dependent transforming growth factor-beta1 regulation of proteoglycan 4 secretion by human knee articular cartialge. Arthritis Rheum 2012; (in revision).

64. Mankin HJ, Dorfman H, Lipiello L, Zarins A. Biochemical and metabolic abnormalities in articular cartilage from osteoarthritic human hips. II. Correlation of morphology with biochemical and metabolic data. J Bone Joint Surg Am 1971; 53-A: 523-537.

65. Custers RJ, Creemers LB, Verbout AJ, van Rijen MH, Dhert WJ, Saris DB. Reliability, reproducibility and variability of the traditional Histologic/Histochemical Grading System vs the new OARSI Osteoarthritis Cartilage Histopathology Assessment System. Osteoarthritis Cartilage 2007; 15: 1241-1248.

66. Pearson RG, Kurien T, Shu KS, Scammell BE. Histopathology grading systems for characterisation of human knee osteoarthritis--reproducibility, variability, reliability, correlation, and validity. Osteoarthritis Cartilage 2011; 19: 324-331.

67. Pauli C, Whiteside R, Heras FL, Nesic D, Koziol J, Grogan SP, Matyas J, Pritzker KP, D'Lima DD, Lotz MK. Comparison of cartilage histopathology assessment systems on human knee joints at all stages of osteoarthritis development. Osteoarthritis Cartilage 2012; 20: 476-485.

68. Rutgers M, van Pelt MJ, Dhert WJ, Creemers LB, Saris DB. Evaluation of histological scoring systems for tissue-engineered, repaired and osteoarthritic cartilage. Osteoarthritis and cartilage / OARS, Osteoarthritis Research Society 2010; 18: 12-23.

69. Pritzker KP, Gay S, Jimenez SA, Ostergaard K, Pelletier JP, Revell PA, Salter D, van den Berg WB. Osteoarthritis cartilage histopathology: grading and staging. Osteoarthritis Cartilage 2006; 14: 13-29.

70. Amir G, Pirie CJ, Rashad S, Revell PA. Remodelling of subchondral bone in osteoarthritis: a histomorphometric study. Journal of clinical pathology 1992; 45: 990-992.

71. Benske J, Schunke M, Tillmann B. Subchondral bone formation in arthrosis. Polychrome labeling studies in mice. Acta orthopaedica Scandinavica 1988; 59: 536-541.

72. Intema F, Hazewinkel HA, Gouwens D, Bijlsma JW, Weinans H, Lafeber FP, Mastbergen SC. In early OA, thinning of the subchondral plate is directly related to cartilage damage: results from a canine ACLT-meniscectomy model. Osteoarthritis Cartilage 2010; 18: 691-698.

73. Hulth A, Johnell O, Lindberg L, Heinegard D. Sequential appearance of macromolecules in bone induction in the rat. J Orthop Res 1993; 11: 367-378.

74. Collins DH, McElligott TF. Sulphate (35SO4) uptake by chondrocytes in relation to histological changes in osteo-arthritic human articular cartilage. Ann Rheum Dis 1960; 19: 318-??

75. Ostergaard K, Petersen J, Andersen CB, Bendtzen K, Salter DM. Histologic/histochemical grading system for osteoarthritic articular cartilage: reproducibility and validity. Arthritis Rheum 1997; 40: 1766-1771.

76. Shapiro F, Glimcher MJ. Induction of osteoarthrosis in the rabbit knee joint. Histologic changes following menisectomy and meniscal lesions. Clin Orthop Relat Res 1980; 147: 287-295.

77. Mainil-Varlet P, Aigner T, Brittberg M, Bullough P, Hollander A, Hunziker E, Kandel R, Nehrer S, Pritzker K, Roberts S, Stauffer E. Histological assessment of cartilage repair: a report by the Histology Endpoint Committee of the International Cartilage Repair Society (ICRS). J Bone Joint Surg Am 2003; 85-A Suppl 2: 45-57.

78. Gurcan MN, Boucheron LE, Can A, Madabhushi A, Rajpoot NM, Yener B. Histopathological image analysis: a review. IEEE reviews in biomedical engineering 2009; 2: 147-171.

79. Moussavi-Harami SF, Pedersen DR, Martin JA, Hillis SL, Brown TD. Automated objective scoring of histologically apparent cartilage degeneration using a custom image analysis program. J Orthop Res 2009; 27: 522-528.

80. Stockwell RA. The cell density of human articular and costal cartilage. J Anat 1967; 101: 753-763.

81. Yamada K, Healey R, Amiel D, Lotz M, Coutts R. Subchondral bone of the human knee joint in aging and osteoarthritis. Osteoarthritis and cartilage 2002; 10: 360-369.

82. McEvoy MD, Hand WR, Furse CM, Field LC, Clark CA, Moitra VK, Nietert PJ, O'Connor MF, Nunnally ME. Validity and reliability assessment of detailed scoring checklists for use during perioperative emergency simulation training. Simulation in healthcare : journal of the Society for Simulation in Healthcare 2014; 9: 295-303.

83. Keszei AP, Novak M, Streiner DL. Introduction to health measurement scales. Journal of psychosomatic research 2010; 68: 319-323.

84. Bland JM, Altman DG. Agreement between methods of measurement with multiple observations per individual. Journal of biopharmaceutical statistics 2007; 17: 571-582.

85. Mankin HJ. The reaction of articular cartilage to injury and osteoarthritis (Part I). N Engl J Med 1974; 291: 1285-1292.

86. Buckwalter JA, Mankin HJ. Articular cartilage. Part II: degeneration and osteoarthrosis, repair, regeneration, and transplantation. J Bone Joint Surg Am 1997; 79-A: 612-632.

87. Buckwalter JA, Mankin HJ. Articular cartilage: tissue design and chondrocyte-matrix interactions. Instr Course Lect 1998; 47: 477-486.

88. Martin JA, Brown TD, Heiner AD, Buckwalter JA. Chondrocyte senescence, joint loading and osteoarthritis. Clin Orthop Relat Res 2004: S96-103.

89. You BM, Siy P, Anderst W, Tashman S. In vivo measurement of 3-D skeletal kinematics from sequences of biplane radiographs: application to knee kinematics. IEEE Trans Med Imaging 2001; 20: 514-525.

90. Smith PN, Refshauge KM, Scarvell JM. Development of the concepts of knee kinematics. Archives of physical medicine and rehabilitation 2003; 84: 1895-1902.

91. Lafortune MA, Cavanagh PR, Sommer HJ, 3rd, Kalenak A. Three-dimensional kinematics of the human knee during walking. J Biomech 1992; 25: 347-357.

92. Bae WC, Payanal MM, Chen AC, Hsieh-Bonassera ND, Ballard BL, Lotz MK, Coutts RD, Bugbee WD, Sah RL. Topographic patterns of cartilage lesions in knee osteoarthritis. Cartilage 2010; 1: 10-19.

93. Temple MM, Bae WC, Chen MQ, Lotz M, Amiel D, Coutts RD, Sah RL. Age- and site-associated biomechanical weakening of human articular cartilage of the femoral condyle. Osteoarthritis Cartilage 2007; 15: 1042-1052.

94. Eggli PS, Hunziker EB, Schenk RK. Quantitation of structural features characterizing weight- and less-weight-bearing regions in articular cartilage: a stereological analysis of medial femoral condyles in young adult rabbits. Anat Rec 1988; 222: 217-227.

95. Arokoski ME, Tiitu V, Jurvelin JS, Korhonen RK, Fick JM. Topographical investigation of changes in depth-wise proteoglycan distribution in rabbit femoral articular cartilage at 4 weeks after transection of the anterior cruciate ligament. Journal of orthopaedic research : official publication of the Orthopaedic Research Society 2015; 33: 1278-1286.

96. Chang DG, Iverson EP, Schinagl RM, Sonoda M, Amiel D, Coutts RD, Sah RL. Quantitation and localization of cartilage degeneration following the induction of osteoarthritis in the rabbit knee. Osteoarthritis Cartilage 1997; 5: 357-372.

97. Ghadially JA, Ghadially FN. Evidence of cartilage flow in deep defects in articular cartilage. Virchows Arch Abt B Zellpath 1975; 18: 193-204.

98. Squires GR, Okouneff S, Ionescu M, Poole AR. The pathobiology of focal lesion development in aging human articular cartilage and molecular matrix changes characteristic of osteoarthritis. Arthritis Rheum 2003; 48: 1261-1270.

99. Bruns J, Kersten P, Silbermann M, Lierse W. Cartilage-flow phenomenon and evidence for it in perichondrial grafting. Arch Orthop Trauma Surg 1997; 116: 66-73.

100. Turunen SM, Lammi MJ, Saarakkala S, Koistinen A, Korhonen RK. Hypotonic challenge modulates cell volumes differently in the superficial zone of intact articular cartilage and cartilage explant. Biomechanics and modeling in mechanobiology 2012; 11: 665-675.

101. Cecil DL, Johnson K, Rediske J, Lotz M, Schmidt AM, Terkeltaub R. Inflammation-induced chondrocyte hypertrophy is driven by receptor for advanced glycation end products. Journal of immunology 2005; 175: 8296-8302.

102. Lotz MK, Otsuki S, Grogan SP, Sah R, Terkeltaub R, D'Lima D. Cartilage cell clusters. Arthritis Rheum 2010; 62: 2206-2218.

103. Eckstein F, Lemberger B, Gratzke C, Hudelmaier M, Glaser C, Englmeier KH, Reiser M. In vivo cartilage deformation after different types of activity and its dependence on physical training status. Ann Rheum Dis 2005; 64: 291-295.

104. Schmidt TA, Schumacher BL, Han EH, Klein TJ, Voegtline MS, Sah RL. Synthesis and secretion of lubricin/superficial zone protein by chondrocytes in cartilage explants: modulation by TGF-b1 and IL-1a. Trans Orthop Res Soc 2004; 29: 577.

105. Klein TJ, Schumacher BL, Blewis ME, Schmidt TA, Voegtline MS, Thonar EJ, Masuda K, Sah RL. Tailoring secretion of proteoglycan 4 (PRG4) in tissue-engineered cartilage. Tissue Eng 2006; 12: 1429-1439.

106. Grogan SP, D'Lima DD. Joint aging and chondrocyte cell death. Int J Clin Rheumtol 2010; 5: 199-214.

107. O'Brien KA, Muscarella DE, Bloom SE. Differential induction of apoptosis and MAP kinase signaling by mitochondrial toxicants in drug-sensitive compared to drug-resistant B-lineage lymphoid cell lines. Toxicol Appl Pharmacol 2001; 174: 245-256.

108. Kabeya Y, Mizushima N, Ueno T, Yamamoto A, Kirisako T, Noda T, Kominami E, Ohsumi Y, Yoshimori T. LC3, a mammalian homologue of yeast Apg8p, is localized in autophagosome membranes after processing. The EMBO journal 2000; 19: 5720-5728.

109. Ewers BJ, Dvoracek-Driksna D, Orth MW, Haut RC. The extent of matrix damage and chondrocyte death in mechanically traumatized articular cartilage explants depends on rate of loading. J Orthop Res 2001; 19: 779-784.

110. Waller KA, Zhang LX, Elsaid KA, Fleming BC, Warman ML, Jay GD. Role of lubricin and boundary lubrication in the prevention of chondrocyte apoptosis. Proc Natl Acad Sci U S A 2013; 110: 5852-5857.

111. Outerbridge RE. The etiology of chondromalacia patellae. J Bone Joint Surg Br 1961; 43-B: 752-757.

112. DuRaine G, Neu CP, Chan SM, Komvopoulos K, June RK, Reddi AH. Regulation of the friction coefficient of articular cartilage by TGF-beta1 and IL-1beta. J Orthop Res 2009; 27: 249-256.

113. Neu CP, Khalafi A, Komvopoulos K, Schmid TM, Reddi AH. Mechanotransduction of bovine articular cartilage superficial zone protein by transforming growth factor beta signaling. Arthritis Rheum 2007; 56: 3706-3714.

114. Bian L, Lima EG, Angione SL, Ng KW, Williams DY, Xu D, Stoker AM, Cook JL, Ateshian GA, Hung CT. Mechanical and biochemical characterization of cartilage explants in serum-free culture. J Biomech 2008; 41: 1153-1159.

115. Eckstein F, Hudelmaier M, Putz R. The effects of exercise on human articular cartilage. J Anat 2006; 208: 491-512.

116. Elmore S. Apoptosis: a review of programmed cell death. Toxicol Pathol 2007; 35: 495-516.

117. Treppo S, Koepp H, Quan EC, Cole AA, Kuettner KE, Grodzinsky AJ. Comparison of biomechanical and biochemical properties of cartilage from human knee and ankle pairs. J Orthop Res 2000; 18: 739-748.

118. Raub CB, Hsu SC, Chan EF, Shirazi R, Chen AC, Chnari E, Semler EJ, Sah RL. Microstructural remodeling of articular cartilage following defect repair by osteochondral autograft transfer. Osteoarthritis Cartilage 2013; 21: 860-868.

119. Moussavi-Harami SF, Pedersen DR, Martin JA, Hillis SL, Brown TD. Automated objective scoring of histologically apparent cartilage degeneration using a custom image analysis program. Journal of orthopaedic research : official publication of the Orthopaedic Research Society 2009; 27: 522-528.

120. Buckwalter JA, Mankin HJ. Articular cartilage: degeneration and osteoarthritis, repair, regeneration, and transplantation. Instr Course Lect 1998; 47: 487-504.

121. Smith RL, Trindade MC, Ikenoue T, Mohtai M, Das P, Carter DR, Goodman SB, Schurman DJ. Effects of shear stress on articular chondrocyte metabolism. Biorheology 2000; 37: 95-107.

122. Grogan SP, Duffy SF, Pauli C, Koziol JA, Su AI, D'Lima DD, Lotz MK. Zone-specific gene expression patterns in articular cartilage. Arthritis and rheumatism 2013; 65: 418-428.